5-2010

SIGNALING MECHANISMS THAT CONTROL GAP JUNCTIONAL COUPLING BETWEEN RETINAL NEURONS

Wade Kothmann

Recommended Citation

The TMC LIBRARY
Health Sciences Resource Center

SIGNALING MECHANISMS THAT CONTROL GAP JUNCTIONAL

COUPLING BETWEEN RETINAL NEURONS

by

W. Wade Kothmann

APPROVED:

_____
John O'Brien, Ph.D., Supervisory Professor

_____
Carmen W. Dessauer, Ph.D.

_____
Stephen C. Massey, Ph.D.

_____
Stephen L. Mills, Ph.D.

_____
Daniel S. Wagner, Ph.D.

APPROVED:

_____
Dean, The University of Texas Graduate School of Biomedical Sciences

SIGNALING MECHANISMS THAT CONTROL GAP JUNCTIONAL

COUPLING BETWEEN RETINAL NEURONS

A

DISSERTATION

Presented to the Faculty of
The University of Texas
Health Science Center at Houston
and
The University of Texas
M.D. Anderson Cancer Center
Graduate School of Biomedical Sciences
in Partial Fulfillment

of the Requirements

for the Degree of

DOCTOR OF PHILOSOPHY

by

William Wade Kothmann
Houston, Texas

May 2010

This work is dedicated to my family

<u>Acknowledgements</u>

There are so many people to thank for their roles in shaping both the work presented here and my development as a scientist. First and foremost among them is my advisor, John O'Brien. When I came to John and expressed my interest in his research, I had very little background in molecular and cellular neuroscience. Despite this, John accepted me as a rotation student and then as his graduate trainee, thus setting off the chain of events that has led to this dissertation. In addition, a number of other things have come to be because of that first step, including what I expect will be my lifelong fascination with the retina and visual science. John has been the consummate mentor to me, providing his advice and guidance at every step of my training while also allowing me a degree of autonomy in selecting my research model and experimental directions. The fact that his door remains open daily and that I have so rarely ever had to wait a day or even an hour to discuss my latest data or thoughts with him is, in my opinion, one of his best qualities. The example he has set is one I hope to follow one day, should I have the opportunity to train students of my own.

The faculty members of the Ophthalmology department have also been invaluable teachers and friends to me in Houston. My weekly trips to the Ginger Man with Steve Massey will be sorely missed, as will all the conversations and advice, scientific and otherwise. I am also quite certain that most of my developmental strides in confocal microscopy are due to that first, half-in-jest comment he made on one of my images. I am grateful for the many discussions I've had with Steve Mills here and at ARVO, and for all his insight and thoughtful comments. Finally, Steven Wang has set an example of

how to work hard and then play hard, and I am grateful as well for his advice, encouragement, and friendship.

I have made many lasting friendships while at UT, and I am especially glad to have met Matt Swulius. Matt has become a good friend of mine, and has provided much perspective on neuroscience and graduate school during our time here. I am also glad to have had good labmates throughout my time in John's lab, especially Hongyan Li.

Finally, I want to acknowledge my family. My parents, Don and Sheila Kothmann, my sister, Kara Kothmann, and my grandparents, Hildegarde Kothmann and Jesse and Louise Gregg, are all inspirations to me and their constant love and support is the best thing in my life. Meeting my wife, Vani Pariyadath, is without question the best thing that happened to me in graduate school, and I look forward to many years of life, love, and learning with her. There is nothing in the world more valuable to me than my family, nor anyone who has shaped me more than them; thus, as with everything I hope to accomplish, this is for them.

Abstract

Signaling mechanisms that control gap junctional coupling between retinal neurons

Gap junctions between neurons form the structural substrate for electrical synapses. Connexin 36 (Cx36, and its non-mammalian ortholog connexin 35) is the major neuronal gap junction protein in the central nervous system (CNS), and contributes to several important neuronal functions including neuronal synchronization, signal averaging, network oscillations, and motor learning. Connexin 36 is strongly expressed in the retina, where it is an obligatory component of the high-sensitivity rod photoreceptor pathway. A fundamental requirement of the retina is to adapt to broadly varying inputs in order to maintain a dynamic range of signaling output. Modulation of the strength of electrical coupling between networks of retinal neurons, including the Cx36-coupled AII amacrine cell in the primary rod circuit, is a hallmark of retinal luminance adaptation. However, very little is known about the mechanisms regulating dynamic modulation of Cx36-mediated coupling. The primary goal of this work was to understand how cellular signaling mechanisms regulate coupling through Cx36 gap junctions. We began by developing and characterizing phospho-specific antibodies against key regulatory phosphorylation sites on Cx36. Using these tools we showed that phosphorylation of Cx35 in fish models varies with light adaptation state, and is modulated by acute changes in background illumination. We next turned our focus to the well-studied and readily identifiable AII amacrine cell in mammalian retina. Using this model we showed that

increased phosphorylation of Cx36 is directly related to increased coupling through these gap junctions, and that the dopamine-stimulated uncoupling of the AII network is mediated by dephosphorylation of Cx36 via protein kinase A-stimulated protein phosphatase 2A activity. We then showed that increased phosphorylation of Cx36 on the AII amacrine network is driven by depolarization of presynaptic ON-type bipolar cells as well as background light increments. This increase in phosphorylation is mediated by activation of extrasynaptic NMDA receptors associated with Cx36 gap junctions on AII amacrine cells and by Ca^{2+}-calmodulin-dependent protein kinase II activation. Finally, these studies indicated that coupling is regulated locally at individual gap junction plaques. This work provides a framework for future study of regulation of Cx36-mediated coupling, in which increased phosphorylation of Cx36 indicates increased neuronal coupling.

Table of Contents

List of Figures

Chapter 4

<u>Chapter 1</u>

Introduction

Gap Junctions: An Overview

Gap junctions are membrane-bound, dodecameric protein channels that connect two neighboring cells by forming an aqueous pore through which metabolic and electrical communication can occur. These channels aggregate into plaques in the lipid bilayer which contain from tens to thousands of individual gap junctions (Yeager, 2009). Each individual gap junction is composed of two docked hemichannels, or connexons, one hemichannel being contributed by each cell in a coupled pair of cells. Each hemichannel is in turn composed of six protein subunits called connexins, which are organized as a hexagonal ring to form the pore (Yeager, 2009). Connexin subunits each contain four transmembrane domains, as well as two characteristic extracellular loops which mediate the docking interaction (Yeager, 2009). The remaining intracellular components (N-terminus, intracellular loop, and C-terminal tail) show considerable variability across different connexin genes and are targets for regulation of the protein (Lampe and Lau, 2004).

The human connexin gene family has 21 members, while only 20 are known in mice (Beyer and Berthoud, 2009). Connexin genes are expressed in virtually every tissue in the body over the course of development, and in adulthood gap junctions are found in most organs. A number of connexin genes are also linked to diseases, which due to the wide expression of the various connexin proteins range from genetic neuropathies to various skin diseases, from congenital deafness to cataracts (Beyer and Berthoud, 2009). The work presented hereafter will focus on the role of gap junctions in the central nervous system (CNS).

Gap Junctions in Neurons: Basic Properties

Gap junctions between neurons form the structural substrate for electrical synapses. Because gap junctions form aqueous pores which are permeable to the common ions used by neurons to control their membrane voltage (Na^+, K^+, Ca^{2+}, Cl^-), when two neurons coupled by a gap junction have unequal membrane potentials current will flow through the gap junction proportional to the size of the voltage difference. Thus gap junctions between neurons act as Ohmic resistors.

Communication between two neurons through electrical synapses contrasts in several ways with the more common chemical synapses. First, electrical synapses are faster than chemical synapses since there is no delay imposed by release, diffusion, and binding of neurotransmitter molecules to receptors. Second, electrical synapses are always sign conserving; depolarization of one cell in a coupled pair will always cause a depolarization in the second coupled cell. Third, electrical synapses do not (in and of themselves) show signal amplification; depolarization of one cell in a coupled pair will cause a smaller depolarization in the second coupled cell inversely proportional to the resistance of the gap junctions. The ratio voltage change in the second cell to voltage change in the first (initially depolarized) cell is termed the coupling coefficient. Additionally, when the input resistances of a coupled cell pair are unequal, the cell with the lower input resistance will exert a greater influence on the cell with the higher input resistance. Finally, electrical synapses are bidirectional, as a depolarization in either cell relative to the other will cause current to flow through the gap junctions.

Despite the many differences between electrical and chemical synapses, they do share some common functional properties, although the underlying causes of the

properties may be different. For instance, electrical synapses undergo synaptic

potentiation (short- and long-term) and depression (Yang et al., 1990; Pereda and Faber,

1996; Landisman and Connors, 2005), similar to chemical synapses. The major goal of

the research presented herein was to further understand the molecular processes that

underlie regulation of gap junctional coupling in neurons. These processes are likely to

be the basis for potentiation and depression observed at electrical synapses.

Gap Junctions in Neurons: Connexin Identity and Implications for Disease

A number of connexins are expressed in neurons in the CNS, including

Cx30.2, Cx36, Cx37, Cx40, Cx45, Cx50, and Cx57 (Massey et al., 2003; Kreuzberg et

al., 2008; Connors, 2009). Of these, Cx36 is both the best studied and the most widely

expressed in the CNS (Connors, 2009). Cx36 gap junction expression occurs throughout

the brain, but is particularly notable in the retina, olfactory bulb, hippocampus,

cerebellum, cerebral cortex, reticular nucleus of the thalamus, inferior olive, striatum, and

spinal cord (Condorelli et al., 1998). In many of these regions specific cell types coupled

by Cx36 have been identified and studied (Connors, 2009).

Neuronal coupling via gap junctions has been suggested to contribute to the

generation and maintenance of neural synchrony underlying seizures (Carlen et al., 2000;

Perez Velazquez and Carlen, 2000). The gene coding for Cx36 has been associated by

linkage studies with juvenile myoclonic epilepsy (Mas et al., 2004; Hempelmann et al.,

2006), and experimental studies have provided some further support for a role of Cx36 in

epilepsy (Maier et al., 2002). These include observations that induced epileptiform

activity is reduced in Cx36-null mice and altered Cx36 expression in animal models of

epilepsy (Sohl et al., 2000; Gajda et al., 2003; McCracken and Roberts, 2006).

Additionally, drugs that block gap junctional coupling have anticonvulsive effects in

seizure models, including drugs with partial specificity for Cx36 (Jahromi et al., 2002;

Uusisaari et al., 2002; Gajda et al., 2003; Gajda et al., 2005; Bostanci and Bagirici, 2007).

Thus, understanding the mechanisms which mediate regulated changes in coupling

through Cx36 gap junctions may have future relevance for novel epilepsy interventions.

Connexin 36: Channel Properties

      Cx36 gap junctions have the smallest unitary conductance, around 10-15 pS,

measured out of all functional gap junction channels (Srinivas et al., 1999; Teubner et al.,

2000). Coupling through Cx36 gap junctions is relatively insensitive to transjunctional

voltage changes (Srinivas et al., 1999), making them ideal for electrical communication

between neurons. Intracellular acidification causes minor increases in the conductance of

Cx36 gap junctions, while alkilinization causes a somewhat sharper reduction of

conductance (Gonzalez-Nieto et al., 2008). However, modulation of channel

conductance by pH within physiological ranges alters conductance less than 25% from

baseline coupling at pH 7.25.

      Studies using small tracer molecules have indicated that Cx36 shows some

charge selectivity, preferentially passing positively charged tracers while restricting

diffusion of negatively charged tracers (Vaney, 1985, , 1991; Mills et al., 2001b;

Charpantier et al., 2007). The preferred tracer for studying Cx36 has been biotin

ethylenediamine (Neurobiotin; MW 286 Da, net charge +1), which readily diffuses

through these junctions. Larger biotin-conjugated tracers show increasingly reduced

permeability through Cx36 junctions as size increases, with biotin-XX cadaverine (MW 555 Da, net charge +1) showing ~80% reduced permeability (Mills and Massey, 2000). Negatively charged tracers within the same size range (Lucifer yellow, MW 443 Da, net charge -2; 6-carboxyfluorescein, MW 376 Da, net charge -1) show very little permeation of Cx36 gap junctions (Vaney, 1985, , 1991; Charpantier et al., 2007).

Fewer studies have addressed the permeation of Cx36 by more biologically relevant molecules. It has been shown that Cx36 is relatively impermeant to the second messenger cAMP (Bedner et al., 2003; Bedner et al., 2006), which is not surprising given its net negative charge. It is known that Ca^{2+} permeates Cx36 gap junctions (citations), which is quite significant for neuronal signaling.

Connexin 36: Role in Neuronal Circuits

Owing to its wide expression throughout the CNS, it is not surprising that a number of studies have identified important roles of Cx36 in neuronal function. Multiple types of inhibitory interneurons are electrically coupled in neocortex, where they drive synchronized inhibition of excitatory neurons (Gibson et al., 1999; Beierlein et al., 2000). Cx36 gap junctions are critical for the generation of this synchronous inhibition (Deans et al., 2001). Electrical coupling of neurons in the reticular nucleus of the thalamus by Cx36 gap junctions likewise mediate correlated spiking patterns within these neurons, which in turn provide inhibition onto thalamic relay cells (Landisman et al., 2002; Long et al., 2004). Cx36 gap junctions between neurons in the inferior olive mediate synchronization of subthreshold membrane oscillations (Long et al., 2002). Loss of Cx36 gap junctions between these olivary neurons causes deficits in cerebellar motor learning

(Van Der Giessen et al., 2008). Cx36-null mice also show selective impairment of gamma-frequency oscillation in the hippocampus (Hormuzdi et al., 2001; Buhl et al., 2003)., which are thought to be involved in binding of spatially separated information processing.

In the retina, Cx36 gap junctions are expressed by every class of neuron except horizontal cells (Feigenspan et al., 2001a; Mills et al., 2001b; Hidaka et al., 2002; Lee et al., 2003; Feigenspan et al., 2004a; Zhang and Wu, 2004; Han and Massey, 2005; Schubert et al., 2005). Coupling between photoreceptors leads to signal averaging between neighbors which can lead to significant improvement of the signal to noise ratio (Schwartz, 1975c; Lamb and Simon, 1976; DeVries et al., 2002) and also expands the effective voltage response range of rods (Attwell et al., 1987). Additionally, coupling between rods and cones provides an alternative pathway for rod signals to enter the cone circuitry (Schwartz, 1975d; Deans et al., 2002; Bloomfield and Volgyi, 2009). Coupling between retinal ganglion cells, many of which express Cx36 (Pan et al., ; Hidaka et al., 2002; Schubert et al., 2005), contributes to synchronous spiking activity (Hu and Bloomfield, 2003).

Perhaps the best known function of Cx36 gap junctions in the retina is coupling between AII amacrine neurons (Kolb and Famiglietti, 1974; Famiglietti and Kolb, 1975; Feigenspan et al., 2001a; Mills et al., 2001b; Veruki and Hartveit, 2002a). AIIs receive excitatory input from rod bipolar cells (Kolb and Famiglietti, 1974; Strettoi et al., 1990), and share this input with their neighboring AIIs through Cx36 gap junctions. The AII network also outputs the signal through gap junctions, which are composted of Cx36 on the AII side, to ON-cone bipolar cells (Kolb and Famiglietti, 1974; Mills and

7

Massey, 1995; Mills et al., 2001b; Veruki and Hartveit, 2002b). Since rod bipolar cells do not synapse onto retinal ganglion cells, loss of Cx36 eliminates transmission through the primary, high-gain rod photoreceptor pathway (Deans et al., 2002; Volgyi et al., 2004). In addition to the loss of this direct pathway for ON signals, loss of Cx36 also eliminates the highest-sensitivity OFF pathway, which relies on glycine release from the lobular dendrites on AII amacrine cells (Volgyi et al., 2004). Loss of Cx36 does not directly prevent this inhibitory output from the AII, but rather lowers its sensitivity to light. This is because coupling between AIIs is thought to underlie summation of synchronous signals and subtraction of asynchronous noise at very low light-levels, thus increasing the overall sensitivity of the cells output (Smith and Vardi, 1995; Vardi and Smith, 1996; Bloomfield and Volgyi, 2004).

The Retina: An Overview

Human vision begins when photoreceptor neurons in the retina transduce absorbed photons into electrical signals. These signals diverge from a small number of photoreceptor types (one high-sensitivity rod photoreceptor and three [or two to five, in other vertebrates] lower-sensitivity cone photoreceptor types with differing spectral sensitivities) at glutamatergic synapses onto a larger number (roughly 10, depending on species) of bipolar cell types. Bipolar cell types are broadly classified into types that depolarize to light increments (ON-types, which includes the single type of rod bipolar cell), and types that hyperpolarize to light (OFF-types). Signals in bipolar cells then diverge further at glutamatergic synapses onto a larger number (between 15 and 20, depending on species) of ganglion cell types. These ganglion cells then output the

8

information processed in the retina to the rest of the brain as spike trains carried along their axons, forming a number of parallel information pathways equal to the number of ganglion cell types (Roska and Werblin, 2001; Dacey et al., 2003; Roska et al., 2006; Field and Chichilnisky, 2007). Each pathway carries information extracted from particular components that make up the visual environment, which will then be further processed by higher-order neurons in the brain to give rise to visual perception (Roska and Werblin, 2001; Dacey et al., 2003; Roska et al., 2006; Field and Chichilnisky, 2007).

In addition to fundamental differences in the biophysical properties of photoreceptors, bipolar cells, and ganglion cells, two key components of retinal circuitry necessary for fine-tuning each parallel pathway are horizontal and amacrine cell inhibitory interneurons. Horizontal cells (between 2 and 4, depending on species) and amacrine cells (25 types and up, depending on species) are thought to contribute largely to the spatial and temporal processing properties of photoreceptors, bipolar cells, and ganglion cells (Roska and Werblin, 2001; Roska et al., 2006; Field and Chichilnisky, 2007).

The Necessity of Adaptation

In addition to the divergence of photoreceptor signals detailed above, there is also a high degree of convergence evident in many retinal pathways, especially the rod photoreceptor pathway (Volgyi et al., 2004; Dunn et al., 2006). Because signals from up to 10,000 rods may converge onto one ganglion cell the retina has exquisite sensitivity to light, but is also in constant danger of saturation (Dunn et al., 2006). And although the various specializations of the retina allow us to perceive the visual world over at least a

9

10^9-fold range of background light intensities, the output range of retinal ganglion cells (in terms of spike rate modulation) is only 10^2 (Rodieck, 1998; Rieke and Rudd, 2009). Thus adaptation is absolutely necessary to preserve dynamic range of signaling, preventing saturation yet preserving our ability to perceive meaningful differences in our environment. Adaptation takes place at many different levels in the retina, from the biochemical phototransduction cascade in photoreceptors (Rodieck, 1998) to individual synapses between retinal neurons (Rieke and Rudd, 2009; Wark et al., 2009). One hallmark of luminance adaptation in the retina is regulated changes in coupling between horizontal cells and AII amacrine cells (Xin and Bloomfield, 1997, , 1999; Bloomfield and Volgyi, 2004).

The Role of Connexin 36 in Retinal Adaptation

Both types of rabbit horizontal cells and AII amacrine cells display inverted "U"-shaped coupling functions with relation to background light intensity (Xin and Bloomfield, 1997, , 1999; Bloomfield and Volgyi, 2004). Since horizontal cells do not use Cx36, the focus here will be on the role of regulated coupling changes in AII amacrine cells. AIIs are relatively uncoupled in well dark-adapted retina, when ambient background light is below rod photoreceptor threshold. Increasing background illumination to just above rod photoreceptor threshold sharply increases coupling, both electrical (as measured by receptive field size) and tracer (Neurobiotin diffusion), 4 to 5-fold. Coupling continues to increase along a much shallower trajectory as background illumination is raised over several log units, until eventually it again decreases somewhat sharply back towards baseline levels. As dopamine also uncouples AII amacrine cells via

10

activation of D1 receptors (Hampson et al., 1992; Mills and Massey, 1995), and since

dopamine is considered a light-adaptive signal in the retina (Witkovsky, 2004) that is

released by light-stimulation (Mills et al., 2007; Zhang et al., 2007), it is widely thought

that the falloff in coupling at higher background intensities is mediated by dopamine

signaling. Less attention has been given to potential mechanisms underlying the

background light-driven increase in coupling, although it has the appearance of an

activity-dependent process.

Much thought has been given to the functional significance of regulated

changes in AII amacrine cell coupling in retinal adaptation. The prevailing line of

thinking is that AIIs are uncoupled in darkness in order to maximize the effect of any

single-photon absorptions in individual rods. When photons are this scarce, preventing

the lateral spread of depolarization in the AII network will enhance the transfer of the

signal into coupled ON-cone bipolar cells and then on to a ganglion cell. As background

illumination increases to a level reliably above rod threshold, the chance increases that

two rods within a given distance of each other will absorb photons within the same

integration period. In such a case, much enhanced coupling between AIIs will allow the

summation of synchronous signals and subtraction of asynchronous signals, as noted

previously. Computational modeling (Vardi and Smith, 1996) and experimental evidence

(Dunn et al., 2006) support this, demonstrating that coupling in the AII network increases

the signal to noise ratio of the AII's light response. The further increase in coupling as

lighting increases in the scotopic range may contribute to gain control as well, as

shunting of increasing excitatory currents in AIIs caused by increasing rod bipolar input

may help to prevent saturation. Finally, as background light enters the cone-

photoreceptor operating range, uncoupling of AIIs likely serves a two-fold purpose.

First, it likely optimizes the amount of rod input and cone input mixing in cone bipolar

cells in the mesopic range where both rods and cones are active. Second, as background

light enters the photopic range the AII switches its "duty" and receives its input directly

from coupled ON-cone bipolar cells, triggering release of glycine by the AII onto OFF-

cone bipolar cells and some ganglion cells (Manookin et al., 2008; Murphy and Rieke,

2008; Munch et al., 2009; van Wyk et al., 2009). Uncoupling of the AII network in this

range will increase the spatial localization of this inhibition when photons are abundant

enough to activate the cone pathways of the retina.

Regulation of Connexin 36: Initial Studies

Coupling at AII-AII gap junctions is preferentially regulated by dopamine

signaling and cAMP-dependent processes, while coupling between AII-cone bipolar gap

junctions is preferentially regulated by nitric oxide signaling and cGMP-dependent

processes (Mills and Massey, 1995). Alteration of protein kinase activity is a common

effector of these pathways, and thus initial studies of the regulation of Cx36 targeted

kinase pathways. Addition of a cAMP analog was shown to reduce currents through

Cx35 gap junctions expressed in *Xenopus* oocytes, and this reduction required a PKA

consensus sequence (Mitropoulou and Bruzzone, 2003). Further studies in HeLa cells

stably transfected with fish Cx35 identified two phosphorylation sites, Ser110 and Ser276

were required for regulation of coupling by PKA activity (Ouyang et al., 2005).

Activation of PKA caused decreased HeLa coupling in these experiments, while

inhibition of PKA increased coupling. Serine to alanine mutation of either residue alone

reduced regulation by PKA activity, while mutation of both sites eliminated this

regulation. Repeating these experiments with HeLa cells transiently transfected with

mouse Cx36 showed that this regulation by PKA activity is conserved at both

phosphorylation sites in mammals (our unpublished observations). Several studies have

indicated that multiple kinases can phosphorylate both of these sites *in vitro*, including

PKA, PKG, and CamKII (Ouyang et al., 2005; Patel et al., 2006; Urschel et al., 2006).

Other kinases are predicted or known to phosphorylate one or the other of these sites

(Ouyang et al., 2005; Urschel et al., 2006). The convergence of multiple kinases,

representing the effectors of various signaling pathways, upon each of these

phosphorylation sites suggests their critical involvement in regulation of Cx36-mediated

coupling.

In addition to phosphorylation, protein-protein interactions are also likely to

contribute to regulation of Cx36-mediated coupling. It is known that calmodulin binds to

the C-terminal tail of Cx36 with a low-micromolar $K_{1/2}$ for Ca^{2+} (Burr et al., 2005). The

necessity of this relatively high intracellular concentration of Ca^{2+} for binding indicates

that this interaction would likely be most common at sites such as synapses, where such

elevations of Ca^{2+} occur. The functional significance of calmodulin binding to Cx36 is

still not well understood. In addition to calmodulin binding, the tip of the C-terminal tail

of Cx36 is a PDZ-domain binding target (Li et al., 2004). This mediates known

interactions with the PDZ-domain-containing scaffolding protein ZO-1 (Li et al., 2004;

Flores et al., 2008), and potentially with several other scaffolding proteins. This

interaction likely does not regulate Cx36 directly, but evidence suggests that it is

important for localizing regulatory proteins to the site of Cx36 gap junctions. For

instance, when the tip is truncated, regulation by PKA activity is reversed, such that activation of PKA leads to increased coupling and vice versa (Ouyang et al., 2005). Such interactions may prove to control cell-specific schemes of Cx36 regulation, particularly those involving different kinase or phosphatase proteins.

Starting Hypotheses

The following work tested several hypotheses concerning the regulation of Cx36 by phosphorylation in retinal neurons and the signaling pathways responsible for this regulation. These chapters follow one another fairly linearly as they progress towards their goal of furthering our understanding of the signaling mechanisms which control regulated changes in neuronal coupling.

Chapter 2 focuses on the development and characterization of antibodies specific for Cx35/36 proteins phosphorylated at either of the two key regulatory serine residues. These antibodies have proven to be uniquely valuable tools for understanding how Cx36 regulation occurs in physiologically intact systems. Following the characterization of the antibodies, they are used to test the hypotheses that the phosphorylation state of Cx36 is modulated by light-adaptation state and also by acute changes in background illumination.

Chapter 3 seeks to establish the exact relationship between the phosphorylation state of Cx36 gap junctions and the coupling state of the networks expressing them. In it we test the hypothesis that dopamine-mediated uncoupling of AII amacrine cells is mediated by increased phosphorylation of Cx36. The experimental data generated argued for rejection of this hypothesis. Therefore, we then test the hypotheses

that dopamine-stimulated uncoupling of AII amacrine cells required PKA activation, and that PKA-mediated uncoupling of AII amacrine cells required activation of a protein phosphatase.

Chapter 4 explores the signaling mechanisms responsible for increasing the coupling of AII amacrine cells. Based on observations of the expression pattern of NMDA receptors on AIIs, we test the hypotheses that NMDA receptor activation mediates increased phosphorylation of Cx36, and that such increases in phosphorylation are mediated by Ca^{2+} influx and activation of CamKII. Additionally, we test whether influx of Ca^{2+} through NMDA receptors is amplified by Ca^{2+}-induced Ca^{2+}-release, and whether increased phosphorylation is mediated by activation of ON-bipolar cells either pharmacologically or by light increments.

Chapter 2

Phosphorylation of connexin 35 at regulatory sites is modulated by light-adaptation state and acute light increments

The quoted material in this chapter was previously published as:

"Connexin 35/36 is phosphorylated at regulatory sites in the retina"

in

Visual Neuroscience (2007), **24**, 363-375.

Figures 1-5 in this chapter represent experiments performed by my adviser, John

O'Brien, Ph.D. (Figures 1-4), or by a former postdoc in our lab, Xiaofan Li, Ph.D.

(Figure 5). Their careful work to develop and biochemically characterize the phospho-

specific antibodies against Cx35/36 laid the foundation for my experiments in the rest of

this chapter, and indeed for the rest of my experiments in this thesis. For this I am

indebted to them.

"

Introduction

Gap junctions form a key component of retinal neural circuitry, and are present in every major class of retinal neuron (Cook and Becker, 1995). The identity of several connexins that form retinal gap junctions has been elucidated in the last decade. Connexin 35/36 (O'Brien *et al.*, 1996; Condorelli *et al.*, 1998; O'Brien *et al.*, 1998) was the first neuron-specific connexin identified. It has been found in a large number of neurons in the retina and central nervous system. In the retina this connexin is associated with AII amacrine cell gap junctions (Feigenspan et al., 2001b; Mills et al., 2001a), cone photoreceptor gap junctions (Feigenspan et al., 2004b; O'Brien et al., 2004), and rod photoreceptor gap junctions in some species (Zhang and Wu, 2004). It is also apparent that a large number of other neurons use this connexin (O'Brien *et al.*, 2004). Disruption of the Cx36 gene in mice results in deficits in visual transmission through the rod pathway (Guldenagel *et al.*, 2001; Deans *et al.*, 2002), consistent with disruption of AII amacrine-cone ON bipolar cell and rod-cone gap junctions. Cx36-null mice also showed impaired firing synchrony in the neocortex (Deans *et al.*, 2001) and gamma-frequency oscillations in the hippocampus (Hormuzdi *et al.*, 2001), as well as anomalous patterns of sharp-wave bursts and ripple oscillations in the hippocampus (Maier *et al.*, 2002; Pais *et al.*, 2002).

Electrical coupling forms functional networks within which signals are shared, and can have many consequences. For example, gap junctions between photoreceptors spread responses through adjacent terminals, improving the

signal:noise ratio under many conditions (Schwartz, 1975a; Lamb and Simon, 1976), and expanding the voltage range through which a synaptic response is possible (Attwell *et al.*, 1987). Rod-cone gap junctions also provide a pathway through which high-sensitivity rod signals may enter the cone pathways and chromatic or high frequency cone signals may enter the rod pathway (Schwartz, 1975b; Wu and Yang, 1988; Krizaj et al., 1998).

During visual adaptation the extent of coupling between cells is modulated, which has significant effects on the sensitivity and resolution of the retina. Light adaptation has profound effects on receptive field size and tracer coupling in cone-driven horizontal cells (Baldridge and Ball, 1991; Lankheet et al., 1993; Bloomfield et al., 1995) and AII amacrine cells (Bloomfield *et al.*, 1997). Smaller but still significant changes are observed in some photoreceptors. Cone-cone coupling increases with light adaptation in the turtle (Copenhagen and Green, 1987), as does rod-cone coupling in salamander (Yang and Wu, 1989). These changes influence the functional efficacy of the output synapse (Smith *et al.*, 1986) as well as rod input into the cone system.

The effect of light on photoreceptors is partially mimicked by dopamine D2/D4-like receptor activation (Krizaj *et al.*, 1998), which results in reduction of adenylyl cyclase activity and cytoplasmic cAMP concentration (Cohen *et al.*, 1992; Nir *et al.*, 2002). In other retinal networks, the opposite effect is mediated by dopamine D1-type receptors. This effect results from elevation of cytoplasmic cAMP and is mediated by cAMP-dependent protein

kinase (PKA). It uncouples gap junctions in horizontal cells (Lasater, 1987; DeVries and Schwartz, 1989) and AII amacrine cells (Hampson *et al.*, 1992).

The effect of PKA activity on coupling in AII amacrine cells has been duplicated with Cx35 stably expressed in a mammalian cell line (Ouyang *et al.*, 2005). Activation of PKA causes uncoupling while PKA inhibition causes an increase in coupling. Uncoupling requires phosphorylation at two sites on Cx35, Ser110 in the intracellular loop and Ser276 in the carboxyl terminal tail. These same two sites are also the target of phosphorylation by cGMP-dependent protein kinase (PKG) *in vitro*, suggesting that several signaling pathways may converge on these regulatory residues (Patel *et al.*, 2006). We reasoned that the phosphorylation state of Ser110 and Ser276 should be indicative of the degree of coupling possible through Cx35 gap junctions. In this study we made antibodies against the two regulatory phosphorylation sites of Cx35 and examined whether these sites are phosphorylated in the retina. A previous study has suggested that Cx36 is not phosphorylated in bovine retina (Sitaramayya *et al.*, 2003). However, our study finds that it is phosphorylated in both fish and mammalian retina, and that phosphorylation state varies with lighting conditions.

Methods

Sequence analysis

DNA sequences obtained from GenBank were analyzed with GeneTool software (Biotools, Inc., Edmonton, AB) and translated to amino acid sequences. Amino acid sequences were analyzed with PepTool software

(Biotools) to identify consensus phosphorylation sequences. Some sequence alignments were performed with Clustal W (Thompson *et al.*, 1994).

Development of phospho-specific antibodies

Phosphorylated synthetic peptides corresponding to the two major regulatory PKA phosphorylation sites of perch Cx35 (Ouyang *et al.*, 2005) were made at the M.D. Anderson Cancer Center Synthetic Antigen Laboratory. The sequence of the phosphorylated Ser110 peptide was CKERRYS(PO$_4$)TVYLT and the sequence of the phosphorylated Ser276 peptide was CARRKS(PO$_4$)IYEIRN. The corresponding non-phosphorylated peptides were also synthesized. The phosphorylated peptides were crosslinked to *Limulus* hemocyanin (Sigma Chemical Co., St. Louis, MO) via the cysteine thiol group using N-[ε-Maleimidocaproyloxy] succinimide ester (EMCS; Pierce Chemical Co., Rockford, IL). Hemocyanin at 10 mg/ml in 83 mM NaH$_2$PO$_4$, 0.9 M NaCl, 10 mM EDTA, pH 7.2 was derivatized by incubation with 1.5 mg/ml EMCS for 2 hours at 4 ºC, and desalted over Biogel P-10 resin (Bio-Rad Laboratories, Hercules, CA). For each reaction, 4.8 mg of phospho-peptide was added as dry solid to approximately 6 mg of derivatized hemocyanin and incubated 4 hrs at 4°C. Crosslinking efficiencies were approximately 50% for phospho-Ser110 peptide and 30% for phospho-Ser276 peptide, as determined by the concentration of free thiol measured by derivatization with dithionitrobenzoic acid (DTNB; Sigma) and measurement of absorbance at 412 nm. The hemocyanin-linked peptides were dialyzed for 20 hrs against PBS (137 mM NaCl, 2.7 mM KCl, 10

21

mM Na$_2$HPO$_4$, 1.5 mM KH$_2$PO$_4$, pH 7.4), sterile filtered, and sent to Spring

Valley Laboratories (Sykesville, MD) for development of antisera in rabbits.

Bleeds were screened for cross-reactivity with phosphorylated and non-

phosphorylated Cx35 by western blot against *in vitro* phosphorylated Cx35

intracellular loop or carboxyl terminal domain fusion proteins (see below for

methods).

Bleeds showing significant reactivity against phosphorylated Cx35

were affinity purified. To prepare affinity columns, approximately 3 mg of the

phosphorylated and non-phosphorylated peptides were coupled to Sulfolink

columns (Pierce) according to the manufacturer's instructions. Linking

efficiencies ranged from 80% for non-phospho-Ser110 to 95% for phospho-

Ser276. Antibodies were affinity purified by a modification of the method of

(Tsang and Wilkins, 1991). 25-50 ml of serum were diluted with an equal volume

of PBS and the following additions were made: 1% phosphatase inhibitor cocktail

(Sigma), 4 μg/ml aprotinin, 4 μg/ml leupeptin, 10 mM benzamidine, 10 mM NaF,

and 0.15% Igepal CA-630. The diluted sera were passed over the phosphopeptide

columns twice, and the columns washed with 100 ml BBS (1 M NaCl, 100 mM

boric acid, 20 mM Na borate, 0.1% Tween-20), followed by 6 ml HBS (25 mM

Hepes, pH 7.4, 0.25 M NaCl, 0.01% NaN$_3$). The columns were then eluted with

15 ml EtMg (3 M MgCl$_2$, 25% ethylene glycol, 75 mM Hepes, pH 7.2), followed

by 6 ml 0.1 M acetic acid, 0.1 M NaCl, 25% ethylene glycol. The acid eluate was

immediately neutralized by addition of 1 M Tris base until the pH was >7. The

eluates were combined and dialyzed for 20 hr against PBS plus 0.05% NaN_3 and 0.05% Igepal CA-630.

Dialyzed, affinity-purified antibodies were passed over the corresponding non-phosphopeptide columns twice and the flow-through fractions were concentrated using Centriprep centrifugal filtration devices (Millipore, Billerica, MA). Antibodies that bound to the non-phosphopeptide columns were washed, eluted, dialyzed, and concentrated as before to obtain "pan-specific" antibody fractions.

In vitro phosphorylation

GST fusion proteins containing the cytoplasmic intracellular loop and carboxyl terminal domains of perch Cx35 (Burr *et al.*, 2005; Ouyang *et al.*, 2005) were expressed in *E. coli* strain BL21 and purified by binding to glutathione sepharose 4B (Amersham, Piscataway, NJ). Fusion proteins (0.5 to 1 µg protein per reaction) were incubated with 0.5 units cAMP-dependent protein kinase (PKA) catalytic subunit (mouse α isoform; New England Biolabs, Beverly, MA) for 90 min. at 37°C. The final solution contained 50 mM Tris-Cl (pH 7.5), 10 mM $MgCl_2$, 300 µM ATP, 27 mM NaCl, 0.5 mM KCl, 2 mM Na_2HPO_4, 0.3 mM KH_2PO_4, and 10% glycerol. The incubation mixtures were dissolved in an equal volume of 2x SDS sample buffer, electrophoresed in varying amounts, and blotted to nitrocellulose membranes for screening antisera and affinity-purified antibodies.

Retinal membrane preparations

Hybrid striped bass (*Morone saxatilis/M. americana*) were obtained from the Texas A&M University Department of Wildlife and Fisheries Sciences and were maintained in circulating tanks in the laboratory on a 12hr light:12hr dark cycle. Fish were taken either 2 hr prior to the onset of light (dark-adapted) or 2 hr after the onset of light (light-adapted), anesthetized with 0.3% 2-aminobenzoic acid methyl ester (Sigma), and sacrificed. Retinas were dissected out and homogenized by sonication in ice-cold 0.32 M sucrose, 10 mM Tris-Cl, pH 7.2, 2 mM EGTA, 5 mM $MgCl_2$, 1 μM okadaic acid, 1% protease inhibitor cocktail (Sigma). For dark eyes, procedures were performed under dim red safelight illumination through the homogenization steps. The suspension was centrifuged for 5 min at 1000 x g to remove large particulates, and then the supernatant was centrifuged for 1 hr at 100,000 x g to pellet membranes. The membrane pellet was resuspended in the homogenization medium without protease or phosphatase inhibitors. Protein concentration was measured by the BCA technique (Pierce).

Daytime, light-adapted rabbit eyes were obtained from Dr. Michael Mauk (University of Texas Medical School at Houston) from animals sacrificed for other experiments. Retinas were dissected out and membrane preparations made as for hybrid bass. Daytime, light-adapted mouse eyes were obtained from Dr. Steven Wang (University of Texas Medical School at Houston) from animals sacrificed for other experiments. Membrane preparations were prepared in a similar manner except that high-speed centrifugation was performed in a

Beckman airfuge for 30 min at approximately 100,000 x g. All procedures performed on animals were approved by the institutional animal care and use committee.

For each membrane preparation, a portion of the preparation was digested with bacterial alkaline phosphatase. The membrane preparations were diluted to 2 mg protein/ml with alkaline phosphatase assay buffer (final buffer composition 10 mM Tris-Cl, 10 mM $MgCl_2$, 0.5% Igepal CA-630, plus 15-28% of the membrane homogenization buffer), and digested with 17-25 units alkaline phosphatase (Fermentas, Hanover, MD) per mg protein for 30 min at 37°C plus an additional 2 hr at 50°C. The samples were then diluted to 1 mg protein/ml with 2x SDS sample buffer. Comparable non-digested samples were prepared at the same concentration with alkaline phosphatase buffer but no enzyme.

Western blot

Samples of *in vitro* phosphorylated fusion proteins or retinal membrane preparations were resolved on SDS-PAGE minigels by standard procedures. Proteins were transferred to nitrocellulose (for *in vitro* phosphorylated proteins) or PVDF (for retinal membrane preparations) membranes electrophoretically. For screening crude antisera, portions of the blots were incubated with dilutions of crude serum ranging from 1:500 to 1:50,000 in TBST (137 mM NaCl, 3 mM KCl, 25 mM Tris-Cl, pH 7.4, 0.1% Tween-20). Signals were developed with Cy3-conjugated secondary antibodies (Jackson Immunoresearch, West Valley, PA) and viewed with a Typhoon imager (GE

Healthcare Bio-Sciences, Piscataway, NJ). For retinal membrane preparations,

blots were incubated with affinity purified phospho-specific antibodies diluted to

1 µg/ml in high-salt TBST (500 mM NaCl, 3 mM KCl, 25 mM Tris-Cl, pH 7.4,

0.1% Tween-20) plus 2% nonfat dry milk. Blots were also probed with a

monoclonal anti-Cx35/36 antibody (Chemicon, Temecula, CA) that was

developed against the perch Cx35 intracellular loop (O'Brien *et al.*, 2004) at 1

µg/ml in the same solution. Blots were developed with peroxidase-linked

secondary antibodies (Pierce) and detected by chemiluminescence using x-ray

film.

Immunoprecipitation

Daytime, light-adapted bass retinal membrane preparations (240 µg

total protein) were diluted to 400 µl in modified PBST (137 mM NaCl, 3 mM

KCl, 10 mM Na_2HPO_4, 2 mM KH_2PO_4, 2 mM EDTA, 1% Triton X-100, 0.5% Na

deoxycholate, pH 7.4) with 1% protease inhibitor cocktail (Sigma) and incubated

with 1 µg mouse anti-Cx36 antibody (Zymed Laboratories, San Francisco, CA) at

4ºC for 4 hr. The protein-antibody mixture was further incubated with 20 µl of

50% slurry of protein G-agarose resin (Amersham) at 4ºC for 1 hr. This mixture

was centrifuged for 5 min at 1000 x g and the pellet was washed three times with

0.5 ml modified PBST and then resuspended in 2x SDS sample buffer for

electrophoresis. The IP supernatant and a sample of the initial lysate were

acetone precipitated to prepare samples for electrophoresis. Western blot of the

samples was performed as above with this modification: the ReliaBlot kit (Bethyl

Laboratories, Montgomery, TX) was utilized to mask the Ig signal from the immunoprecipitation antibody according to the manufacturer's instruction. Briefly, PVDF membrane with transferred protein samples was blocked in ReliaBlot blocking reagent and then probed with rabbit anti-phospho-S110 antibodies (1.6 μg/ml in Reliablot blocking reagent) overnight at 4°C. The blot was developed with peroxidase-linked secondary antibodies provided in the kit and detected by chemiluminescence using x-ray film.

Immunostaining

Eyecups were prepared from hybrid striped bass either 2 hr before the start of the light-cycle under infrared illumination (dark-adapted) or 2 hr after the start of the light-cycle under normal room lights (light-adapted). The eyecups were incubated in 2000 units/ml hyaluronidase (Sigma) in PBS for 20 min, and then washed twice for 15 min each in PBS. Subsequently all eyecups were fixed for 15 min in fresh 1% *N*-(3-Dimethylaminopropyl)-*N'*-ethylcarbodiimide hydrochloride (Sigma) in fixation buffer (116 mM Tris, 68 mM NaCl, 1.3 mM KCl, 52 mM Na_2HPO_4, 25 mM NaH_2PO_4, 0.9 mM KH_2PO_4, pH 7.5), and then washed three times for 30 min each in PBS. Eyecups were cryoprotected overnight at 4°C in PBS plus 30% sucrose, 0.25% NaN_3, embedded in Tissue-Tek O.C.T. compound (Sakura Finetek, Torrance, CA), and cryosectioned (20 or 40 μm sections). Sections were incubated in PBST (PBS plus 0.5% Triton X-100, 0.1% NaN_3) with 10% normal donkey serum (Jackson) for 5 hours to block nonspecific binding. Sections were then incubated with 2 μg/ml mouse anti-

Cx35/36 (Chemicon) and either rabbit anti-phospho-Ser110 or rabbit anti-phospho-Ser276 (0.8 or 1 μg/ml, respectively) in PBST with 10% normal donkey serum overnight at 4ºC. Sections were washed three times for 10 min each in PBST, and then incubated with Cy3-conjugated donkey anti-mouse IgG (Jackson; 1:250 dilution) and Alexa 488-conjugated donkey anti-rabbit IgG (Molecular Probes, Eugene, OR; 1:250 dilution) for 2.5 hours. Sections were then washed three times for 10 min each in PBST, mounted with Vectashield (Vector Laboratories, Burlingame, CA), and imaged on a Zeiss LSM 510 Meta confocal microscope using 12-bit data acquisition. All specimens were imaged using similar settings to allow comparison of phospho-antibody labeling in different parts of the retina and under different conditions. Images presented are stacks of three confocal slices totaling approximately 1 μm of focal depth. Image processing (Adobe Photoshop; Adobe Systems, San Jose, CA) was limited to applying a uniform threshold (approximately 10%) to all images in all color channels to reduce background haze. One low-power overview image was brightened (figure 6, phospho-Ser276) to make small gap junction plaques visible.

Quantitative Image Analysis

Medium-power, high-resolution images that included the entire inner plexiform layer were collected for quantitative analysis using identical confocal microscope settings. For each condition 3-6 images were collected from each of 3 eyecups which were each from different fish. Images were analyzed with the same settings using SimplePCI software (Compix, Sewickley, PA) to

automatically select regions of interest (ROIs) from the Cx35 plaques, as identified by the mouse anti-Cx35/36 (Chemicon) labeling. Briefly, regions of interest were defined as contiguous pixels with an intensity threshold greater than 20% of the total intensity range, and which covered a minimum area of 16 pixels ($\sim$0.1 μm^2 or larger). Each image was then manually scanned for individual ROIs that included more than one plaque. These were eliminated from the analysis. Mean fluorescence intensity was measured in each channel (monoclonal Cx35 labeling; phospho-Cx35 labeling) for each ROI (hereafter called 'plaques'). The intensity of phospho-Cx35 antibody labeling was then normalized to the intensity of the monoclonal Cx35 antibody labeling for each individual plaque. Cx35 plaques were separated into two subgroups for further analysis based on readily apparent differences between plaques of typical size and "giant plaques" that were distributed symmetrically in two bands in the IPL. Histograms of plaque size were generated in Matlab (The MathWorks, Natick, MA) using 250 pixel ($\sim$1.225 μm^2) bins. A cutoff point (1000 pixels, $\sim$4.9 μm^2) was empirically determined that distinguished the giant plaques apparent upon visual inspection from all other plaques. For each image the mean normalized phospho-Cx35 intensity of each population of plaques ("normal" and "giant") was calculated. Mean values for 3-6 images per eyecup were averaged to yield a grand mean normalized phospho-Cx35 intensity for each population of plaques for each eyecup. Note that each eyecup represents one animal. Unpaired t-tests were performed to compare eyecups across conditions.

Results

Cx35/36 is regulated by phosphorylation at conserved sites

Connexin 35/36 is the most widespread neuronal gap junction protein in the vertebrate central nervous system. A preponderance of evidence from retinal neurons suggests that gap junctional coupling through Cx35/36 can be regulated by environmental conditions such as light exposure and by neurotransmitter signaling pathways. Comparable regulation has been observed directly for Cx35 in cell culture expression systems and has been shown to depend on direct phosphorylation of the connexin (Ouyang *et al.*, 2005; Patel *et al.*, 2006). The outcomes of these studies indicate that two phosphorylation sites are critical for regulation of coupling by the cAMP/PKA pathway, and perhaps the cGMP/PKG pathway as well. Figure 1A shows these two sites, Ser110 in the intracellular loop and Ser276 in the C-terminal domain (Ser276 in teleost, amphibian, and avian Cx35 is equivalent to Ser293 of mammalian Cx36 and Ser273 of skate Cx35), and a putative model of regulation by PKA (adapted from (Ouyang et al., 2005). In this model, phosphorylation at both Ser110 and Ser276 is required to cause substantial uncoupling of Cx35 gap junctions; phosphorylation of either residue alone causes only very modest uncoupling (Ouyang *et al.*, 2005). Furthermore, this behavior can be reversed, i.e. phosphorylation can lead to increased coupling, under conditions that alter the interactions at the tip of the C-terminus. The molecular details of this "switch" are unknown.

A

Extracellular

N-terminus   I-loop   C-terminus

P

Intracellular   P

PKA/PKG   +/- switch

— (+)

B   IL Domain

PKA, **PKG**, CamK, S6KII

PKC   PKA, CamK   PKC

```
Perch Cx35   HQSAKQKERRYSIVYLTLDKD-QDSLK--
Newt Cx35    HQSAKQKERRYSIVFLSLDRD-QDSMK--
Chick Cx35   HQSAKQRERRYSIVFLTLERD-QDSMK--
Mouse Cx36   HQSAKQRERRYSIVFLALDRDPAESIGGP
             ******:*******:*:*::*  :*:
             101        110,111      122
```

CT Domain

PKA, PKG

PKA, **PKG**, CamK, CKII   **PKA**, CamK, S6KII

```
Pe   RGVQARRKSIYEIRNKDLPRMSVPNFGRTQSSDSAYV
Nt   RGVQAKRKSIYEIRNKDLPRMNVPNFGRTQSSDSAYV
Ch   RGVQAKRKSIYEIRNKDLPRMSMPNFGRTQSSDSAYV
Ms   RGAQAKRKSVYEIRNKDLPRVSVPNFGRTQSSDSAYV
     **.**:***:********** .:*************
         276           289        298
```

Figure 1. Regulation of Cx35 by phosphorylation.
A. Phosphorylation of Cx35 at two sites, Ser110 (on the intracellular loop) and
Ser276 (on the carboxyl terminus), cause reductions in coupling through Cx35
gap junctions. Phosphorylation at both sites has a nearly 3-fold larger effect than
phosphorylation at either site alone. This regulation can be reversed by altering as
yet unknown interactions with the end of the C-terminal domain. Model adapted
from (Ouyang et al., 2005). *B*. Alignments of the Cx35/36 sequences
surrounding the regulatory phosphorylation sites from diverse species. Both
regulatory sites are highly conserved. Cx35/36 contains consensus sequences for
phosphorylation by several protein kinases in these domains (listed above the
phosphorylated residues). Phosphorylation by kinases shown in bold has been
verified experimentally (Ouyang *et al.*, 2005; Patel *et al.*, 2006; Urschel *et al.*,
2006). Amino acid residue numbering is for perch Cx35.

Figure 1B shows an alignment of Cx35/36 sequences from several

species in the regions surrounding these regulatory phosphorylation sites.

Sequence analysis shows that these regions contain consensus phosphorylation

sequences for a number of different protein kinases, listed above the sequences.

Those that have been verified experimentally (all through *in vitro* studies) are

shown in bold. It is apparent that the previously identified regulatory

phosphorylation sites are highly conserved across widely divergent vertebrate

species. Furthermore, these sites are potential targets of several protein kinases,

which in turn represent several different signaling pathways. These include

cAMP-dependent protein kinase (PKA), a terminal effector of the dopamine

signaling pathways, and cGMP-dependent protein kinase (PKG), a terminal

effector of nitric oxide signaling, both of which are important in light adaptation

in the retina.

Conserved regulatory phosphorylation sites are phosphorylated in the retina

The convergence of several different signaling pathways on common

regulatory sites suggests that the phosphorylation status of these sites may be used

to estimate the functional state of the gap junctions. To examine this hypothesis

we developed phospho-specific antibodies against both regulatory sites of Cx35.

We examined the specificity of these antibodies with western blots against

bacterially-expressed GST fusion proteins of either the Cx35 intracellular loop

(IL) domain, containing the Ser110 phosphorylation site, or the carboxyl terminal

(CT) domain, containing the Ser276 phosphorylation site. Figure 2A shows a
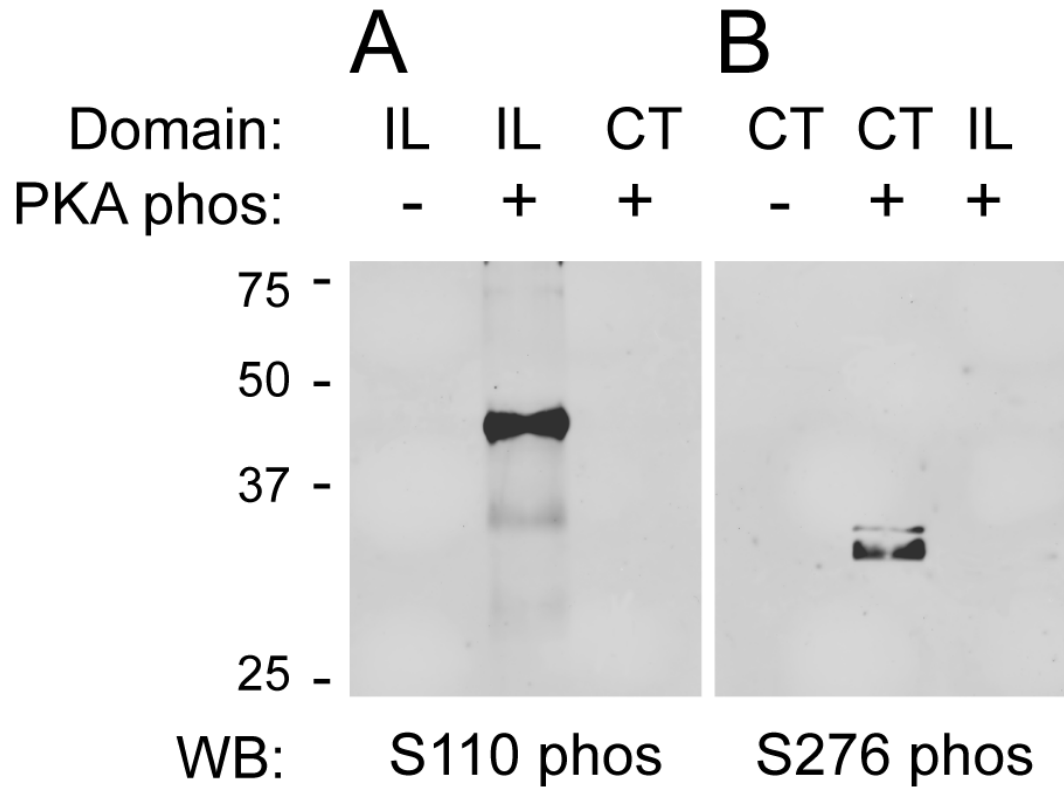
Figure 2. Specificity of the phospho-Cx35 antibodies.
Western blot analysis of GST-fusion proteins phosphorylated *in vitro* with PKA
using two phospho-specific anti-Cx35 antibodies. *A*. The blot was probed with
polyclonal anti-Cx35 phospho-Ser110. The antibody labeled the Cx35
intracellular loop domain (IL) phosphorylated by PKA (middle lane), but not the
non-phosphorylated IL domain (left lane). The IL domain contains the Ser110
site targeted by this antibody. The antibody also failed to recognize the
phosphorylated Cx35 C-terminus (CT; right lane), which contains the Ser276 site.
B. The blot was probed with polyclonal anti-Cx35 phospho-Ser276 antibody.
This antibody labeled the *in vitro* phosphorylated Cx35 CT (middle lane), but did
not label the non-phosphorylated CT (left lane). Phosphorylated Cx35 IL (right
lane) was not labeled. Each lane contains 200 ng GST fusion protein.

western blot with the phosho-Ser110 antibody. This antibody reacted strongly to

the IL domain phosphorylated *in vitro* with PKA, but showed no measurable

reaction to the non-phosphorylated IL domain. Furthermore, this antibody

showed no cross-reaction with the *in vitro* phosphorylated Cx35 CT domain.

Thus the antibody was specific for the phosphorylated form of the protein and did

not cross-react with the other major PKA phosphorylation site. Likewise, figure

2B shows a similar western blot with the phospho-Ser276 antibody. As with the

phospho-Ser110 antibody, this antibody was specific for the phosphorylated form

of the protein and did not cross-react with the Ser110 site.

If phosphorylation of Cx35 is involved in regulation of coupling in

retinal neurons, we would predict that both Ser110 and Ser276 sites would be

phosphorylated to some extent in Cx35 derived from the retina. To test this

prediction we performed western blots on membrane preparations from hybrid

bass retina taken in the dark and light parts of their diurnal cycle. We treated half

of each membrane preparation with alkaline phosphatase (AP) to remove

phosphate groups from the protein. A monoclonal antibody against Cx35 (figure

3, panel A) identified Cx35 as a diffuse band running around 30-32 kDa, in

keeping with previous reports (O'Brien *et al.*, 1998; Pereda *et al.*, 2003; O'Brien *et

al.*, 2004). The phospho-Ser110 antibody (panel B) labeled the same band in

untreated retinal membranes. The labeling was lost in AP digested membranes.

Note that this antibody also labeled several high molecular weight bands in retinal

membranes. That labeling was also lost upon AP digestion, suggesting that these

were phosphorylated proteins with PKA phosphorylation sites similar to that of
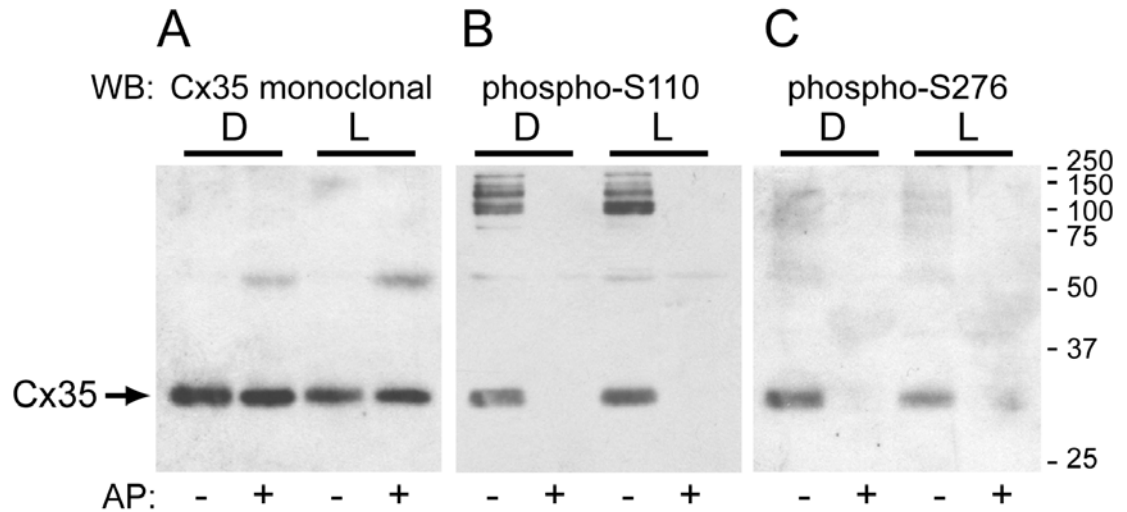
Figure 3. Phospho-Cx35 antibodies recognize Cx35 in hybrid bass retinal membrane preparations.

A. Western blot of membrane preparations from dark-adapted retina (D, left two lanes) and light-adapted retina (L, right two lanes). A monoclonal antibody against Cx35 recognized the appropriate band between 30-32 kDa. Digestion of the membranes with alkaline phosphatase (AP; right lane of each pair) had no effect on this labeling. *B*. Western blot of retinal membranes probed with the phospho-Ser110 antibody. The phospho-Ser110 antibody recognized the same band identified by the monoclonal antibody in preparations from both dark- and light-adapted retinas. Labeling by the phospho-Ser110 antibody was lost in membranes digested with AP. The phospho-Ser110 antibody also recognized high molecular weight bands in the blot, but labeling was lost with AP digestion indicating that these are phospho-proteins. *C*. Western blot of retinal membranes probed with the phospho-Ser276 antibody. The phospho-Ser276 antibody also recognized the Cx35 band in both dark- and light-adapted retinal membranes. Labeling by the phospho-Ser276 antibody was lost in membranes digested with AP. Each lane contains 40 μg retinal membrane protein.

Cx35's Ser110 site. There was little difference in the intensity of phospho-Ser110 labeling on the Cx35 band between dark and light conditions, nor in the total amount of Cx35 between dark and light conditions. The phospho-Ser276 antibody also recognized the Cx35 band in retinal membranes (panel C), and this labeling was lost upon AP digestion. No non-specific bands were detected with this antibody. Again, the difference between dark and light conditions was minimal. These results suggest that Cx35 is indeed phosphorylated in bass retina at both regulatory sites.

The regulatory phosphorylation sites of Cx35 are highly conserved among diverse vertebrate species (e.g. figure 1B), which suggests that regulation by phosphorylation at these two sites is likely also to be conserved. To test whether these sites were phosphorylated in other species we examined retinal membranes from two mammals, mouse and rabbit, for phosphorylation of Cx36 on Ser110 and Ser293 (= Ser276 of teleost Cx35). Figure 4 shows that both phospho-specific antibodies labeled Cx36 in daytime, light-adapted mouse and rabbit retinal membranes. This labeling was destroyed by digestion of the membranes with AP. Although not shown in these blots, labeling of phosphorylated high molecular weight bands in mouse and rabbit retina was again evident with the phospho-Ser110 antibody.

Labeling of phospho-proteins other than Cx35 in western blots using the phospho-Ser110 antibody raises the question of whether this antibody can be used to examine phosphorylation of Cx35 in intact tissues. It is possible that labeling of Cx35 gap junctions by the antibody may represent phosphorylation of
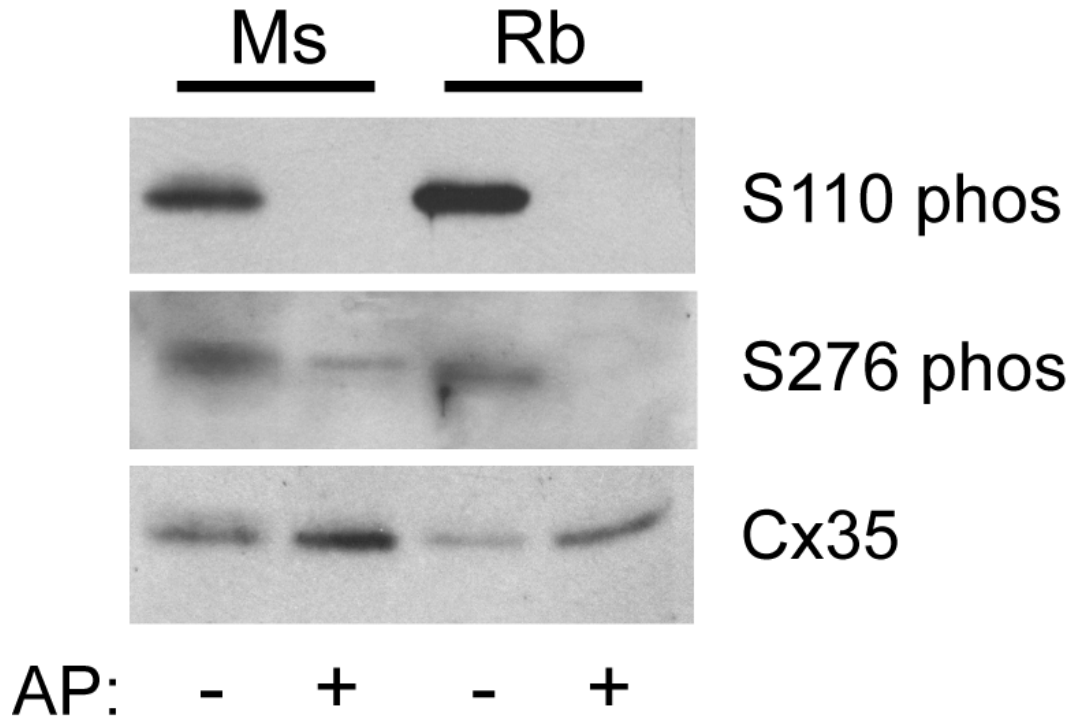
Figure 4. Phospho-Cx35 antibodies recognize Cx36 in mammalian retinal membranes.
Cx36 was labeled by the Cx35 monoclonal antibody (bottom panel) in western blots of membrane preparations from light-adapted mouse (left two lanes) and rabbit (right two lanes) retina. Both the phospho-Ser110 (top panel) antibody and the phospho-Ser276 antibody (middle panel) recognized the same band identified by the monoclonal antibody in both species. This labeling was largely lost in membranes digested with alkaline phosphatase (AP). Each lane contains 40 μg retinal membrane protein.

proteins associated with the Cx35 gap junctions rather than actual phosphorylation of Cx35. To examine this question we performed immunoprecipitation experiments with the monoclonal anti-Cx35 antibody and probed the precipitates with the phospho-Ser110 antibody. Figure 5 shows that the immunoprecipitate containing phosphorylated Cx35 did not contain any of the high molecular weight phospho-proteins found in the original retinal membrane preparation. In contrast, the supernatant from the experiment contained the same complement of high molecular weight phospho-proteins as did the crude membranes. This implies that the phosphorylated proteins recognized by the phospho-Ser110 antibody are not associated with Cx35 in a complex, and thus are not predicted to interfere with analysis of Cx35 gap junctions.

Phosphorylation of Cx35 is controlled at the level of individual gap junctions

We did not see gross changes in Cx35 phosphorylation between dark and light conditions by western blot analysis. However, it is possible that the phosphorylation state, and by inference the coupled state, of Cx35 gap junctions may be regulated at the level of individual gap junctions. To test this hypothesis we examined hybrid bass retina by confocal immunofluorescence techniques using the two phospho-specific Cx35 antibodies. Figure 6 shows the pattern of labeling by the Cx35 phospho-Ser110 antibody (A-C) and the Cx35 phospho-Ser276 antibody (D-F) compared to labeling with a Cx35 monoclonal antibody. Both phospho-Ser110 (A) and phospho-Ser276 (D) antibodies labeled abundant punctate structures in both inner and outer plexiform layers in a pattern similar to
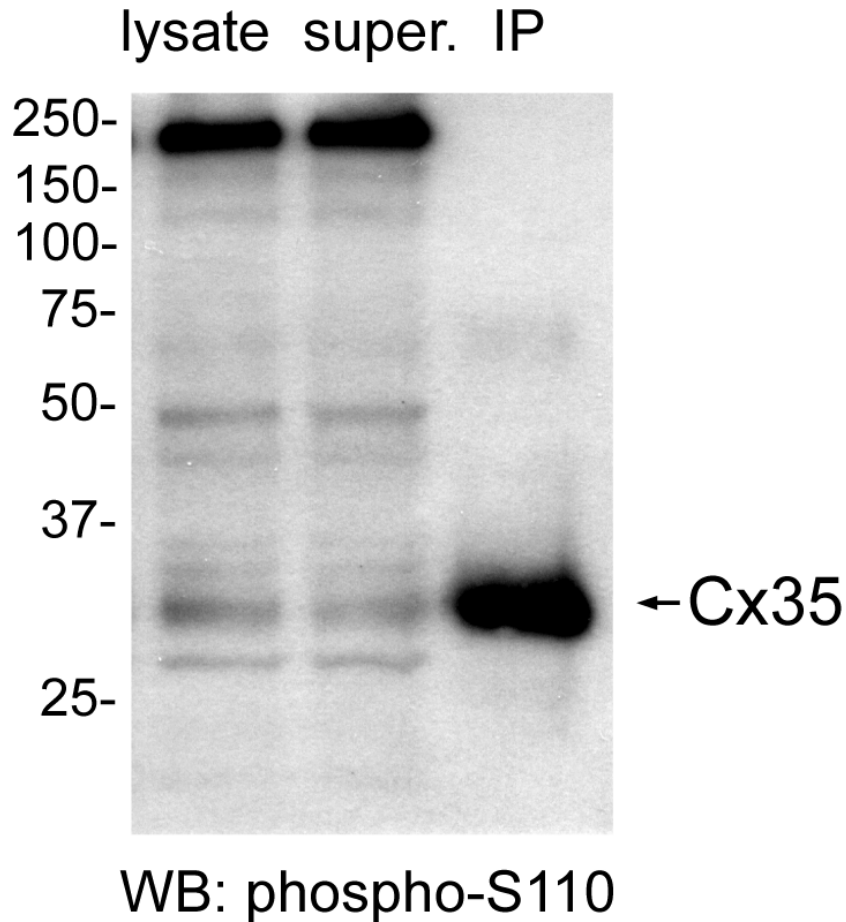
Figure 5. Phospho-proteins non-specifically recognized by the phospho-Ser110 antibody are not associated with Cx35.
Immunoprecipitation of Cx35 from hybrid bass retinal membrane preparations using monoclonal anti-Cx35 and probed with anti-phospho-Ser110. The immunoprecipitate lane (IP) contained phosphorylated Cx35 but none of the high molecular weight phospho-proteins detected in western blots of retinal membranes (lysate lane; see also figure 3B). In contrast, the IP supernatant (super.) contained the same suite of phospho-proteins as found in the lysate. Each lane contains the equivalent of 90 μg retinal membrane protein.

that of Cx35 labeling (B and E). In the merged images it is evident that many

Cx35 plaques were also labeled for phospho-Ser110 (C) or phospho-Ser276 (F).

The phospho-Ser110 antibody also showed strong non-specific labeling of Müller

cells (A and C). This labeling was much less apparent, though present to some

extent, in retina from other species (authors' unpublished observations). The

phospho-Ser276 antibody showed only minor non-specific labeling of blood

vessels in the retina.

Closer examination of the inner plexiform layer revealed that

individual gap junctions labeled with the Cx35 monoclonal antibody (figure 7 B

and C; shown in red) had highly variable labeling for phospho-Ser276 (figure 7 A

and C; green). Some Cx35 plaques showed extensive, bright phospho-Ser276

labeling while others had essentially none (arrow). One readily identifiable group

of Cx35 gap junctions were the extremely large (up to 32 μm^2) plaques distributed

in two bands, one each in sublamina a and sublamina b, that we have previously

reported (O'Brien *et al.*, 2004). The cell type harboring these gap junctions is

unknown, although they fit the description of the large gap junctions between

large-caliber amacrine cell processes identified by (Marc et al., 1988) in TEM

studies of goldfish retina. In nighttime, dark-adapted retina these gap junctions

were highly phosphorylated at Ser276 (figure 7 A and C, triple arrowhead).

However, in daytime, light-adapted retina there was much less immunostaining

for phospho-Ser276 on these gap junctions (figure 7 D and F, triple arrowhead).

At the same time one population of medium-sized Cx35 gap junctions still

showed substantial phosphorylation on the Ser276 site (single arrowheads), while
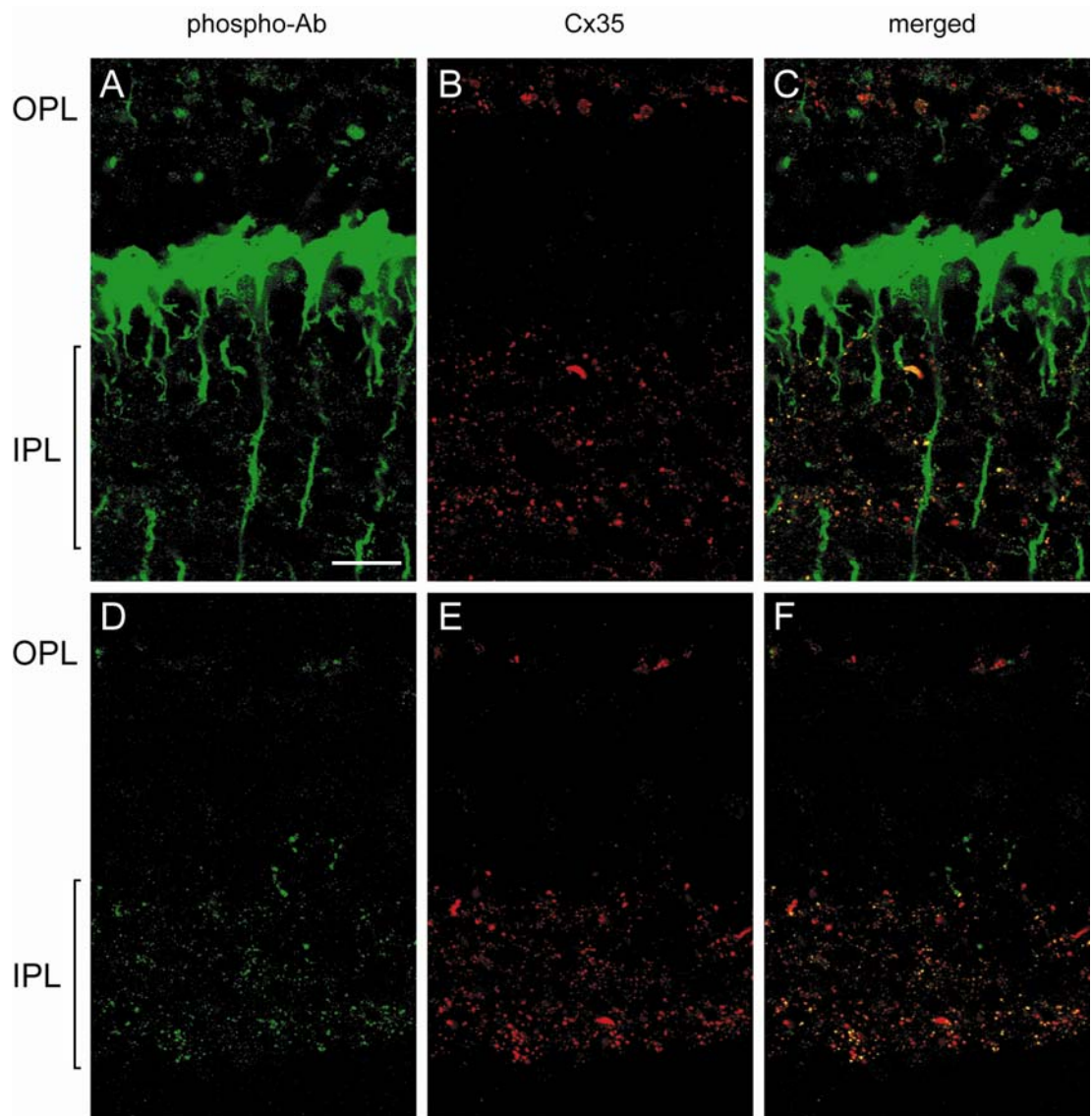
Figure 6. Phospho-Cx35 antibody labeling patterns in hybrid bass retina.
A. Labeling pattern of phospho-Ser110 antibody in light-adapted hybrid bass retina. The phospho-Ser110 antibody labeled abundant punctate structures in the inner and outer plexiform layers (IPL and OPL, respectively). It also strongly labeled Müller cells, as illustrated here by the bright labeling of their somas above the IPL and long trunks descending through the IPL. Scale bar is 20 μm; scale is the same for each image. *B*. Labeling with the monoclonal Cx35 antibody in the same section reveals the distribution of Cx35 in the OPL and IPL. *C*. Merged image of *A* and *B*. Many of the plaques identified as Cx35 by the monoclonal antibody were also labeled by the phospho-Ser110 antibody (co-localization shown in yellow). *D*. Labeling pattern of phospho-Ser276 antibody in light-adapted hybrid bass retina. The phospho-Ser276 antibody also labeled abundant punctate structures in the IPL and OPL. Minor non-specific labeling resembled blood vessels in the retina. *D*. Cx35 monoclonal antibody staining in the same section shows a largely overlapping distribution of signals. *F*. Merged image of

41

D and *E*. Many of the plaques identified as Cx35 by the monoclonal antibody were also labeled by the phospho-Ser276 antibody (co-localization shown in yellow).

again others had none (arrow). We could not determine from these data whether the medium-sized Cx35 gap junctions, some of which were highly phosphorylated and some non-phosphorylated under both dark and light conditions, belonged to the same population or to different ones.

Similar results were observed with the phospho-Ser110 antibody (figure 7 G-L). Again, there was substantially more Ser110 phosphorylation on the giant plaques in dark conditions than in the light. The small to medium sized Cx35 gap junctions showed variable levels of phosphorylation in both light and dark conditions, with some gap junctions showing no phosphorylation (arrow).

To determine if the changes in Cx35 phosphorylation that were observed empirically represent consistent changes we performed quantitative analysis of the phospho-specific antibody labeling on giant Cx35 plaques in the inner plexiform layer. The large size of these giant plaques relative to others in the hybrid bass retina, their typical oblong shape, and their unique distribution were used to segregate them from the total population of plaques for analysis. Figure 8A shows a histogram of the distribution of Cx35 plaques by size in the inner plexiform layer. Plaque abundance decreased steadily with increasing area, and the vast majority of plaques were included in bins containing areas less than 2.5 μm^2. The number of plaques per bin became relatively stable in bins containing areas greater than 4.9 μm^2, and this was chosen as the cutoff point to segregate giant plaques from the total population. Visual inspection of the image data confirmed that all plaques above the cutoff point were of the characteristic size, shape, and distribution described above. Phospho-specific antibody labeling
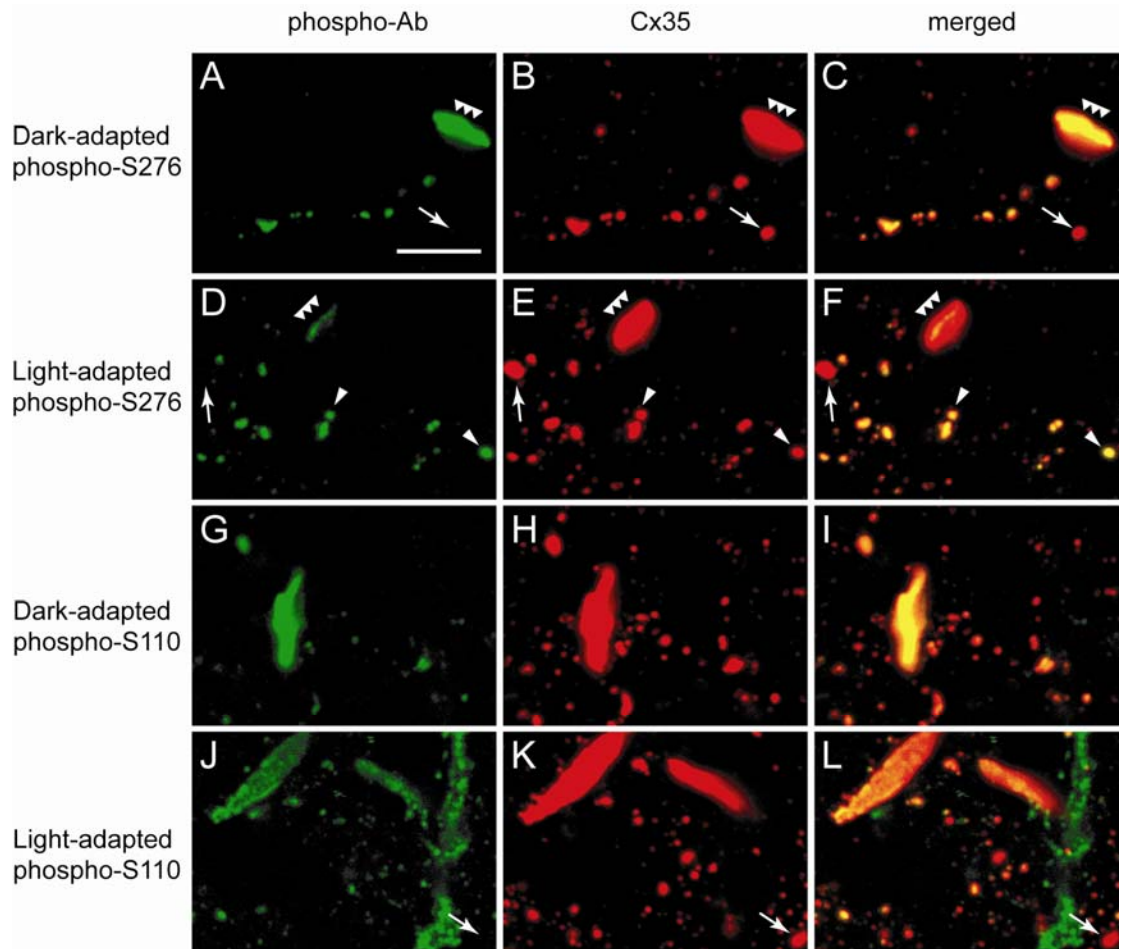
Figure 7. Cx35 phosphorylation varies across gap junction type and with light-adaptation state.
All images are from sublamina b of the inner plexiform layer of hybrid bass retina. *A-C*. Double labeling for phospho-Ser276 (*A*) and monoclonal anti-Cx35 (*B*) in dark-adapted retina. Scale bar is 5 μm; scale is the same for each image. *C*. Merged image of *A* and *B*. Many Cx35 plaques were strongly labeled by the phospho-Ser276 antibody in dark-adapted retina, including the giant plaques described (triple arrowhead), while other plaques were devoid of labeling (arrow). *D-F*. Double labeling for phospho-Ser276 (*D*) and monoclonal anti-Cx35 (*E*) in light-adapted retina. *F*. Merged image of *D* and *E*. Phospho-Ser276 antibody labeling was markedly reduced on Cx35 giant plaques in light-adapted retina (triple arrowhead), and again some plaques showed no labeling at all (arrow). A population of medium-sized plaques continued to show strong labeling in light-adapted retina (single arrowheads). *G-I*. Double labeling for phospho-Ser110 (*G*) and monoclonal anti-Cx35 (*H*) in dark-adapted retina. *I*. Merged image of *G* and *H*. Numerous Cx35 plaques were labeled by the phospho-Ser110 antibody in dark-adapted retina, including strong labeling on the giant plaques. *J-L*. Double labeling for phospho-Ser110 (*J*) and monoclonal anti-Cx35 (*K*) in light-adapted retina. *L*. Merged image of *J* and *K*. Phospho-Ser110 labeling was reduced on Cx35 giant plaques in light-adapted retina. Labeling on other plaques was

44

variable, with most Cx35 gap junctions showing some labeling. However, a few
showed no labeling (arrow). The descending process of a Müller cell non-
specifically labeled by the phospho-Ser110 antibody can be seen on the right side
of the image.

normalized to the monoclonal Cx35 antibody labeling was calculated for each plaque in 3-6 images per animal (see methods). Figure 8B shows the effect of background illumination on Cx35 phosphorylation at Ser110 and Ser276 (n = 3 animals per condition). Giant plaques (figure 8B, right two pairs) showed significantly less phosphorylation at Ser110 and Ser276 in light-adapted retina (unpaired t-test, $p < 0.05$ for each). The remaining smaller plaques (figure 8B, left two pairs) did not show any significant difference in phosphorylation at either Ser110 or Ser276 between dark- and light-adapted retinas.

In the outer plexiform layer, where Cx35 is present in both cone and bipolar cell gap junctions (O'Brien *et al.*, 2004), the phospho-Ser276 antibody labeled several morphologically distinct populations of Cx35 gap junctions (figure 9). Large plaques that varied from round to ellipsoid (arrows), and which may represent bipolar cell gap junctions, showed strong phospho-Ser276 labeling in both dark- and light-adapted retina. Narrow, string-like gap junctions (double arrowheads), which likely represent those found on cone telodendria (O'Brien *et al.*, 2004), were also well-labeled by the phospho-Ser276 antibody in both conditions. Small, round plaques (arrowheads) showed lesser phospho-Ser276 labeling than the other two populations in the dark-adapted retina and almost no labeling in the light-adapted retina.
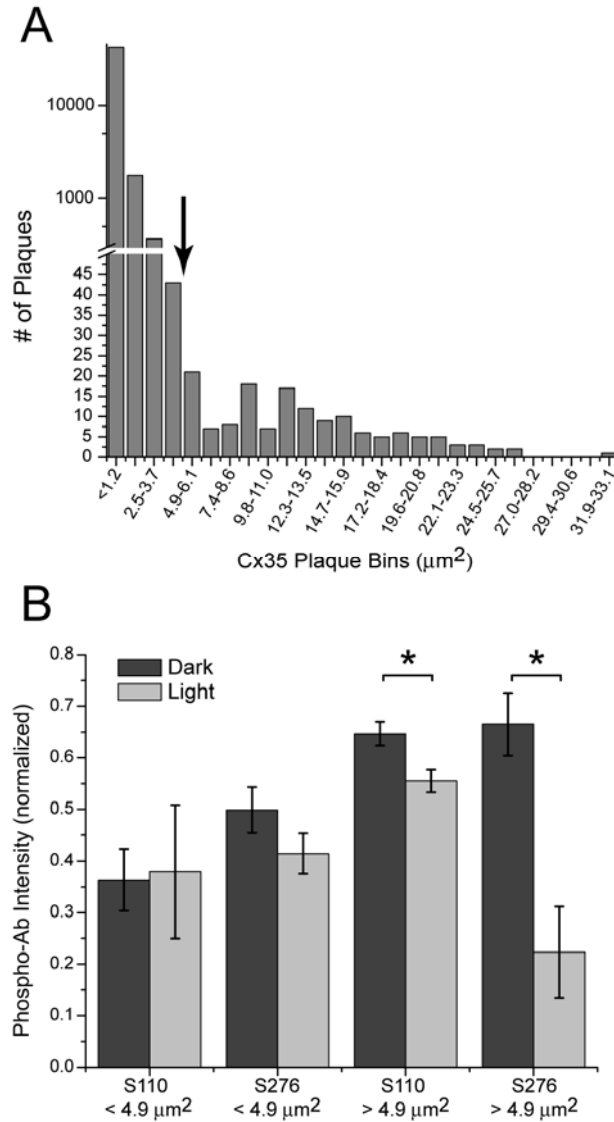
Figure 8. Quantitative analysis of phosphorylation on Cx35 plaques in the inner plexiform layer.
A. Histogram of Cx35 plaque size in the IPL. The arrow indicates the empirically determined cutoff point used to distinguish the giant plaques distributed in two symmetric bands in the IPL from the total population of Cx35 plaques (see methods). Each bin is 250 pixels (~1.225 μm^2). For visual clarity, only every other bin is labeled on the x-axis. Note that scaling on the y-axis switches to logarithmic after the break. Data from six animals are shown (3-6 images per animal). *B*. Effects of background illumination on Cx35 gap junction phosphorylation. Giant plaques (right two pairs) exhibited significantly less phosphorylation at both Ser110 and Ser276 in light-adapted retina than in dark-adapted retina. The remaining smaller plaques (left two pairs) did not show a significant difference in phosphorylation at Ser110 or Ser276 between dark- and light-adapted retina. n = 3 animals per condition. * designates significance at p < 0.05 level.
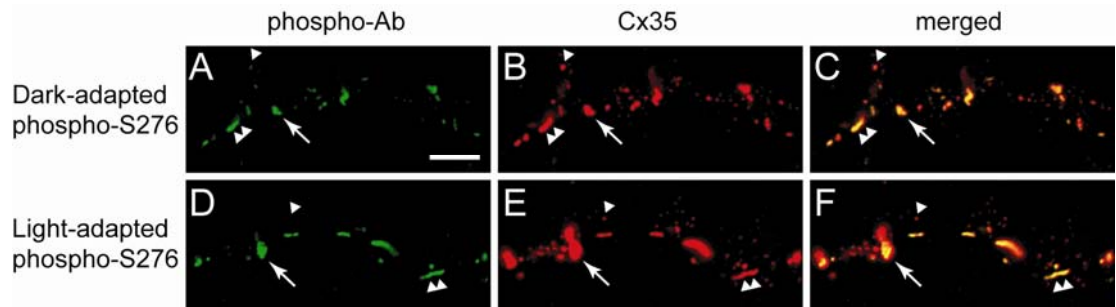
Figure 9. Phosphorylated Cx35 in the outer plexiform layer.
A-C. Double labeling for phospho-Ser276 (*A*) and monoclonal anti-Cx35 (*B*) in dark-adapted OPL. Scale bar is 5 μm; scale is the same for each image. *C*. Merged image of *A* and *B*. Large, round-ellipsoid (arrows) and string-like (double arrowheads) Cx35 plaques were well-labeled by phospho-Ser276 in dark-adapted OPL. Small, round plaques (arrowheads) showed lesser labeling. *D-F*. Double labeling for phospho-Ser276 (*D*) and monoclonal anti-Cx35 (*E*) in light-adapted OPL. *F*. Merged image of *D* and *E*. Phospho-Ser276 antibody labeling on light-adapted OPL was similar to dark-adapted OPL for large, round-ellipsoid (arrows) and string-like (double arrowheads) Cx35 plaques, while small round plaques (arrowheads) showed almost no labeling.

"

Zebrafish are rapidly emerging as a prominent model system for studies of the retina and of disease (Fadool and Dowling, 2007; Lieschke and Currie, 2007). The phospho-specific Cx35 antibodies also label Cx35 gap junctions in zebrafish in confocal light microscopy and in immuno-electron microscopy (Li et al., 2009); John Rash, personal communication). Using these tools we found also found light-dependent changes in the phosphorylation of Cx35 plaques in zebrafish. Exposing dark-adapted zebrafish eyecups to 15 minutes of photopic light triggered decreases in the phosphorylation of a subpopulation of large gap junction plaques at both Ser110 and Ser276 (figure 10). Although smaller in absolute size than the very large plaques in hybrid bass, these gap junctions are similar in all aspects to those in hybrid bass: their large size relative to other Cx35 gap junctions, characteristic oblong morphology, and distribution in sublamina 1 and at the border of sublaminae 4 and 5 in the inner plexiform layer (IPL), and are likely to mediate coupling between the same cell type in zebrafish as the giant plaques do in hybrid bass.
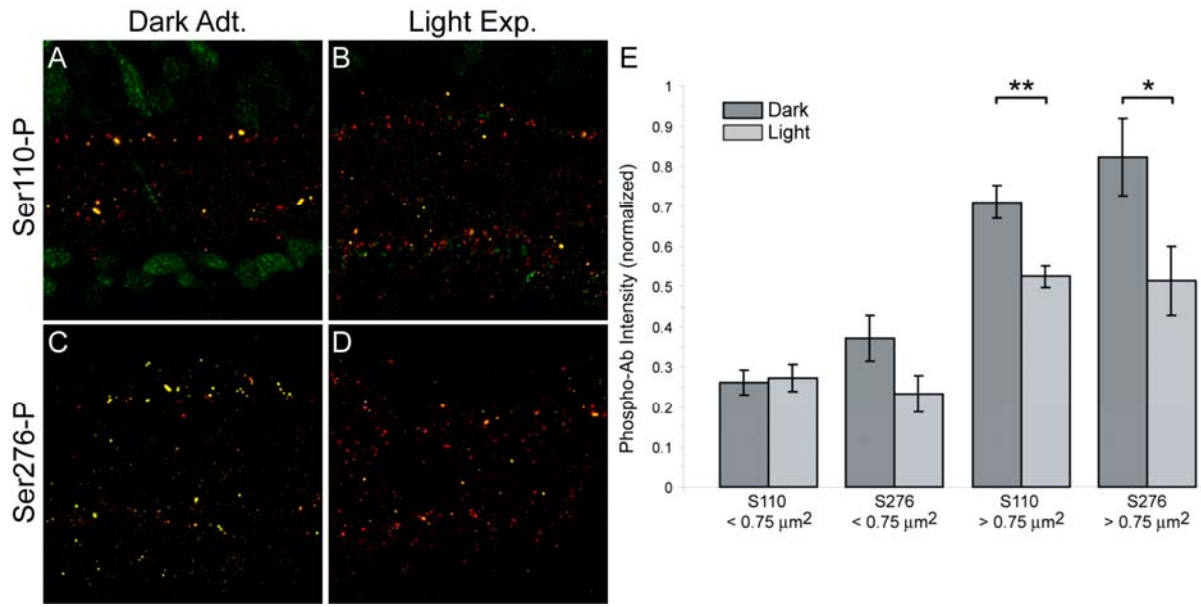
Figure 10. Modulation of Cx35 phosphorylation by acute light exposure in zebrafish retina.
A & C, In dark adapted zebrafish retina, phosphorylation is strong at both Ser110 and Ser276 on the population of largest-sized Cx35 plaques. **B & D,** 15 minutes of photopic light exposure reduced phosphorylation at both Ser110 and Ser276 on the population of largest-sized Cx35 plaques. **E,** Effects of 15 minutes of photopic light exposure on Cx35 gap junction phosphorylation in nightime, dark-adapted zebrafish eyecups. Phosphorylation on the population of largest-sized Cx35 plaques (right two pairs), resembling the "giant" plaques of hybrid bass retina, was significantly reduced at both Ser110 and Ser276 by the exposure to bright light. The remaining smaller plaques (left two pairs) did not show a significant difference in phosphorylation at Ser110 or Ser276 across conditions. The pattern of change in mean phosphorylation in all groups strongly resembles the pattern obtained when comparing dark-adapted and light-adapted hybrid bass retina. n = 5 animals per condition. * designates significance at $p < 0.05$ level, ** designates significance at $p < 0.01$ level.

"

Discussion

The regulation of coupling through Cx35/36 gap junctions by phosphorylation has now been well described. (Mitropoulou and Bruzzone, 2003) found that a consensus PKA recognition sequence in the intracellular loop of perch Cx35 was essential for the 8-Br-cAMP-induced reduction in hemichannel currents observed in *Xenopus* oocytes. They further found that re-creating this recognition sequence in skate Cx35, which was unresponsive to 8-Br-cAMP in its wild-type form in *Xenopus* oocytes, conferred the same behavior to this connexin. This strongly suggested that phosphorylation regulates current flow through Cx35. We subsequently showed that phosphorylation by PKA at Ser110, the target of this PKA recognition sequence, was responsible for reduction of tracer coupling in perch Cx35 expressed in HeLa cells. However, full regulation required concomitant phosphorylation at a second site, Ser276, in addition to Ser110 (Ouyang *et al.*, 2005). Phosphorylation at either site alone caused only a small degree of uncoupling: a 20% reduction in diffusion coefficient in mutants lacking one phosphorylation site compared to a 56% reduction in diffusion coefficient in the wild-type.

PKA phosphorylation at the homologous sites has been confirmed for mouse Cx36 and parallel regulation by PKA phosphorylation has been proposed (Urschel *et al.*, 2006), although direct regulation by phosphorylation was not tested. Nonetheless, the high degree of sequence homology between these connexin gene homologues suggests that the mammalian Cx36 is regulated in the

same fashion as fish Cx35. Our finding that both mouse and rabbit Cx36 were

phosphorylated at both Ser110 and Ser293 (homologous to Ser276 in fish Cx35)

in the retina supports this contention.

It is not yet clear how phosphorylation regulates coupling in Cx35/36

gap junctions. Phosphorylation could have a direct effect on channel properties of

Cx35/36 gap junctions, as has been seen for a number of other connexin channels.

For example, Cx43 channels expressed in SkHep1 cells show a reversible shift

from a 90-100 pS main state to a 60-70 pS subconductance state with activation of

PKC (Moreno *et al.*, 1994; Kwak *et al.*, 1995). These effects are mediated by

phosphorylation of Ser368 by PKC (Lampe *et al.*, 2000). Macroscopic coupling

through Cx45 was also found to be influenced by phosphorylating conditions:

PKC phosphorylation increased conductance, while PKA or tyrosine

phosphorylation decreased conductance (van Veen *et al.*, 2000). However, in this

case subconductance states were not observed to change; changes in the open

probability of the channels were responsible for the changes in macroscopic

conductance. Thus phosphorylation can affect several important characteristics of

gap junction channels that influence functional coupling.

Phosphorylation may also affect assembly or disassembly of gap

junctions. Treatment with phorbol esters increased Cx43 phosphorylation and

inhibited assembly of plasma membrane Cx43 into gap junctions in Novikoff

hepatoma cells (Lampe, 1994). This treatment did not appear to influence

stability of pre-existing gap junctions. In lens fiber cells, Cx50 and Cx46 were

phosphorylated and gap junctions partially disassembled by similar phorbol ester

treatments (Zampighi *et al.*, 2005). Such treatments also resulted in a substantial

decrease in dye coupling, although it is not clear whether the reduction in dye

coupling is a result of gap junction disassembly or changes in channel properties.

Studies of Cx36 have revealed that mutation of the major consensus

phosphorylation sites did not affect trafficking of Cx36 to the plasma membrane

or the formation of gap junctions (Zoidl *et al.*, 2002). The latter suggests that

regulation of Cx35/36 by phosphorylation on the identified regulatory sites is

more likely due to modification of channel properties than of gap junction

assembly.

The requirement for phosphorylation of two separate sites to regulate

Cx35/36-mediated coupling imparts significant flexibility. First, these two

phosphorylation sites have substantially different sequences that may have

different affinities for PKA or the phosphatases that de-phosphorylate them. One

of the sites, Ser276, is also known to overlap with a calmodulin binding site (Burr

et al., 2005). Hence the sites can be considered independent. Second, the two

identified regulatory phosphorylation sites appear to be targets for a number of

signaling pathways in addition to the cAMP/PKA pathway. We have found that

PKG also phosphorylates both of these sites *in vitro* (Patel *et al.*, 2006). These

sites are also consensus phosphorylation sequences for Casein Kinase II, Ca^{2+}-

Calmodulin-dependent kinases, and S6 Kinase II (summarized in figure 1; see

also (Sohl et al., 1998; Urschel et al., 2006). Not all of these kinases are predicted

to phosphorylate both sites, which emphasizes that the sites are not equivalent. It

is possible to construct a number of regulatory schemes that rely on two or more

independent signaling pathways to control the coupling through Cx35/36 gap junctions. Two such pathways, the dopamine pathway routed through cAMP and the nitric oxide pathway routed through cGMP, are both important in light adaptation and known to influence gap junction coupling.

One significant prediction of the requirement for phosphorylation at two sites to regulate coupling is that gap junctions in different cell types could be regulated in different ways. Our phosphorylation data provide evidence that this is the case in the fish retina. The giant Cx35 gap junctions in the IPL showed prominent shifts in phosphorylation state at both Ser110 and Ser276 sites between dark-adapted and light-adapted conditions. Our model predicts that the weakly phosphorylated state of these gap junctions in the light would correlate with strong coupling, while the heavily phosphorylated gap junctions in the dark-adapted state would support reduced coupling. However, the changes in phosphorylation state seen in the very large gap junctions were clearly not global. Many medium sized Cx35 gap junctions in the vicinity of these large plaques were well phosphorylated under both dark- and light-adapted conditions, and a few were virtually non-phosphorylated under both conditions. Since we could not identify the cell types in which these gap junctions reside, we could not determine if they represent relatively invariant gap junctions or rather a shift in phosphorylation status between light- and dark-adapted states in particular cell populations. In either case, the presence of strongly and weakly phosphorylated gap junctions in close proximity indicates that the phosphorylation state of the gap

54

junction is under local control. This implies that adjacent neural circuits regulate their coupled states independently, even though they use the same connexin.

The abundant Cx35 gap junctions in fish retina belong to many cell types. Although we have found them to be present in cone photoreceptor and Mb1 bipolar cell gap junctions, the majority are likely to be in amacrine cells, as revealed by *in situ* hybridization labeling of many cell types in the proximal inner nuclear layer (O'Brien *et al.*, 2004). Tracer coupling and the ultrastructural presence of gap junctions has been described in several types of amacrine cells in the fish retina (Teranishi et al., 1984; Marc et al., 1988; Hidaka et al., 1993; Teranishi and Negishi, 1994; Hidaka et al., 2005). These gap junctions allow expansion of receptive fields beyond the dendritic spread, spike synchronization, and summation of responses (Hidaka *et al.*, 1993; Hidaka *et al.*, 2005). In mammalian AII amacrine cells, homologous coupling provides for summation of rod signals, in part setting the sensitivity of the rod pathway. Regulation of coupling preserves the fidelity of rod signaling through the broad scotopic operating range (Bloomfield and Volgyi, 2004). Unlike the very well studied mammalian AII amacrine cell, very little has been reported regarding changes in fish amacrine cell receptive fields in response to light adaptation.

The striking change in phosphorylation of Cx35 in the giant gap junctions with light adaptation suggests that the cell type harboring these gap junctions re-configures its receptive field during adaptation. Based upon the previous results reported in cell culture systems (Ouyang *et al.*, 2005), we predict that the decrease in phosphorylation at both Ser110 and Ser276 on giant gap

junctions in light-adapted retina will result in increased coupling, which in turn may influence receptive field size and signaling range in the cell type harboring them. Note that this change in coupling in response to light-adaptation would be opposite to that which is observed in the AII amacrine cell (Bloomfield and Xin, 1997). Dopamine signaling is known to increase in light-adapted retina (Kramer, 1971; Iuvone et al., 1978; Dearry and Burnside, 1986) and to cause uncoupling in the AII amacrine cell via D1-type receptors (Hampson *et al.*, 1992). If dopamine also influences the phosphorylation of the Cx35 giant gap junctions we predict that it would do so via D2/D4-type dopamine receptors, such as those found in photoreceptors (Cohen *et al.*, 1992) and dopaminergic interplexiform cells (Harsanyi and Mangel, 1992) and which cause a decrease in cAMP signaling through a g_i protein. The nitric oxide/cGMP/PKG pathway has also been shown to affect Cx35 phosphorylation, and several other signaling pathways are predicted to (Patel *et al.*, 2006). This raises the possibility that phosphorylation of the giant gap junctions is influenced by transmitters other than dopamine. In the absence of physiological data we cannot at present speculate further about the consequences of decreased phosphorylation on giant Cx35 gap junctions in hybrid bass, but presumably such a change would contribute to optimization of signal processing during light adaptation.

"

The modulation of Cx35 phosphorylation in hybrid bass relative to light adaptation state could be controlled by light-stimulated changes in cell signaling, but

circadian control of phosphorylation cannot be ruled out in these experiments since the dark-adapted and light-adapted eyes were collected at different points in the light cycle. However, the finding that acute light exposure modulates phosphorylation of Cx35 in zebrafish provides evidence that regulation of Cx35 by light is controlled, at least in part, by light-stimulated changes in cell signaling. Circadian control may also exist, though future experiments must be done to determine this.

Previous research in several fish species has identified a cell type that is likely to harbor the large or "giant" Cx35 gap junctions that we found in zebrafish and hybrid bass. In an ultrastructural study of the goldfish retina very large gap junction plaques (similar in size to the large plaques in the hybrid bass IPL) were identified in large-caliber amacrine cell dendrites that stratified in sublayer 1 of the IPL (Marc et al., 1988). The cell containing these very large gap junction plaques was inferred to make homologous gap junctions with neighboring cells and to possess transient ON-OFF light responses based on its similarity to a cell in the retinas of carp and roach fish (Djamgoz et al., 1990; Negishi and Teranishi, 1990; Cook and Becker, 1995). The morphology of this cell type has been documented in several fish species (carp, roach, and Japanese dace); it has a fusiform soma located in the inner nuclear layer (INL) immediately adjacent to the IPL (but is also sometimes reported as being interstitial and located in sublayer 1 of the IPL), is bistratified, and makes gap junctions at tip-tip or tip-shank contacts with neighboring cells of the same type (Wagner and Wagner, 1988; Djamgoz et al., 1989; Hidaka et al., 2005). This cell's gap junctions are organized into very large plaques that pass neurobiotin but do not pass Lucifer yellow (Hidaka et al., 2005), a characteristic of Cx35/36 gap junctions (Hampson et al., 1992). These studies suggest that the cell type

harboring the large or "giant" Cx35 gap junctions is common to all teleost fish species, and likely shows modulation of Cx35 phosphorylation by light in the same direction as we observed in hybrid bass and zebrafish.

"

The diversity of neurotransmitter receptors and signaling pathways in retinal neurons allows for vastly different but finely-tuned responses specific to individual cell types. Cx35 gap junctions are a key component of some neural circuits and have the potential to remodel circuit properties in response to signaling. The convergence of multiple signaling pathways at regulatory phosphorylation sites on Cx35 (see figure 1) implies that the coupling state of Cx35-expressing cells can be controlled with a high degree of precision, and our results suggest that this happens at a very local level in retinal neurons.

"

Our results also highlight the need for readily identifiable retinal neuron networks in future studies of the signaling mechanisms regulating Cx35/36 gap junctions. The large number of inner retinal networks that express this protein threaten to "drown out" signaling effects that preferentially modulate phosphorylation of Cx35/36 in only one or two cell types. In this study we were able to bypass this difficulty due to the unique characteristics of the giant gap junctions. Future studies may have similar success by utilizing genetically-altered mice which express GFP in individual retinal neurons (Siegert et al., 2009) that express Cx36, or by utilizing cells types which can be readily

and diffusely immunolabeled, such as the mammalian AII amacrine cell (Massey and

Mills, 1999). The AII amacrine cell is a particularly promising target for such studies as

it is already known that dopamine signaling modulates the coupling state of the AII

network (Hampson et al., 1992).

Chapter 3

Dopamine-stimulated dephosphorylation of connexin 36 mediates AII

amacrine cell uncoupling

The quoted material in this chapter was previously published as:

"Dopamine-stimulated dephosphorylation of connexin 36 mediates AII amacrine cell

uncoupling"

in

The Journal of Neuroscience, November 25, 2009, 29(47):14903-14911.

"

Introduction

Electrical synapses formed by gap junctions between neurons underlie a number of important neural functions, including neuronal synchronization (Deans et al., 2001), signal averaging (DeVries et al., 2002), and network oscillations (Hormuzdi et al., 2001; Buhl et al., 2003), in addition to providing an alternative form of synaptic connection with properties that differ distinctly from the more common chemical synapses. Connexin 36 (Cx36) is the most widely expressed gap junction protein in neurons (Connors, 2009), but little is known about how intercellular coupling mediated by Cx36 is regulated. Loss of Cx36 eliminates electrical coupling and coordinated output in certain cortical interneurons (Deans et al., 2001), impairs gamma frequency oscillations in hippocampus (Hormuzdi et al., 2001; Buhl et al., 2003), causes deficits in cerebellar motor learning (Van Der Giessen et al., 2008), and eliminates the high-gain rod photoreceptor pathway (Guldenagel et al., 2001; Deans et al., 2002; Volgyi et al., 2004). Cx36 is also the dominant connexin in pancreatic beta cells (Serre-Beinier et al., 2008), and loss of these gap junctions causes insulin secretion abnormalities that resemble those observed in type 2 diabetes (Wellershaus et al., 2008). Thus, understanding the regulation of Cx36 channel function is of critical importance to understanding brain and sensory system function as well as endocrine function.

The retina is an ideal tissue for studying regulation of gap junction-mediated coupling; every class of retinal neuron expresses gap junction proteins

(Bloomfield and Volgyi, 2009), and the tissue remains physiologically intact when isolated from the eye. In mammalian retina the AII amacrine cell, which receives input from rod bipolar cells (Strettoi et al., 1990) and is critical for rod-mediated vision (Guldenagel et al., 2001; Deans et al., 2002; Volgyi et al., 2004), is a well-established model for studying Cx36-mediated coupling (Famiglietti and Kolb, 1975; Mills and Massey, 1995; Feigenspan et al., 2001a; Mills et al., 2001b; Veruki and Hartveit, 2002a; Xia and Mills, 2004; Veruki et al., 2008). AII amacrine cells are extensively coupled to each other by Cx36 gap junctions under scotopic background light and are uncoupled in response to photopic background light (Bloomfield et al., 1997; Bloomfield and Volgyi, 2004), dopamine D1-like receptor (D1R) activation (Hampson et al., 1992), and protein kinase A (PKA) activation (Mills and Massey, 1995; Urschel et al., 2006). Studies in cell cultures have identified two phosphorylation sites on the fish homologue of Cx36, Ser110 and Ser276 (Ser293 in mammals), that are required for regulation of Cx36-mediated coupling by PKA (Ouyang et al., 2005). These sites have been shown to undergo dynamic changes in phosphorylation state in the retina (Kothmann et al., 2007). We therefore sought to determine the relationship between Cx36 phosphorylation and regulation of Cx36-mediated coupling by utilizing the well-described AII amacrine cell system.

Methods

Intracellular injection

Care and use of experimental animals was performed in accordance with institutional guidelines at the University of Texas Health Science Center at Houston. All experiments were performed on light-adapted animals in the daytime phase of their light cycle. Adult rabbits were anesthetized with urethane (1.5 g/kg, i.p.), and the eyes removed into Ames medium bubbled with 95% O_2/5% CO_2. Following this, the animals were killed by intracardial injection with an overdose of urethane. The superior portion of the retina was separated into several retina-sclera pieces, which were then incubated with DAPI (4,6-diamino-2-phenylindole; Molecular Probes; Eugene, OR) for 20 minutes to label cell nuclei (this short incubation labels AII amacrine cells preferentially (Mills and Massey, 1991)). Immediately before each piece was to be injected, the retina was isolated and mounted photoreceptor-side down on black nitrocellulose filters. Neurobiotin (3.5%; Vector Laboratories; Burlingame, CA) was injected by iontophoresis (±1 nA, 3 Hz) into AII amacrine cells, as described previously in detail (Xia and Mills, 2004), except that Alexa 488-conjugated biocytin (Molecular Probes) was used to visualize the microelectrode. Injections were performed for 5 minutes on an Olympus BX51WI microscope; this was followed by a 15 minute diffusion period. Each piece was superfused, starting 15 minutes prior to the start of the injection and on through the diffusion period, with either bubbled Ames medium (at 35°C) or Ames medium containing D1R agonist (SKF38393, 10 or 100 μM) or antagonist (SCH23390, 10 or 100 μM). After

tracer injection and diffusion periods, the pieces of retina were fixed for 15 minutes in 4% formaldehyde in 0.1 M phosphate buffer, and subsequently immunolabeled for Cx36 and phospho-Ser293-Cx36 (Kothmann et al., 2007). Dopaminergic drugs were purchased from Tocris (Ellisville, MO).

Pharmacology experiments

Rabbit eyecups with the vitreous removed were separated into superior and inferior portions by chopping along the myelinated band with a razor blade. The central portion of the superior part from a single eye was then further separated into 4 adjacent retina-sclera pieces. Each retina-sclera piece was incubated for 20 minutes in bubbled Ames medium (at 35°C) with the appropriate pharmacologic agent. Thus, each experiment yielded one control piece and three matched pieces subjected to various pharmacological treatments. Following the incubation period, the retina-sclera pieces were fixed for 15 minutes in 4% formaldehyde in 0.1 M phosphate buffer, after which the retina was isolated, mounted photoreceptor-side down on nitrocellulose filters, and immunolabeled for Cx36 and phospho-Ser293-Cx36. The cAMP analogs were purchased from Axxora (San Diego, CA) the microcystin-LR from Calbiochem (San Diego, CA), and the tautomycetin from Tocris.

Immunolabeling

Isolated retina pieces (photoreceptor-side down on nitrocellulose filters) were first blocked overnight at 10°C in immunolabeling buffer (phosphate

buffered saline with 0.5% Triton X-100, 0.1% NaN$_3$, pH 7.4) with 10% normal

donkey serum (Jackson Immunoresearch; West Valley, PA). Pieces were then

labeled with monoclonal mouse anti-Cx36 (mCx36, 1:1,000 dilution; Chemicon;

Temecula, CA) and rabbit anti-phospho-Ser293-Cx36 (Ser293-P, 1:1,000

dilution) (Kothmann et al., 2007) antibodies in immunolabeling buffer with 10%

donkey serum for 5 days at 10°C. Retina pieces from pharmacology experiments

were also labeled with goat anti-calretinin antibodies (1:5,000 dilution;

Chemicon) to label AII amacrine cells. After extensive washing, retina pieces

were labeled with secondary antibodies (1:500 dilutions) in immunolabeling

buffer with 5% donkey serum overnight at 10°C. For retina pieces from injection

experiments, anti-calretinin labeling was replaced with Alexa 488-conjugated

streptavidin (1:250 dilution) to label Neurobiotin in the injected network. Alexa

488-conjugated streptavidin and secondary antibodies were purchased from

Molecular Probes. All other secondary antibodies were Cy3- or Cy5-conjugated

(Jackson). Retina pieces were whole-mounted on slides with Vectashield

(Vector).

Imaging and data quantification

Images were collected on a Zeiss LSM 510 Meta confocal microscope

using a 63x (1.4 N.A.) or 40x (1.3 N.A.) oil immersion objectives. Imaging

settings in the LSM software were identical where comparisons are made.

Coupling between AII amacrine cells was quantified as the diffusion coefficient

for Neurobiotin tracer transfer using a 2-dimensional compartmental diffusion

model (Xia and Mills, 2004). Cx36 phosphorylation was quantified as the ratio of the mean intensity of Ser293-P to mCx36 immunofluorescence at individual regions of interest (ROIs), each identified by the mCx36 label as a single Cx36 gap junction plaque. ROI identification was accomplished using SimplePCI software (Compix; Sewickley, PA) to analyze single optical sections. ROI borders were defined by a 20% intensity threshold in the mCx36 channel and a size threshold of 0.15 μm^2. For the pharmacology experiments, an additional, empirically determined intensity threshold was added in the calretinin channel to include only the Cx36 gap junctions localized on the AII network. In our hands, this represents 96% of the Cx36 gap junctions in stratum 5 of the rabbit inner plexiform layer, in good agreement with a previously reported value of 98% (Mills et al., 2001b). In the case of injected AII networks, single optical sections were collected focused on the distal dendrites of the injected cell, and all gap junctions in the field of view were included. Since 96-98% of the gap junctions at this focus depth in the retina are on AIIs, even when Neurobiotin diffusion was weak there was a very low probability of including Cx36 plaques that were not on AII amacrine cells.

In the pharmacology experiments, six images were collected at mid-peripheral eccentricity from each condition; in the injection experiments, three images were collected on different sides of each injected cell. The ratio of the mean intensity of Ser293-P to mCx36 immunofluorescence was calculated for each ROI and averaged across all ROIs in all images per condition. In this way,

we collapsed the phosphorylation data into one value per condition per animal in order to perform statistical analysis.

In order to calculate the fraction of Cx36 plaques that showed any detectable phospho-Ser293 antibody labeling, regardless of its intensity, we first measured the background labeling in the Ser293-P channel for all images (measured in areas where no mCx36 labeling existed). We then set a threshold for detectable labeling at 200% of the mean background value (this value approximated the mean + 2 s.d. of the background levels observed in the initial experiments). Any Cx36 gap junction plaque with Ser293-P labeling above this threshold was considered "detectably phosphorylated" for purposes of calculating the fraction of plaques showing phosphorylation.

Images presented in the figures were collected using identical settings in the LSM software. Processing was limited to application of a 10% intensity threshold in all channels to minimize background noise.

Statistical analysis

A linear regression was used to find the correlation between relative Cx36 phosphorylation and AII amacrine cell coupling. Unpaired, two-tailed *t*-tests were used to compare each drug-treated condition with the control condition from the same animal. Unpaired, two-tailed *t*-tests were also used to compare two drug-treated conditions that shared one common drug (such as D1R agonist condition vs. D1R agonist plus phosphatase inhibitor).

Results

AII amacrine cell uncoupling is associated with dephosphorylation of Cx36

We combined intracellular injection of the Cx36-permeant tracer

Neurobiotin with immunolabeling for phospho-Ser293-Cx36 in order to measure

AII amacrine cell coupling and Cx36 phosphorylation in isolated rabbit retina. As

previously reported (Hampson et al., 1992), AII-AII coupling was modulated by

dopamine signaling (Fig.1, A-C). Activation of D1Rs (SKF38393, 10 µM)

reduced AII-AII coupling (Fig. 1B), while antagonism of D1Rs (SCH23390, 100

µM) increased coupling (Fig. 1C). Phosphorylation of Cx36 at Ser293 (Ser293-P)

was assessed at gap junctions on the injected AII amacrine cell dendrites and

those nearby (Fig. 1, D-F; see Methods). Ser293-P was decreased by D1R

activation (Fig. 1H) relative to control (Fig. 1G). Consistent with this, D1R

antagonism increased Ser293-P (Fig. 1I). In order to quantify AII amacrine cell

coupling, we used a compartmental diffusion model to estimate the diffusion

coefficient of the Neurobiotin tracer (Xia and Mills, 2004). We quantified

Ser293-P as a ratio of the mean fluorescence intensity of the phospho-Ser293-

Cx36 antibody to the mean fluorescence intensity of a monoclonal Cx36 antibody

at each individual gap junction plaque (for full details see Methods section). We

collected three images focused on the dendrites of each injected AII amacrine

cell, calculated the mean Ser293-P for all Cx36 plaques detected across all three

images, and plotted this against the diffusion coefficient for Neurobiotin tracer

transfer measured for that AII amacrine network (Fig. 1J). A strong correlation

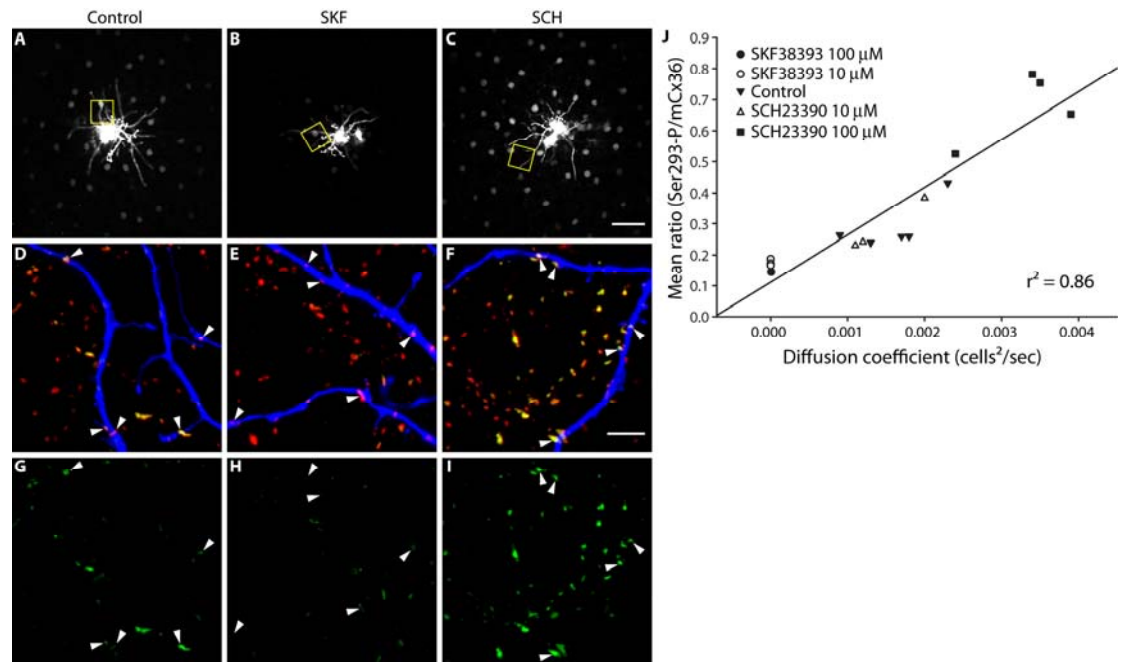($r^2 = 0.86$) was found between AII amacrine cell coupling and Cx36

Figure 1 | AII amacrine cell coupling is directly related to Cx36 phosphorylation at Ser293. A-C, Neurobiotin tracer coupling between AII amacrine cells is modulated by dopamine D1R signaling. D1R activation (**B**, SKF38393, 10 μM) reduced the extent of Neurobiotin diffusion relative to control (**A**). D1R antagonism (**C**, SCH23390, 100 μM) increased tracer diffusion. Images are mini-stacks (2 μm in z-depth) focused on the somas of the AII amacrine cells. Yellow boxes highlight areas shown in **D-I** (at different focal depth). **D-F,** Cx36 gap junctions, labeled with mCx36 antibody (red) and Ser293-P antibody (green), on and around the dendrites of the injected AII amacrine cell, labeled with fluorophore-conjugated Streptavidin (blue). The Cx36 gap junctions not on the injected cell are primarily on other AII amacrine cells (see Methods). Arrowheads identify prominent Cx36 gap junctions on the injected cells. **G-I,** Phosphorylation of Cx36 at Ser293, a site known to regulate coupling through Cx36 gap junctions (Ouyang et al., 2005), is also modulated by dopamine D1R signaling. Arrowheads identify the locations of the same Cx36 gap junctions identified in **D-F**. D1R activation (**H**, SKF38393, 10 μM) reduced Ser293-P labeling relative to control (**G**). D1R antagonism (**I**, SCH23390, 100 μM) increased Ser293-P labeling. **J,** Quantification of the relationship between AII amacrine cell coupling and Cx36 phosphorylation at Ser293. The mean ratio of Ser293-P intensity to mCx36 intensity (across all Cx36 gap junctions in 3 images per injection) is plotted against the diffusion coefficient for Neurobiotin tracer transfer calculated for each injected AII amacrine cell network. The strong correlation of the data ($r^2 = 0.86$) indicates a direct relationship between AII amacrine cell coupling and Cx36 phosphorylation at Ser293. Images are 2 μm-deep stacks. Scale bar in **C** is 50 μm; bar in **F** is 5 μm.

phosphorylation at Ser293. Since Ser293 is known to regulate coupling through

Cx36 gap junctions (Ouyang et al., 2005), this finding leads us to conclude that

phosphorylation at this site increases coupling.

D1R-stimulated dephosphorylation of Cx36 is mediated by PKA

The canonical D1R signaling pathway involves a Gs-protein that

activates adenylyl cyclase, thereby elevating $[cAMP]_i$ to activate PKA (Neve et

al., 2004). We therefore examined the role of PKA activity in controlling Cx36

phosphorylation state downstream of D1R signaling using retina-sclera

preparations (Fig. 2; see Methods). D1R activation (SKF38393, 100 μM) caused

a 3.5-fold reduction in Ser293-P intensity (Fig. 2D). Inhibition of PKA (Rp-8-

CPT-cAMPS, 20 μM) significantly suppressed the effect of D1R activation (Fig.

2F), resulting in intermediate Cx36 phosphorylation that was below control levels

but above the levels seen with D1R activation alone. D1R antagonism

(SCH23390, 100 μM) caused a 2-fold increase in Cx36 phosphorylation (Fig.

2H). As a second measure of the effects of these treatments, we determined if

they altered the fraction of Cx36 plaques that showed detectable Ser293-P

labeling, regardless of fluorescence intensity. Detectable Ser293-P labeling was

defined as 200% of the background fluorescence in that channel (see Methods);

this equated approximately to a 5% threshold in the Ser293-P channel. This

measure yielded results consistent with the mean Ser293-P measurements (Fig.

2J). Histograms of the ratio of Ser293-P to mCx36 fluorescence from one

representative experiment showed that D1R activation caused a leftward-shift
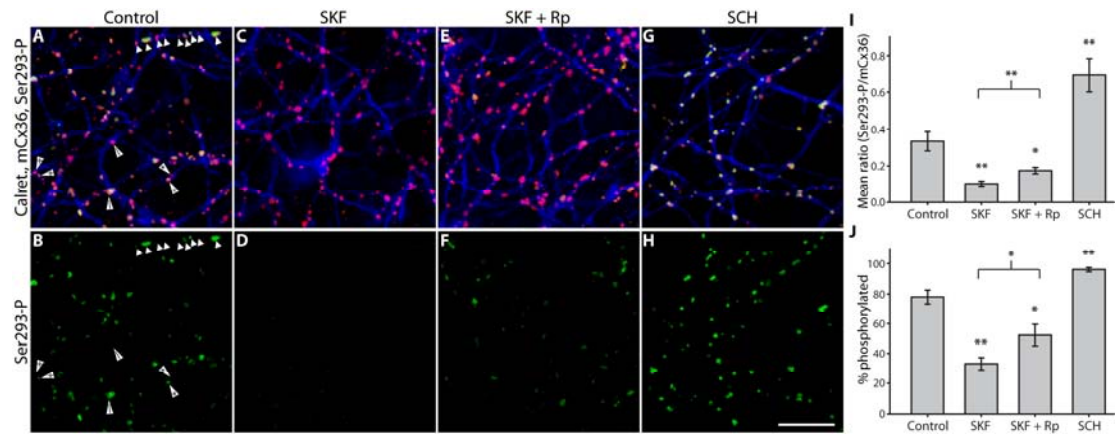
Figure 2 | PKA mediates D1R-dependent dephosphorylation of Cx36 at Ser293 in AII amacrine cells. A & B, Under control conditions Ser293-P (green) labeling of Cx36 gap junctions (mCx36, red) on AII amacrine cells (calretinin, blue) was heterogeneous. Annotated arrowheads indicate pairs of Cx36 plaques along single dendrites that are in different phosphorylation states. The close proximity of Cx36 plaques with widely varying Ser293-P labeling implies that regulation is locally controlled at individual plaques. **C & D,** D1R activation (SKF38393, 100 μM) greatly diminished Ser293-P labeling. **E & F,** Inhibition of PKA (Rp-8-CPT-cAMPS, 20 μM) attenuated the dramatic reduction in Ser293-P labeling caused by SKF38393 (100 μM). **G & H,** Antagonism of D1Rs (SCH23390, 100 μM) increased Ser293-P labeling. **I,** Summary of data shows that inhibition of PKA significantly suppressed the reduction in Ser293 phosphorylation caused by D1R activation. **J,** Summary of data shows that changes in the percentage of Cx36 plaques that show detectable Ser293-P labeling follows the same pattern established for relative Ser293-P measurements in **I**. Error bars are s.e.m, n = 6. Asterisk denotes $P < 0.05$, two asterisks denote $P < 0.01$. Images are 1 μm-deep stacks. Scale bar in **H** is 10 μm.
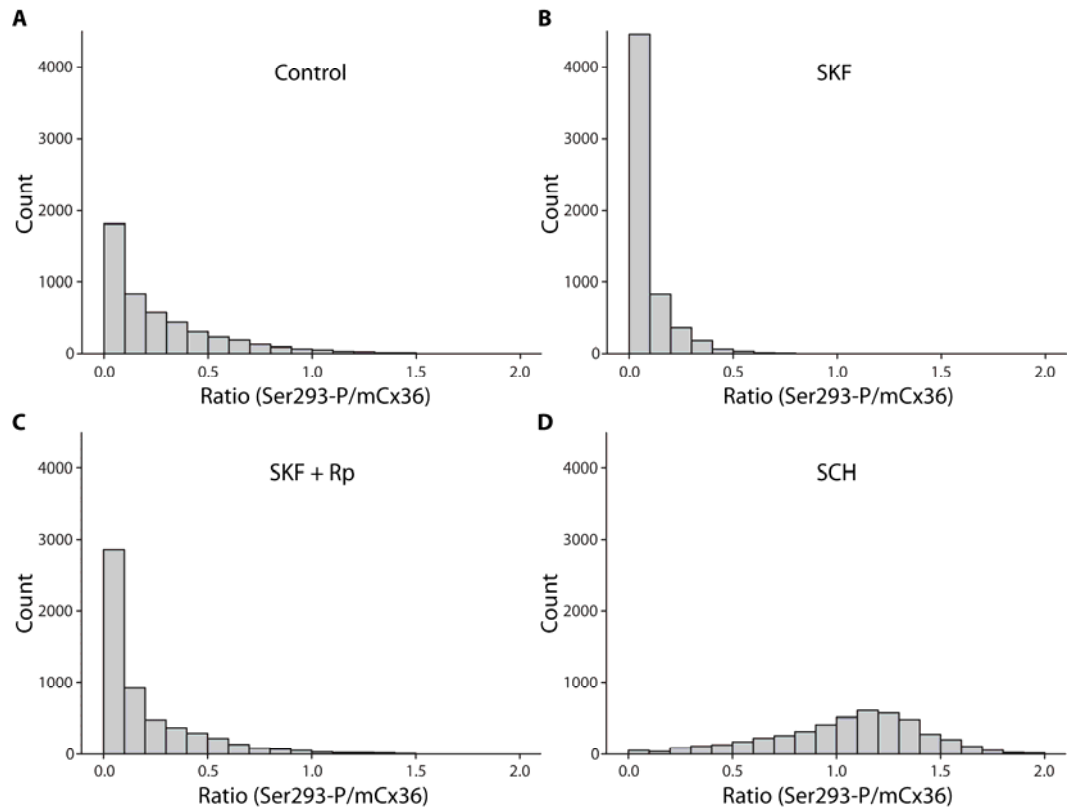
Figure S1 | PKA mediates a D1R-stimulated leftward-shift in the relative phosphorylation of Cx36 at Ser293 in AII amacrine cells. A, Histogram displaying the distribution of relative Ser293 phosphorylation (ratio of Ser293-P to mCx36 intensity) on Cx36 plaques under control conditions. Data are from one representative experiment displayed in Figure 2. **B,** D1R activation (SKF38393, 100 μM) caused a leftward-shift in the distribution. The majority of Cx36 plaques showed relatively little or no Ser293 phosphorylation. **C,** PKA inhibition (Rp-8-CPT-cAMPS, 20 μM) blocked the leftward-shift caused by D1R activation (SKF38393, 100 μM). **D,** D1R antagonism (SCH23390, 100 μM) caused a strong rightward-shift in the distribution. Cx36 plaques located in the center of the distribution (±1 s.d.) showed relatively strong phosphorylation.

(reduction in Ser293-P) in the population of Cx36 plaques which was blocked by inhibition of PKA, while D1R antagonism caused a rightward-shift (increase in Ser293-P) in the Cx36 population (Fig. S1). These results lead us to conclude that activation of PKA is a component of the pathway regulating Cx36-mediated coupling of AII amacrine cells. However, these results are not consistent with direct phosphorylation of Ser293 by PKA, since inhibition of this kinase led to a net increase in Cx36 phosphorylation.

We also tested the effects of dopamine itself on Cx36 phosphorylation at Ser293 in AII amacrine cells. Consistent with the effects of D1R agonist, dopamine application (1 μM) caused a 4-fold reduction in Ser293-P intensity (control, mean ratio 0.41 ± 0.06 s.e.m.; dopamine, mean ratio 0.096 ± 0.02 s.e.m.; n = 4, $p < 0.01$), as well as a similar reduction in the percentage of Cx36 plaques that showed detectable Ser293-P labeling (control, mean $69 \pm 6\%$; dopamine, mean $19 \pm 8\%$; n = 4, $p < 0.01$) (Fig. S2). This concentration of dopamine represents the upper end of estimates of the physiological extracellular dopamine concentration in the vertebrate retina (Witkovsky et al., 1993), and is known to strongly uncouple AII amacrine cells (Hampson et al., 1992; Mills and Massey, 1995). Thus, endogenous levels of dopamine should be sufficient to drive dephosphorylation of Cx36.

Modulation of Cx36 phosphorylation at Ser293 could alter coupling between AII amacrine cells in several ways. It could modulate the permeability of Cx36 gap junctions to the Neurobiotin tracer, stimulate insertion or removal of gap junction proteins from the plasma membrane at each Cx36 plaque, or cause
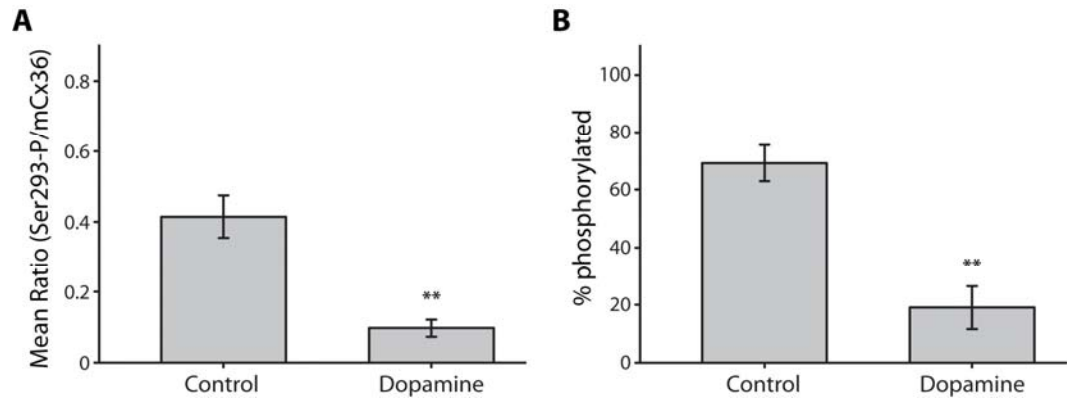
Figure S2 | Exogenous dopamine application causes dephosphorylation of Cx36 at Ser293 in AII amacrine cells. A, Summary of data shows that exogenous application of dopamine (1 μM) caused a strong reduction in the intensity of Ser293-P labeling on Cx36 gap junction plaques. This concentration of dopamine represents the upper end of estimates of the physiologic extracellular dopamine concentration in the vertebrate retina (Witkovsky et al., 1993), and is known to strongly uncouple AII amacrine cells (Hampson et al., 1992; Mills and Massey, 1995). **B,** Summary of data shows that changes in the percentage of Cx36 plaques that show detectable Ser293-P labeling follows the same pattern established for relative Ser293-P measurements in **A**. Error bars are s.e.m, n = 4. Two asterisks denote $P < 0.01$.
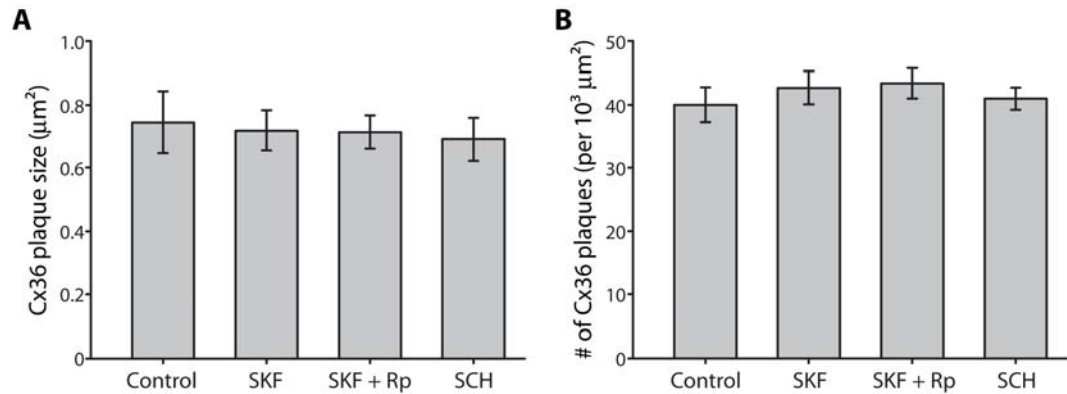
Figure 3 | Phosphorylation of Ser293 on Cx36 does not alter trafficking or distribution of the protein. A, Conditions that altered Cx36 phosphorylation at Ser293 (D1R activation, SKF38393, 100 μM; D1R antagonism, SCH23390, 100 μM) had no effect on the size of Cx36 plaques in AII amacrine cells. Inhibition of PKA (Rp-8-CPT-cAMPS, 20 μM) also had no effect on Cx36 plaque size. **B,** Conditions that altered Cx36 phosphorylation at Ser293 (D1R activation, SKF38393, 100 μM; D1R antagonism, SCH23390, 100 μM) had no effect on the overall distribution of Cx36 plaques in AII amacrine cells. Inhibition of PKA (Rp-8-CPT-cAMPS, 20 μM) also had no effect on Cx36 plaque distribution. Error bars are s.e.m, n = 5. No significant changes were found.

changes in the number of gap junction plaques between AII amacrine cells.

Changes in Ser293-P caused by D1R receptor activation (SKF38393, 100 μM) or

antagonism (SCH23390, 100 μM) had no effect on the mean plaque size of Cx36

gap junctions or the mean number of plaques on AII dendrites in a given area

(Fig. 3). Thus, the changes in tracer coupling between AII amacrine cells

presented above cannot be attributed to changes in the trafficking of Cx36

proteins or the number of Cx36 gap junctions connecting AII amacrine cells.

Rather, it appears that phosphorylation of Ser293 must modulate the permeability

of Cx36 to the Neurobiotin tracer.

PP2A is required for D1R-stimulated dephosphorylation of Cx36

Because D1R activation reduced Ser293-P, we hypothesized that

dopamine signaling increases overall phosphatase activity at Cx36 gap junctions

in AII amacrine cells. In eukaryotic cells protein phosphatase 1 (PP1) and protein

phosphatase 2A (PP2A) are the most abundant phosphatases (Virshup and

Shenolikar, 2009); thus, we initially targeted these proteins as potential effectors

of D1R-stimulated dephosphorylation of Cx36. We tested the ability of D1R

agonist to reduce Ser293-P in the presence of different phosphatase inhibitors at

concentrations that preferentially inhibit either PP1 or PP2A. Microcystin-LR

(0.5 nM), an inhibitor with higher affinity for PP2A (IC_{50} = 40 pM) than for PP1

(IC_{50} = 1.7 nM) (Honkanen et al., 1990), completely blocked the reduction of

Ser293-P caused by D1R activation (SKF38393, 10 μM) (Fig. 4F). Application

of microcystin-LR alone significantly increased Ser293-P levels relative to
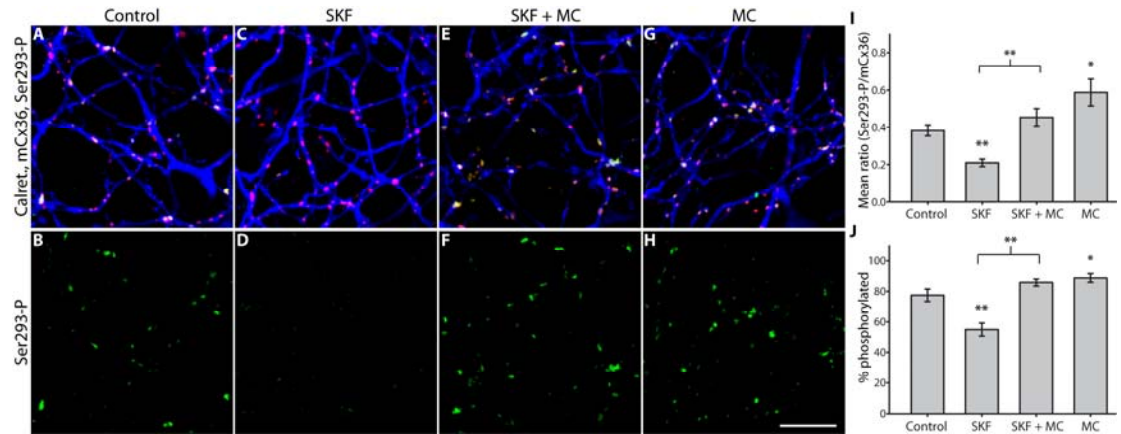
Figure 4 | PP2A is required for D1R-dependent dephosphorylation of Cx36 at Ser293 in AII amacrine cells. **A & B,** Control; color scheme and antibodies are the same as Figure 2. **C & D,** D1R activation (SKF38393, 10 μM) greatly diminished Ser293-P labeling. **E & F,** Inhibition of PP2A (microcystin-LR, 0.5 nM) completely blocked the reduction in Ser293 phosphorylation caused by D1R activation. **G & H,** Inhibition of PP2A alone led to increased phosphorylation of Ser293. **I,** Summary of data shows that inhibition of PP2A significantly blocked the reduction in Ser293 phosphorylation caused by D1R activation, and that PP2A inhibition alone significantly increased Ser293 phosphorylation. **J,** Summary of data shows that changes in the percentage of Cx36 plaques that show detectable Ser293-P labeling follows the same pattern established for relative Ser293-P measurements in **I**. Error bars are s.e.m, n = 6. Asterisk denotes $P < 0.05$, two asterisks denote $P < 0.01$. Images are 1 μm-deep stacks. Scale bar in **H** is 10 μm.

control (Fig. 4H), similar to the effect of D1R antagonist application. Contrasting

these results, tautomycetin (10 nM), an inhibitor with higher affinity for PP1 (IC_{50}

= 1.6 nM) than for PP2A (IC_{50} = 62 nM) (Mitsuhashi et al., 2001), did not prevent

the D1R-mediated reduction of Ser293-P (Fig. 5F). Interestingly, inhibition of

PP1 with tautomycetin in the absence of D1R activation was sufficient to cause a

robust reduction in Ser293-P (Fig. 5H). As shown in the previous experiments,

the percentage of Cx36 plaques showing detectable Ser293-P labeling followed

the same pattern revealed by measuring the mean Ser293-P for both PP2A and

PP1 inhibitors (Fig. 4J and 5J). These results provide a measure of confidence

that the concentrations of microcystin-LR and tautomycetin used were selective

for PP2A and PP1, respectively, as only microcystin-LR was able to block the

effects of D1R activation, and since they had opposite effects on Cx36

phosphorylation when applied alone. Together, these experiments argue that

PP2A is a necessary component of the D1R pathway regulating Cx36

phosphorylation and coupling strength between AII amacrine cells, and these

results are consistent with direct dephosphorylation of Ser293 by PP2A. These

experiments also provide evidence that PP1 is involved in regulating Cx36-

mediated coupling of AII amacrine cells. However, these results are not

consistent with PP1 acting directly on Ser293. Rather, they indicate that PP1

negatively regulates the pathway leading to dephosphorylation of Ser293,

although the exact mechanism for this action is unclear.
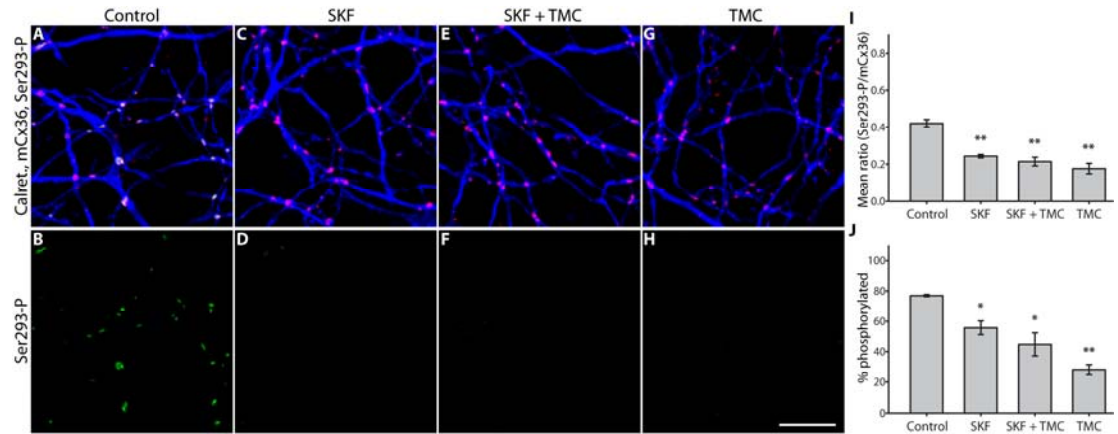
Figure 5 | PP1 negatively regulates the dephosphorylation of Cx36. A & B,
Control; color scheme and antibodies are the same as Figure 2. **C & D,** D1R
activation (SKF38393, 10 μM) greatly diminished Ser293-P labeling. **E & F,**
Inhibition of PP1 (tautomycetin, 10 nM) did not alter the effects of D1R
activation. **G & H,** Inhibition of PP1 alone was sufficient to cause a strong
reduction in Ser293-P labeling. **I,** Summary of data shows that inhibition of PP1
did not prevent the reduction in Ser293 phosphorylation caused by D1R
activation, and that PP1 inhibition alone significantly reduced Ser293
phosphorylation. **J,** Summary of data shows that changes in the percentage of
Cx36 plaques that show detectable Ser293-P labeling follows the same pattern
established for relative Ser293-P measurements in **I**. Error bars are s.e.m, n = 4.
Asterisk denotes *P* < 0.05, two asterisks denote *P* < 0.01. Images are 1 μm-deep
stacks. Scale bar in **H** is 10 μm.

PKA drives PP2A-mediated dephosphorylation of Cx36

Based on the results showing that both PKA and PP2A are downstream of D1R activation, we next asked if PP2A itself is activated by PKA in AII amacrine cells. Such a pathway has recently been described in medium-sized, spiny neurons in the striatum, where D1R-stimulated activation of PKA causes phosphorylation of the regulatory subunit of PP2A and thus increases the activity of the phosphatase (Ahn et al., 2007). These striatal neurons bear certain similarities to AII amacrine cells (namely, D1R and DARPP-32 expression) (Partida et al., 2004; Svenningsson et al., 2004; Witkovsky et al., 2007). In order to test this hypothesis, we bypassed D1Rs and directly stimulated PKA. PKA activation (Sp-8-CPT-cAMPS, 20 μM) strongly reduced mean Ser293-P in AII amacrine cells (Fig. 6D), just as D1R activation did. Inhibition of PP2A (microcystin-LR, 0.5 nM) completely blocked the PKA-mediated reduction in Ser293-P (Fig. 6F). Inhibition of PP2A alone caused a trend toward increased phosphorylation of Ser293-P (Fig. 6I), similar to the to the significant increase noted above (Fig. 4). As before, the percentage of Cx36 plaques showing detectable phospho-antibody labeling followed the same pattern established by measuring the mean Ser293-P intensity (Fig. 6J). These results confirm that PP2A is required for PKA-dependent dephosphorylation of Cx36 in AII amacrine cells, and support the existence of the D1R → PKA → PP2A pathway in these neurons.
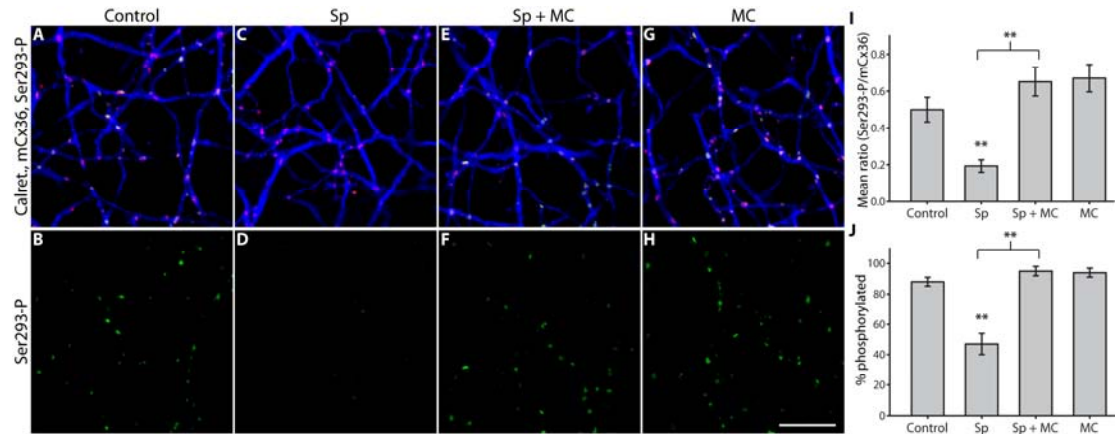
Figure 6 | PP2A is required for PKA-dependent dephosphorylation of Cx36 at Ser293 in AII amacrine cells. A & B, Control; color scheme and antibodies are the same as Figure 2. **C & D,** PKA activation (Sp-8-CPT-cAMPS, 20 μM) greatly diminished Ser293-P labeling, just as D1R activation did. **E & F,** Inhibition of PP2A (microcystin-LR, 0.5 nM) completely blocked the reduction in Ser293 phosphorylation caused by PKA activation. **G & H,** Inhibition of PP2A alone slightly increased Ser293 phosphorylation relative to control. **I,** Summary of data shows that inhibition of PP2A significantly blocked the reduction in Ser293 phosphorylation caused by PKA activation. We observed a trend towards increased Ser293 phosphorylation when PP2A alone was inhibited, similar to the significant increase we observed previously with the same treatment (Fig. 4). **J,** Summary of data shows that changes in the percentage of Cx36 plaques that show detectable Ser293-P labeling follows the same pattern established for relative Ser293-P measurements in **I**. Error bars are s.e.m, n = 5. Two asterisks denote *P* < 0.01. Images are 1 μm-deep stacks. Scale bar in **H** is 10 μm.

Phosphorylation of Cx36 is controlled independently at each gap junction plaque

We frequently observed that Cx36 gap junctions in close proximity of each other existed in very different phosphorylation states, even across gap junctions positioned along a single dendrite. This was most apparent in control conditions (Fig. 2A & B, arrowheads; also Fig. S1 D). Pharmacologic activation of D1Rs reduced the heterogeneity observed in Ser293-P by causing a strong reduction in the relative degree of phosphorylation at each Cx36 plaque. Conversely, antagonism of D1Rs led to an increase in the relative degree of phosphorylation at each Cx36 plaque, indicating that dopamine-driven dephosphorylation of Cx36 is opposed by an unknown process. Thus, it appears that our control condition represents a near-equilibrium point, where conditions at some gap junction plaques favor phosphorylation of Cx36 and conditions at others favor dephosphorylation of Cx36. The observation that this variation exists even for pairs of Cx36 plaques within a micron of one another suggests that each Cx36 gap junction plaque functions as an individual unit, the regulation of which is at least partially controlled by very local processes.

Overall, we have quantitatively demonstrated the relationship between AII amacrine cell uncoupling and Cx36 dephosphorylation. Our results describe a D1R → PKA → PP2A pathway that mediates the dephosphorylation of Cx36 at Ser293, and thus the D1R-mediated uncoupling of AII amacrine cells (Fig. 7). PP1 activity negatively regulates this dephosphorylation pathway at an unknown point. Our results indicate regulation is likely controlled at the level of individual
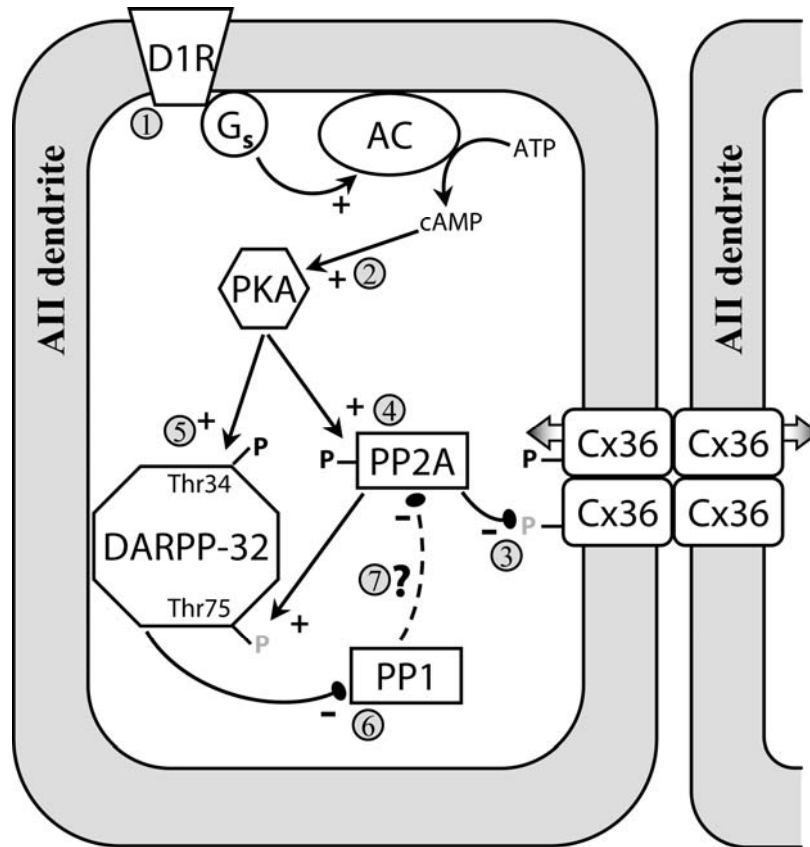
Figure 7 | Model of D1R-dependent regulation of Cx36-mediated coupling between AII amacrine cells. Activation of D1Rs (1) initiates a cascade leading to activation of PKA (2); both D1R and PKA activation are sufficient to uncouple AII amacrine cells (Hampson et al., 1992; Mills and Massey, 1995). In this study we showed that D1R-dependent dephosphorylation (grey P's) of Ser293 on Cx36 uncouples AII amacrine cells (3). We show that PP2A is required for both D1R- and PKA-stimulated dephosphorylation of Ser293 (4). This provides evidence that the D1R → PKA → PP2A pathway, which was recently described in spiny neurons in the striatum and led to dephosphorylation of Thr75 on DARPP-32 (Ahn et al., 2007), is also present in the AII amacrine cell. AII amacrine cells also express DARPP-32 (Partida et al., 2004; Witkovsky et al., 2007), and dephosphorylation of Thr75 on DARPP-32 facilitates PKA-mediated phosphorylation (black P's) of Thr34 (5), which converts DAPRR-32 into an inhibitor of PP1 (6) (Svenningsson et al., 2004). We found that PP1 negatively regulates the dephosphorylation of Cx36, possibly by opposing PKA-mediated activation of PP2A (7). Our results indicate that the D1R → PKA → PP2A pathway is not limited to striatal neurons, and may represent a common pathway in neurons expressing D1Rs and DARPP-32.

Cx36 plaques, and that phosphorylation of Ser293 appears to influence permeability of these gap junctions, but not the trafficking of Cx36.

Discussion

One fundamental function of the retina is to adapt to fluctuating background illumination. Electrical coupling between AII amacrine cells increases the signal to noise ratio of their response to light (Vardi and Smith, 1996; Dunn et al., 2006). Modulation of coupling strength between AII amacrine cells serves to optimize signal to noise ratio for prevailing background illumination, and is one mechanism the retina uses to accomplish luminance adaptation (Bloomfield and Volgyi, 2004). In darkness AIIs are relatively uncoupled, thus preserving single-photon responses in a small group of AIIs. Coupling increases greatly under low scotopic to mesopic illumination, allowing for summation of coincident signals and improved signal to noise ratio. The AII network is uncoupled under photopic illumination by dopamine signaling. This may act to prevent contamination of cone photoreceptor signals in cone bipolar cells by saturated rod signals in AII amacrine cells. In addition, AIIs provide inhibitory glycinergic input to Off cone bipolar cells (Strettoi et al., 1992) and some Off ganglion cells (Manookin et al., 2008; Murphy and Rieke, 2008; Munch et al., 2009). Thus uncoupling of the AII network should also act to increase the spatial resolution of On cone bipolar cell-driven feed-forward inhibition of Off cone bipolar and retinal ganglion cells.

Previously it was unclear what molecular mechanism modulates coupling through Cx36 gap junctions. Although increased phosphorylation of Cx36 has been implicated as a mechanism for uncoupling gap junctions based on the dependence on PKA activity (Ouyang et al., 2005; Urschel et al., 2006), this has not been directly assessed. By making quantitative measures of tracer diffusion between AII amacrine cells and the relative phosphorylation of Cx36 gap junctions between these cells, we have determined that dephosphorylation of Ser293 is associated with uncoupling of the AII amacrine cell network. Decreases in both coupling and phosphorylation are triggered by dopamine D1R signaling and are mediated (at least in part) by activation of PKA. This finding, together with the previous finding that the Ser293 phosphorylation site is one of two that are required for regulation of Cx36 coupling by PKA activity (Ouyang et al., 2005), provides strong evidence that dephosphorylation of Cx36 at Ser293 is the mechanism by which Cx36 gap junctions are uncoupled.

It has been reported that SCH23390 (10 μM) blocks the uncoupling effect of exogenous dopamine (100 nM) application (Hampson et al., 1992). It is thus curious that in our hands 10 μM SCH23390 did not alter AII amacrine cell coupling, but 100 μM SCH23390 increased coupling. However, technical differences between our tracer coupling measurements and those made in the previous study preclude direct comparison. Hampson et al. (1992) used a more sensitive but nonlinear (peroxidise amplification) tracer detection method and 3 to 4-fold longer diffusion periods, potentially amplifying small effects. It is difficult to precisely identify the reason that a high concentration of SCH23390 was

required to increase coupling in our experiments. It is possible that the non-specific binding of the drug to other targets with low-affinity binding sites (Leonard et al., 2006; Ekelund et al., 2007) caused network effects that led to increased AII amacrine cell coupling. However, given that both the D1R agonist SKF38393 (10 μM) and dopamine (1 μM) effectively drove reductions in AII amacrine cell coupling, the specific action of SCH23390 on D1-like dopamine receptors seems most likely.

The molecular mechanism by which phosphorylation of Ser293 alters coupling through Cx36 gap junctions is still a topic for further study. We have excluded changes in the trafficking of Cx36 proteins and reduction in the absolute number of Cx36 gap junctions on AII amacrine cells as potential mechanisms by which dephosphorylation of Cx36 reduces coupling. Thus, it seems likely that dephosphorylation of Cx36 reduces its permeability to the Neurobiotin tracer. The question of what dephosphorylation of Cx36 does to the single-channel conductance and/or open probability or open duration of the channel is of more biological significance in neurons. Although our experiments here cannot directly address this measure of channel function, it has recently been shown that the junctional conductance between pairs of AII amacrine cells can change dynamically up to six-fold (Veruki et al., 2008). This increase was time-dependent and was observed with low-resistance patch pipettes, but not with high-resistance pipettes, leading the authors to suggest that the increase in coupling was due to gradual washout of an endogenous regulatory system in the AII

amacrine cell. Washout of cAMP is the most prominent initial candidate, and should result in a gradual increase in the phosphorylation of Cx36.

Our results indicate that the D1R- and PKA-dependent dephosphorylation of Cx36 in AII amacrine cells requires PP2A activation. A D1R → PKA → PP2A pathway also exists in medium-sized spiny neurons of the striatum, in which Thr75 of dopamine- and cyclic-AMP-regulated phosphoprotein (DARPP-32) is one substrate for PP2A (Ahn et al., 2007). This dephosphorylation allows PKA to phosphorylate Thr34 of DARPP-32, thereby converting it into a potent inhibitor of PP1 (Svenningsson et al., 2004). DARPP-32 is also expressed by AII amacrine cells (Partida et al., 2004; Witkovsky et al., 2007), and we show that while PP1 inhibition does not mediate D1R-stimulated dephosphorylation of Cx36, PP1 inhibition alone is sufficient to cause Ser293 dephosphorylation. As PKA activation of PP2A in the striatal spiny neuron was caused by phosphorylation of the regulatory subunit of PP2A (Ahn et al., 2007), one explanation for our finding is that PP1 activity may oppose PKA-dependent activation of PP2A by phosphorylation (Fig. 7), although we did not explicitly test this hypothesis. It is clear from our results that the dopamine D1R → PKA → PP2A pathway is not limited to the striatal neurons where it was first described, but is also a component of dopamine signaling in other neurons, such as the AII amacrine cell.

In the retina, dopamine signaling originates from dopaminergic amacrine cells and is associated with light adaptation (Witkovsky, 2004). In addition to the AII amacrine cell, dopamine modulates the coupling state of other

Cx36-coupled retinal neurons, such as cone photoreceptors (Lee et al., 2003; O'Brien et al., 2004; Zhang and Wu, 2004; Ribelayga et al., 2008) and OFF α ganglion cells (Hidaka et al., 2002; Mills et al., 2007). In both of these cases, however, activation of D2-like dopamine receptors triggers the uncoupling. This suggests that in cones and OFF α ganglion cells, reduced $[cAMP]_i$ and reduced PKA activity mediate uncoupling. Based on the relationship between Cx36 phosphorylation and AII amacrine coupling strength that we describe here, we would predict that in cones and OFF α ganglion cells PKA acts directly on Cx36 proteins, rather than activating a phosphatase effector, and in cones this appears to be the case (H. Li, A. Chuang, & J.O., 2009; manuscript submitted for publication). Previous reports support this possibility, as we and others have shown that PKA can directly phosphorylate regulatory residues on Cx36 *in vitro* (Ouyang et al., 2005; Urschel et al., 2006; Kothmann et al., 2007). Thus, regulation of Cx36-mediated coupling is specific to individual neuronal subtypes in the retina and is dependent on the signaling pathways they express.

The specificity of regulation that we observe in retinal neurons indicates that the signaling pathways that control coupling are likely to vary in other Cx36-coupled networks, such as those found in cortex, hippocampus, cerebellum and inferior olive, and elsewhere. For instance, several kinases converge onto the regulatory phosphorylation sites of Cx36 *in vitro*, including PKA, PKG, and CamKII (Ouyang et al., 2005; Patel et al., 2006; Urschel et al., 2006; Kothmann et al., 2007; Alev et al., 2008), suggesting that many common signaling pathways can modulate coupling. The importance of regulation of

Cx36-mediated coupling in other networks is currently not well understood, as most studies have focused on the consequences of complete loss of Cx36-mediated coupling (Deans et al., 2001; Buhl et al., 2003; Van Der Giessen et al., 2008). The results we present here provide a framework for future study of coupling in these systems, where increased phosphorylation of Ser293 indicates increased coupling, and vice versa.

We commonly observed heterogeneity of Cx36 phosphorylation within individual AII amacrine cells under control conditions. This observation implies that Cx36 phosphorylation, and thus coupling, is controlled at the level of individual gap junction plaques. This possibility evokes comparisons to the postsynaptic density found at chemical synapses, where complexes of signaling proteins are assembled and provide synapse-specific modulation of important synaptic elements, such as glutamate receptors (Soderling and Derkach, 2000; Feng and Zhang, 2009). The C-terminal tail of Cx36 binds PDZ domain-containing proteins (Li et al., 2004), and may bind some of the same molecules that form the scaffolding complex at the postsynaptic density. Additionally, CamKII can bind directly to Cx36 (Alev et al., 2008), providing the means for localization of one potential regulator of coupling.

Local control of coupling would allow for the possibility of activity-dependent regulation of individual electrical synapses. This is particularly interesting to consider in the case of the AII amacrine cell, which shifts from uncoupled in dark-adapted retina to well-coupled through most of the scotopic range of vision, and which finally becomes uncoupled again under photopic visual

conditions (Bloomfield and Volgyi, 2004) as a result of dopamine signaling. What causes the increase in coupling when background illumination increases from darkness to scotopic levels? One possibility is that glutamate release from rod bipolar cells causes Ca^{++} influx in the AII dendrites, leading to activation of CamKII and phosphorylation of Cx36, thus increasing coupling in a manner dependent on presynaptic activity. There are several potential sources of Ca^{++} on AII dendrites, including Ca^{++}-permeable AMPA receptors and NMDA receptors (Hartveit and Veruki, 1997; Morkve et al., 2002). One possible role for locally increasing coupling in an activity-dependent manner is to allow the spread and summation of signals from active rod bipolar cells in AII amacrine cells when photon catch is very low (near visual threshold). Gap junctions not in the vicinity of an active rod bipolar cell would remain uncoupled, and thus reduce the sharing of noisy fluctuations in the AII membrane potential. This could be particularly important in AIIs, which are inherently noisy due to the nature of the rod bipolar to AII amacrine synaptic inputs (Dunn et al., 2006). As background light intensity increases in the scotopic range, additional rod bipolar cells will become active, and continue to increase AII amacrine cell coupling, as has been described (Bloomfield and Volgyi, 2004).

"

Chapter 4

Presynaptic activity and NMDA receptor activation drive phosphorylation of connexin 36 on AII amacrine cells

Figures 1-3 in this chapter represent experiments performed by Brady Trexler, Ph.D., a former postdoc with Steve Massey, Ph.D. (Figures 1 and 3), or by Wei Li, Ph.D., a former student with Steve Massey, Ph.D. (Figure 2). Their unpublished observations (represented in these figures) stimulated me to develop and test the hypotheses concerning the role of NMDA receptors in regulating Cx36 gap junctions on AII amacrine cells. Thus, I have included them here for logical continuity. I am indebted to them for their contributions to this research.

Introduction

One requirement for a well-functioning sensory system is the ability to adapt to fluctuations in prevailing environmental conditions. For instance, in the course of one day the retina must maintain its ability to reliably encode the visual environment and transmit this code to the brain, despite the fact that the mean level of background luminance will shift over 10^9-fold from night to day (Rodieck, 1998; Rieke and Rudd, 2009). Adaptation serves to maintain appropriate dynamic range of signaling, preventing saturation yet preserving discrimination of relevant differences, thus optimizing sensory system function. A hallmark of luminance adaptation in the retina is modulation of the strength of electrical coupling between horizontal and amacrine cell interneuron networks (Bloomfield et al., 1997; Xin and Bloomfield, 1999; Bloomfield and Volgyi, 2004). Modulation of coupling strength in these networks alters receptive field size, and consequently changes the spatial extent of feedback and feedforward inhibition. In the AII amacrine cell interneuron network, electrical coupling also improves the signal-to-noise ratio of the light response (Vardi and Smith, 1996; Dunn et al., 2006).

The AII amacrine cell is an obligatory component of the high-sensitivity rod photoreceptor pathway (Guldenagel et al., 2001; Deans et al., 2002; Volgyi et al., 2004), and is extensively coupled to neighboring AIIs by connexin 36 (Cx36) gap junctions (Kolb and Famiglietti, 1974; Famiglietti and Kolb, 1975; Vaney, 1991; Feigenspan et al., 2001a; Mills et al., 2001b; Veruki and Hartveit, 2002a). AII amacrine cells display a complex inverted U-shaped pattern of electrical and tracer coupling modulation relative to increasing background illumination (Bloomfield et al., 1997; Bloomfield and Volgyi, 2004). In well dark-adapted retina, the AII network is relatively uncoupled. When

background illumination is increased to just above rod photoreceptor threshold, coupling increases dramatically, and continues to increase modestly with increasing illumination through the rod photoreceptor-dominated range of vision. If background illumination is increased further, into the cone photoreceptor-dominated range of vision, coupling is driven back down towards baseline levels. This reduction of coupling is thought to occur through increased dopamine signaling (Hampson et al., 1992; Witkovsky, 2004). Recent work has demonstrated a direct relationship between the phosphorylation state of Cx36 and tracer coupling in the AII network, and shown that dephosphorylation of the protein mediates the uncoupling caused by dopamine signaling (Kothmann et al., 2009). However, the mechanism responsible for increasing coupling in the AII network in the rod-dominated visual range is still unclear.

The observation that AII amacrine cells increase their coupling once background illumination exceeds rod photoreceptor threshold, and that coupling continues to increase with increasing illumination, suggests an activity-dependent process driven by the ON pathways in retinal circuitry. AII amacrine cells express functional NMDA receptors (Hartveit and Veruki, 1997; Zhou and Dacheux, 2004), which commonly mediate activity-dependent changes in postsynaptic neurons. However, to date no study has described a physiological role for these receptors in the AII. In this study, we sought to determine if the NMDA receptors expressed by AII amacrine cells contribute to processes that increase phosphorylation of Cx36 gap junctions, and thus drive increased coupling in the AII network.

Methods

Electrophysiology

The inferior portions of rabbit eyecups were cut into strips and attached to filter paper, vitreal side down. The sclera and choroid were removed and the retinas were bathed in a modified Ames medium (see below). Retinas were then stored at 10°C for later recording. Slices were cut on a vertical slicer to varying thickness (120 – 200 μm) and transferred to the recording chamber. Experiments measuring light responses were performed on retinas from rabbits that were dark adapted for 2 hrs prior to enucleation; surgery, isolation of the retina, and preparation of slices were done under dim red light.

A modified Ames solution was used for storing retinas, bath perfusion of slices, and puffer application of drugs. The salts common to all external solutions consisted of (in mM) 115 NaCl, 3.1 KCl, 1.24 $MgCl_2$, 2 $CaCl_2$, 0.1 $BaCl_2$, 6 glucose, 2 succinate, 1 malate, and 1 lactate. For the storage solution, 10 mM HEPES, 12 mM $NaHCO_3$, and 1 mM pyruvate were added and pH was adjusted to 7.4 with NaOH. For bath perfusion, 24 mM $NaHCO_3$ and 1 mM pyruvate were added and the solution was bubbled with 95% O_2/5% CO_2. The perfusate was heated to 37°C with an inline heater (Warner Instruments, Hamden, CT). Drugs were diluted from stock solutions into the external solution buffered with 20 mM HEPES, pH = 7.4.

Patch pipette filling solution consisted of (in mM) 110 potassium gluconate, 10 CsCl, 10 NaCl, 10 HEPES, 10 EGTA, 2 $MgCl_2$, 5 K^+ATP, 0.5 Na^+GTP. The pH was adjusted to 7.2 with KOH. Lucifer yellow (0.5 mg/ml) or 0.1 mM Alexa-488 (Molecular Probes, Eugene, OR) were included in the patch solutions to confirm cell identity by epifluorescent visualization after recording. All chemicals and pharmacological agents

were obtained from Sigma-Aldrich (St. Louis, MO) unless otherwise noted. Drug

solutions were delivered by single or triple barrel puffer pipettes. A single barrel would

contain two or more drugs for testing the effects of simultaneous application, rather than

perfusion from multiple barrels.

Patch electrodes were pulled on a Flaming-Brown horizontal puller from

Sutter Instruments (Novato, CA) and fire polished on a Narishige MF-83 microforge

(East Meadow, NY) to a resistance of 7 to 10 MΩ (in KCl pipette solutions, pipette

resistances were 5 to 7 MΩ, due to the higher mobility of chloride relative to gluconate).

Seals in the cell attached configuration ranged from 8 to 20 gigaohms. Upon obtaining a

whole cell patch, series resistance was estimated from the peak of the capacitive

transients due to a square wave voltage pulse and ranged from 20 to 30 MΩ.   Series

resistance was not compensated but was monitored periodically by the method of

capacitive transients. Cell currents and voltages were amplified by Axopatch 200 B

patch clamp amplifiers (Axon Instruments, Foster City, CA) in resistive feedback mode.

Current and voltage signals were filtered on [?] the amplifiers at 2 kHz and sampled at 10

kHz using a PCI-MIO16XE-10 data acquisition board from National Instruments (Austin,

TX). Custom software was used for data acquisition and analysis.

Light Stimuli

Light responses were recorded from slices visualized using infrared

photomicroscopy with DIC optics. Light stimuli were delivered to the slice through the

objective from a source consisting of 20 LEDs (525 nm peak, ±17 nm at half-width). The

LEDs were mounted facing into a plastic sphere, which acted as a diffuser and provided a

uniform field of illumination. The LEDs were driven by digital counter/timers on the data acquisition board, and light intensity was varied by pulse width modulation of a 1 kHz square wave as well as neutral density filters moved into the light path. Maximum output was 5×10^5 photons $\mu m^{-2} s^{-1}$, measured at the focal plane of the slice using an IL-1700 radiometer (International Light, Newburyport, MA) and apertures of 100 or 400 μm (Lenox Laser, Glen Arm, MD)..

Pharmacology experiments

Rabbit retina-sclera preparations were made and pharmacology experiments performed as described in Chapter 3, except as described below. For dark-adapted experiments, the whole superior portion of the eyecup was stored in bubbled Ames at room temperature inside a light-tight chamber for a minimum of 100 minutes. The light-tight chamber consisted of two nested cardboard boxes wrapped in dual layers of aluminum foil. A rubber tube carrying the O_2/CO_2 mix was threaded through a small, hole in the outer box, which was then covered with foil. Secondary silicone tubes fed into the inner box and bubbled the Ames medium. The light-tight chamber was then kept in a dark room for the duration of the adaptation. After the adaptation period, the eyecup was cut into four pieces as described in Chapter 3, except that this was performed under infrared illumination. Once separated, the pieces were incubated with pharmacologic agents in bubbled Ames back inside the light-tight chamber

Immunolabeling

Immunolabeling was performed as described in Chapter 3. Additional antibodies used were rabbit anti-NR1 (1;100 dilution; Chemicon) and mouse monoclonal antibodies against PKCα (1:500 dilution; Transduction Laboratories, Lexington, KY) and kinesin II (1:100 dilution, Convance, Richmond, CA).

Imaging and data quantification

Images presented in Figures 2 and 3 were acquired on a Zeiss LSM-410 confocal microscope with a 63x objective (1.4 N.A.). Alignment for all three channels and resolution were checked at x8 zoom using 1μm fluorescent spheres (Molecular Probes, Eugene, OR). The average distribution of synaptic structures around NMDAR clusters was obtained by clipping sections of the image centered on NMDARs, aligning these frames and signal averaging for all three channels. Results were displayed as surface plots using custom software. This is a method to analyze the average distribution of labeling in the other two channels around a repeated neuronal structure. In this paper, it was used as a method to assess the average distribution of synaptic ribbons, rod bipolar terminals, and Cx36 plaques around NMDAR clusters.

All other confocal images were collected on a Zeiss LSM 510 Meta confocal microscope using a 63x (1.4 N.A.) objective. Imaging settings in the LSM software were identical where comparisons are made. Cx36 phosphorylation was quantified as the ratio of the mean intensity of Ser293-P to mCx36 immunofluorescence at individual regions of interest (ROIs), each identified by the mCx36 label as a single Cx36 gap junction plaque. ROI identification was performed as described in Chapter 3.

Five-six images were collected at mid-peripheral eccentricity from each condition in the pharmacology experiments. The ratio of the mean intensity of Ser293-P to mCx36 immunofluorescence was calculated for each ROI and averaged across all ROIs in all images per condition. In this way, we collapsed the phosphorylation data into one value per condition per animal in order to perform statistical analysis.

Images presented in the figures were collected using identical settings in the LSM software. Processing was limited to application of a 10% intensity threshold in all channels to minimize background noise.

Statistical analysis

Unpaired, two-tailed *t*-tests were used to compare each drug-treated condition with the control condition from the same animal. Unpaired, two-tailed *t*-tests were also used to compare two drug-treated conditions that shared one common drug (such as D1R agonist condition vs. D1R agonist plus phosphatase inhibitor).

Results

NMDA receptors do not contribute to the light response of AII amacrine cells

Much work has been done to characterize the glutamate-driven ionic currents present in AII amacrine cells (Hartveit and Veruki, 1997); (Morkve et al., 2002); (Veruki et al., 2003; Zhou and Dacheux, 2004), but at present it is unclear if the NMDA receptors on these cells play a role in the response to light. We began this study by reproducing the NMDA-mediated currents previously characterized by others (Hartveit and Veruki, 1997; Zhou and Dacheux, 2004). AII amacrine cells were identified for recording in retinal
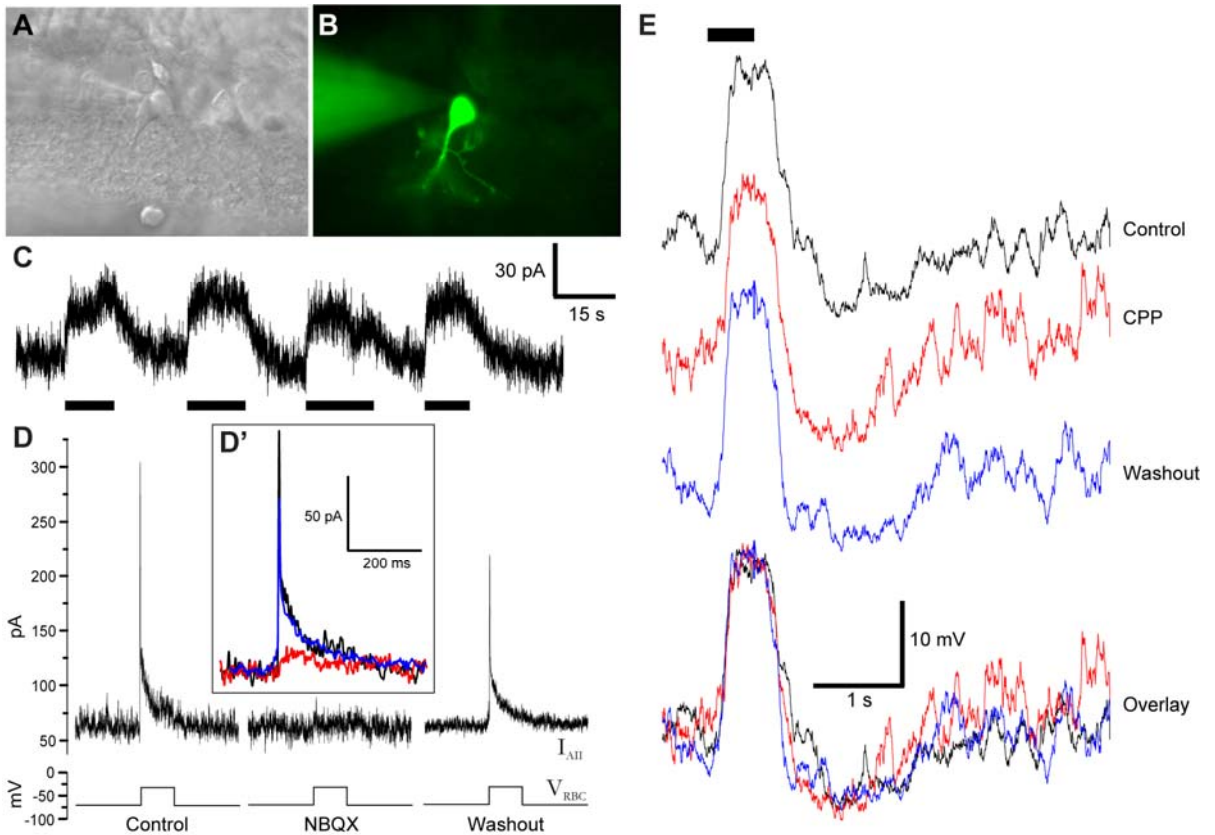
Figure 1 | NMDA currents in AII amacrine cells do not contribute to the light response.

A) Image of an AII amacrine cell targeted for recording under DIC illumination; **B)** Lucifer yellow fluorescence in the cell confirms its identity after recording; **C)** Puffs of NMDA (500 μM, black bars) in the presence of 4 μM Co^{2+}, 1 μM glycine, 2 μM strychnine, and 2 μM TTX elicit an outward current in an AII amacrine held at +60 mV; **D)** Current responses in an AII held at +60 mV in response to depolarization of a presynaptic rod bipolar cell. The outward current elicited was almost entirely blocked by NBQX (20 μM), an AMPA & kainate receptor antagonist. Averaging of 5 recorded pairs (inset **D')** revealed a low amplitude, slow onset current that suggests activation of extrasynaptic NMDA receptors; **E)** A 500 ms dim light flash (1 R* rod^{-1} s^{-1}, black bar) elicited a 20 mV depoloarization followed by a slight hyperpolarization after light off. Application of CPP (20 μM), an NMDA receptor antagonist, did not alter the amplitude or waveform of the light response, indicating that NMDA receptors do not influence light evoked responses in AII amacrine cells.

slices by their distinctive small somas and stout primary dendrites that descend through

the inner plexiform layer (IPL) (Figure 1A). Patch pipettes contained fluorescent dyes

for visualization of the cells after recording. Cell identity was confirmed by the existence

of characteristic lobular appendages in sublaminae 2 and 3 of the IPL in addition to fine

dendritic arbors in sublaminae 4 and 5 (Figure 1B). Puffs of NMDA (500 μM) were

applied to the dendritic arbor via puffer pipette. The Ames medium bath was

supplemented with the coagonist glycine (1 μM), Co^{2+} (4 mM) to block polysynaptic

effects, strychnine (2 μM) to block activation of glycine receptors, and TTX (2 μM) to

block voltage-gated sodium channels on AIIs. At a holding potential of +60 mV AIIs

responded to NMDA puffs with an outward current (Figure 1C). Currents were also

recorded using a ramp protocol that varied the membrane potential of the cell from -60 to

+60 mV in the presence of NMDA. This was repeated with the addition of the NMDA

receptor antagonist CPP (20 μM). Subtraction of the NMDA + CPP current from the

NMDA current alone yielded a J-shaped I-V curve that reversed close to 0 mV

(Supplemental Figure 1), characteristic of NMDA receptors (Dingledine et al., 1999).

These results were consistent across 5 recorded AIIs.

At synapses where AMPA and NMDA receptors colocalize in the

postsynaptic membrane, both receptor types contribute to evoked and spontaneous

EPSCs (Bekkers and Stevens, 1989). Current evidence suggests that spontaneous EPSCs

in AII amacrine cells are mediated solely by AMPA receptors (Veruki et al., 2003),

indicating that NMDA receptors on AIIs may be extrasynaptic. We directly tested

whether evoked glutamate release from rod bipolar cells could activate EPSCs in AII

amacrine cells when AMPA receptors were blocked. To do this we performed dual
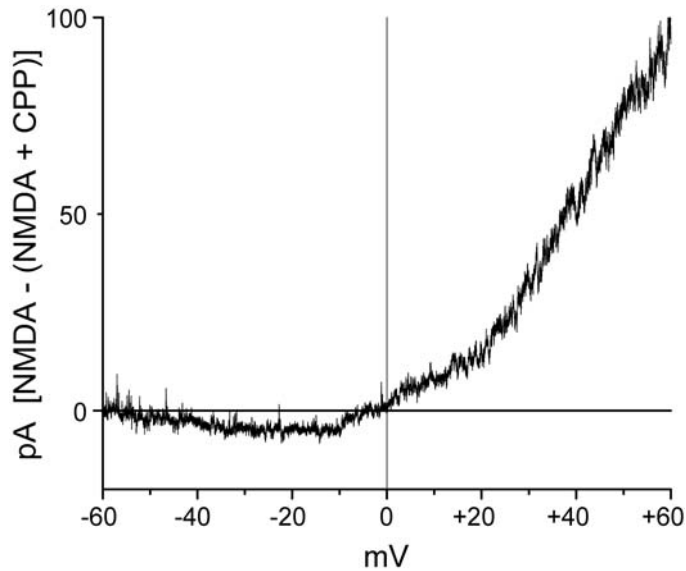
Figure S1 | I-V relationship of NMDA activated conductance on AII amacrine cells.
Shown is an example of the current-voltage relationship of the NMDA activated
conductance (shown in Figure 1). With 4 μM Co^{2+}, 1 μM glycine, 2 μM strychnine and 1
μM TTX in all perfused solutions, the AII was ramped from -60 to +60 mV. Currents
were recorded and averaged in response to 20 voltage ramps. Shown is the difference
current between ramps with NMDA and those with NMDA + CPP, an NMDA receptor
antagonist. Subtraction of the NMDA+CPP current from the current in NMDA alone
yielded a characteristic J-shaped I-V curve that reversed at 0 mV.

whole-cell patch clamp experiments on rod bipolar cell-AII amacrine cell pairs with and without the selective AMPA/Kainate antagonist NBQX in the bath. In order to maximize the possibility of detecting small NMDA-mediated EPSCs, the postsynaptic AII was held at +60 mV to alleviate the Mg^{2+} block of NMDA receptors, and the Ames medium was supplemented as above, with the exception that Co^{2+} was not included. Rod bipolar cells were held at -70 mV and stepped to -30 mV, evoking large, fast inward currents in postsynaptic AIIs (Figure 1D). These were virtually eliminated when NBQX (20 μM) was included in the bath, and recovered upon washout of the drug, as expected if AMPA receptors alone are located at the synapse. Similar results were observed in a total of 5 recorded pairs. However, when the currents from all rod bipolar-AII pairs were averaged, a small, slow inward current was revealed (Figure 1D'). Such low-amplitude, long-latency currents are characteristic of extrasynaptic NMDA receptors (citations). This current cannot be explained by electrical input due to spikes in neighboring AIIs, as TTX (2 μM) was co-applied with NBQX. While it is clear that the majority of rod bipolar cell input to AIIs is mediated by AMPA receptors, this residual current suggests that glutamate released from rod bipolar cells may also bind to putative extrasynaptic NMDA receptors on AII amacrine cells.

We next asked whether the NMDA receptors on AII amacrine cells contribute to the light response of these neurons by flashing dim light on dark adapted retinal slices while recording from AIIs in current clamp. It is known that glutamate spillover occurs at the rod bipolar-AII synapse, as stimulating release of glutamate from one rod bipolar elicits a glutamate transporter-coupled anion current in neighboring rod bipolar cells (Veruki et al., 2006). We therefore sought to activate the majority of rod bipolar cells in
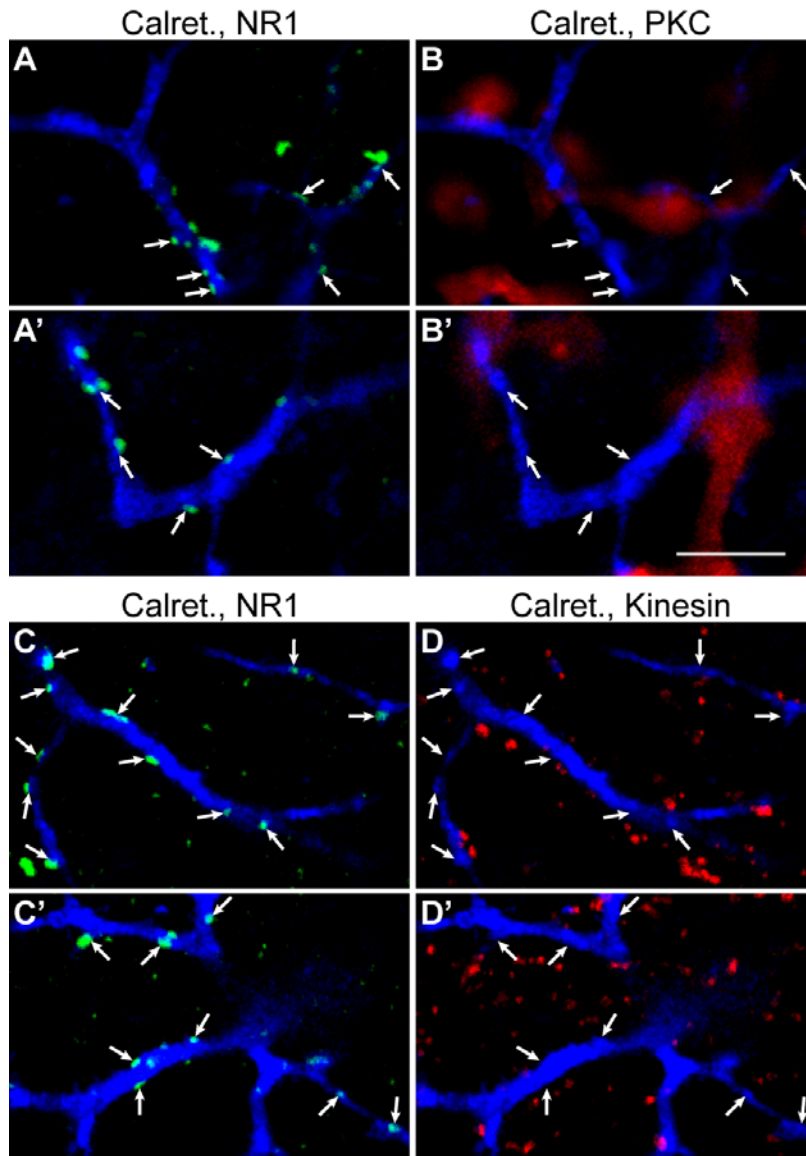
Figure 2 | NMDA receptors on AII amacrine cells are extrasynaptic.
A) and **A')** High magnification images show the location of NMDA receptors, labeled by antibodies against the NR1 subunit (green), on AII amacrine cell dendrites, labeled by calretinin antibodies (blue). Arrows indicate the locations of several NR1 puncta. **B)** and **B')** Rod bipolar cell terminals, labeled by antibodes against PKCα (red), associated with the same AII dendrites. The arrows indicating the positions of the NR1 puncta show that NMDA receptors on AIIs are not associated with rod bipolar cell inputs to the AII dendrites. **C)** and **C')** As described in **A**, but from a different piece of tissue. **D)** and **D')** Labeling of synaptic ribbons by kinesin II antibodies (red) in bipolar cell terminals; the arrows indicating the positions of the NR1 puncta show that NMDA receptors on AIIs are not associated with sites of glutamate release. For contrast, compare with the association of kinesin II labeling and AMPA receptors on AII dendrites (Li et al., 2002). Scale bar in **B'** is 5 μm.

the slice in hopes of maximizing the chances of spillover glutamate binding to putative

extrasynaptic NMDA receptors. To accomplish this we chose a light flash intensity of 1

R* rod^{-1} s^{-1}, which will activate multiple rod bipolar cells presynaptic to each AII

amacrine cell. We found that the AII response to a 500 ms light flash was unaffected by

CPP (20 μM) (Figure 1E), indicating that NMDA receptors do not contribute to the AII's

light response even when it receives input from multiple rod bipolar cells. This is

perhaps unsurprising given the very large ratio of AMPA to non-AMPA current

stimulated by glutamate release from a single rod bipolar cell (Figure 1D). As this

experiment's results did not support a traditional role for the NMDA currents in AII

amacrine cells (i.e. contribution to the light response), we next performed several

immunolabeling experiments to localize the NMDA receptors on AIIs. The rationale for

this was that the anatomical location of the receptors might hint at their function in AII

physiology.

NMDA receptors on AII amacrine cells are extrasynaptic

NMDA receptors are heterotetramers composed of two NR1 subunits and two

NR2 subunits; NR2 subunits are further divided in four types, A-D, all of which are

expressed in the retina (Grunder et al., 2000). Whole mount retinas were labeled with

polyclonal antibodies against the NR1 subunit in order to label the maximum number of

NMDA receptors at once for our localization of NMDA receptors on AII amacrine cells.

AII amacrine cells were labeled diffusely with antibodies against the Ca^{2+}-binding

protein calretinin (Massey and Mills, 1999). Finally, we included antibodies against

PKCα or kinesin II to label rod bipolar cells or synaptic ribbons in presynaptic bipolar
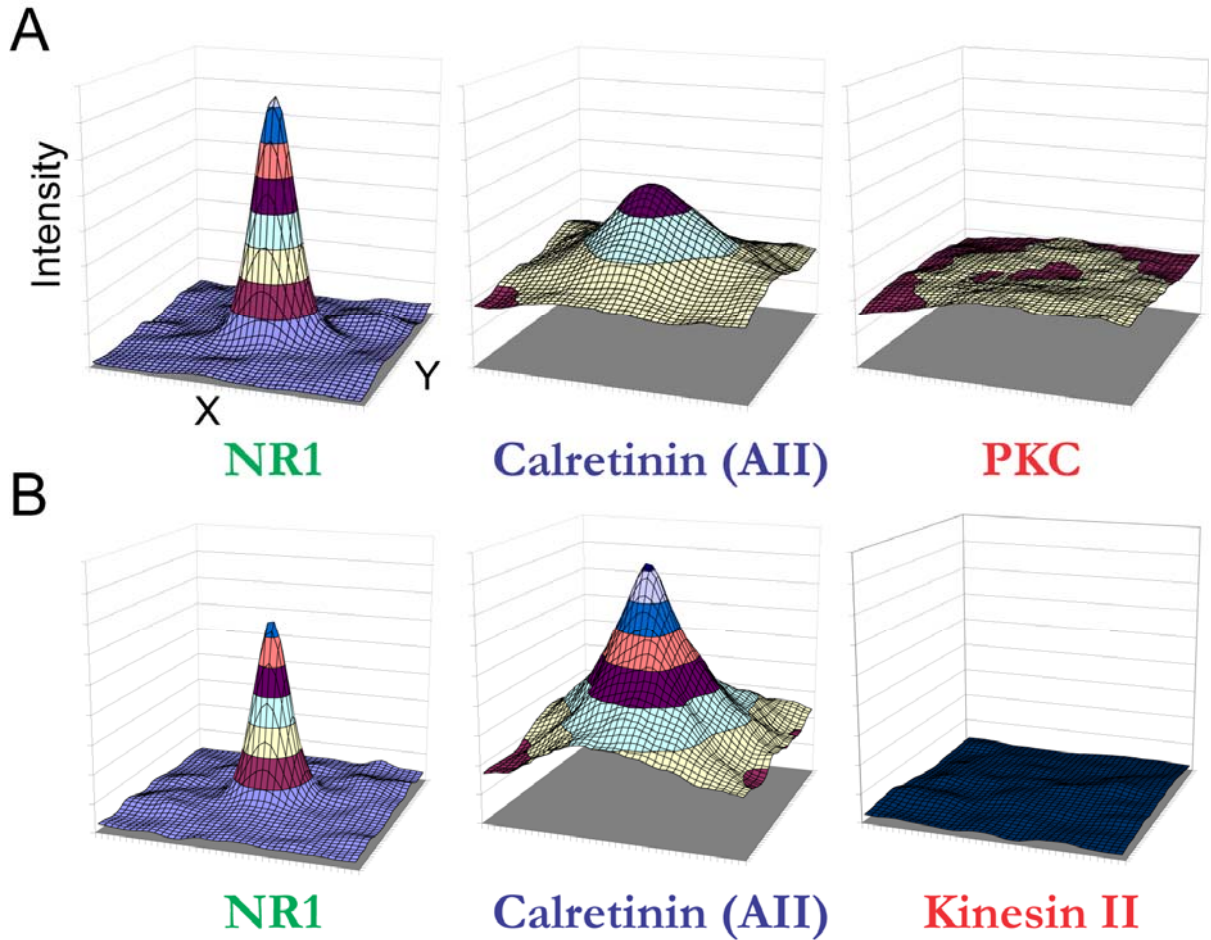
Figure S2 | Spatial fluorescence intensity averages show that NMDA receptors on AIIs are not associated with rod bipolar terminals or presynaptic ribbons.
A) Signal averaging analysis shows a random pattern of PKC immunoreactivity in relation to NR1 puncta associated with AIIs. There is no central peak in the PKC plot corresponding to the two central peaks in the NR1 and calretinin plots. Instead, the PKC plot is flat indicating no association with NR1 or calretinin. **B)** Signal averaging analysis shows a random pattern of kinesin II immunoreactivity in relation to NR1 puncta associated with AIIs. There is no central peak in the kinesin II plot corresponding to the two central peaks in the NR1 and calretinin plots. In fact, the kinesin II plot is flat, indicating that nearly total absence of label in the sampling boxes. The size of the sampling squares used in the analysis was 2 μm, indicating that ribbons and NR1 puncta were not consistently found within 1 μm of each other.

cells, respectively. NR1 labeling was localized on the fine dendrites of AII amacrine cells in sublamina b of the IPL (Figure 2, A & C). AIIs were nearly devoid of NR1 labeling in sublamina a, where the lobular dendrites of the AII ramify (data not shown). Arrows in Figure 2 were placed to indicate the location of NR1 labeling associated with AII amacrine cell dendrites. Examination of rod bipolar cell labeling (Figure 2B) showed that most NMDA receptors on the AII dendrites are not closely apposed to rod bipolar cell terminals. Further investigation of the synaptic ribbon labeling (Figure 2D) revealed that most NMDA receptors on AIIs were not closely apposed to sites of glutamate release from any nearby bipolar cells. Since the kinesin II labels synaptic ribbons in both rod and cone bipolar cells, it appears that the NMDA receptors on AIIs do not receive direct synaptic input at all. This interpretation is reinforced when contrasted against a similar immunolabeling experiment showing close association of kinesin II-labeled ribbons and synaptic AMPA receptors on AII amacrine cells (Li et al., 2002).

        To further analyze the relationship between NR1 puncta and rod bipolar cell terminals or synaptic ribbons, square sampling boxes (2 μm per side) were placed centered on NR1 puncta located on AII dendrites (see Methods). The spatial intensity distributions of fluorescence for each antibody was calculated and then averaged across all sampling boxes (Supplemental Figure 2). The flatness of the PKC and kinesin II channel averages indicates that there was no reliable relationship between NR1 labeling on AII dendrites and presynaptic rod bipolar cells or glutamate release sites in nearby bipolar cells. All together, this evidence further argues that NMDA receptors on AII amacrine cells are localized extrasynaptically.
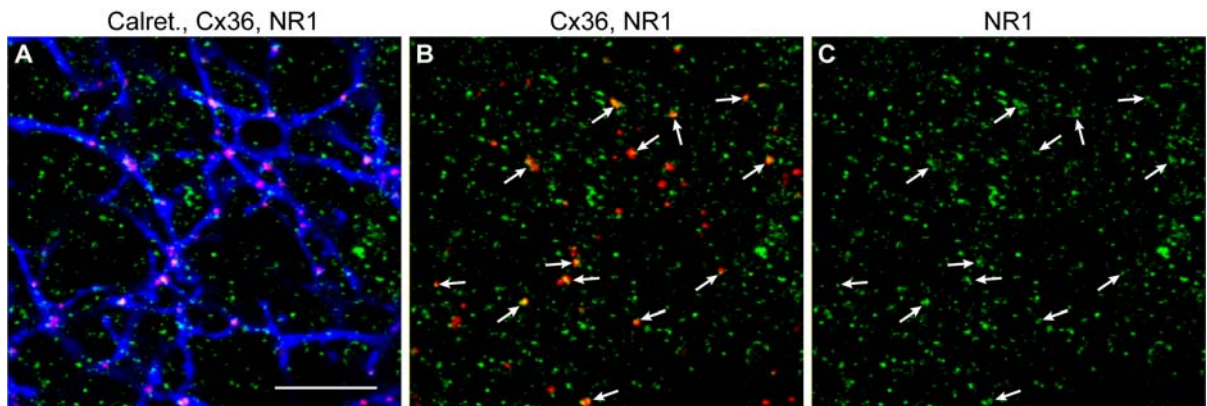
Figure 3 | NMDA receptors colocalize with Cx36 gap junctions on AII amacrine cells.
A) Triple labeling shows AII amacrine cells labeled by calretinin antibodies (blue), Cx36 gap junctions (red), and NMDA receptors labeled with NR1 antibodies (green). White spots indicate the colocalization of all strong signals in all three channels. **B)** Arrows indicate the locations of selected Cx36 gap junctions. **C)** The arrows showing the locations of Cx36 gap junctions show that NR1 puncta are colocalized with most Cx36 gap junctions on the AII network. Scale bar in **A** is 10 μm.

NMDA receptors on AII amacrine cells colocalize with Cx36 gap junctions

Although NMDA receptors do not appear to participate in the light response of AII amacrine cells in the rod-photoreceptor operating range (Figure 1E), we showed that blockade of AMPA receptors on AIIs revealed a small residual current (Figure 1D'). This residual current resembled the profile for extrasynaptic NMDA receptors in that it was small, had a long latency to onset, and did not appear to inactivate. It remains possible that glutamate spillover might activate very small currents mediated by extrasynaptic NMDA receptors in the AII amacrine cell that minimally influence the voltage response of the cell to light, but which cause significant Ca^{2+} influx in a very local domains. Both NMDA receptor activation and Ca^{2+} influx are required for activity-dependent potentiation of Cx35-mediated electrical coupling at the mixed electrical/chemical synapses in goldfish Mauthner cells (Yang et al., 1990; Pereda and Faber, 1996) (Cx35 is the non-mammalian ortholog of mammalian Cx36). Since increasing background illumination increases coupling between AII amacrine cells throughout the rod-photoreceptor operating range (Bloomfield et al., 1997; Bloomfield and Volgyi, 2004), we investigated whether NMDA receptors were localized near Cx36 gap junctions on AIIs, and thus in a position to influence gap junctional coupling in the AII network. Whole mount retinas were labeled with antibodies against calretinin, the NR1 subunit of NMDA receptors, and Cx36 gap junctions (Figure 3A). Nearly all Cx36 gap junctions on AII amacrine cell dendrites were colocalized or closely associated with NR1 puncta (Figure 3B). Arrows in Figure 3 indicate locations on AII dendrites where Cx36 gap junctions colocalize with strong NR1 puncta. As before, we analyzed the spatial intensity distribution of fluorescence for each antibody channel, with each square
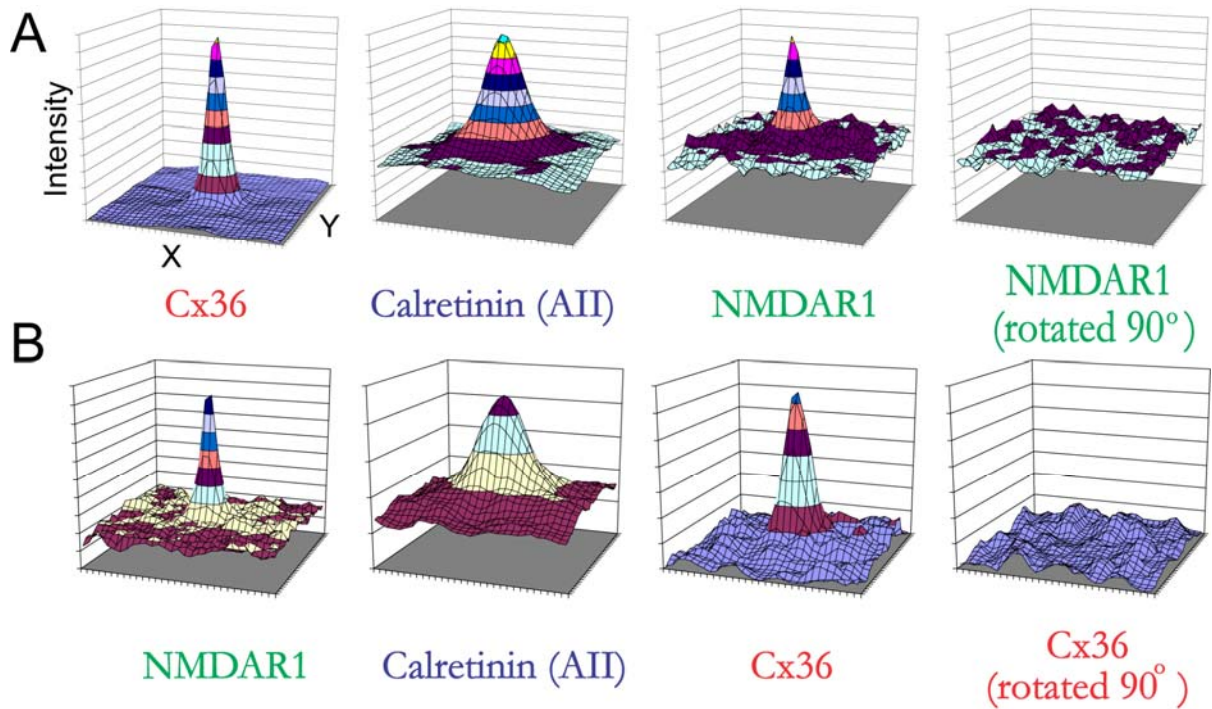
Figure S3 | Spatial fluorescence intensity averages show that Cx36 gap junctions are associated with NMDA receptors on AII amacrine cells.
A) Signal averaging of 228 Cx36 plaques from a larger area of retina that included the area shown in Figure 3 was used to analyze the association between Cx36 and NR1. 5.4 μm sampling boxes were placed around Cx36 plaques on AII dendrites. The NR1 signal was hidden to avoid bias. No distinction was made between plaques at AII dendritic crossings and plaques on single dendrites. The existence of 3 distinct peaks from all three signals indicates that the three structures are repeatedly associated. Loss of a central peak upon rotation of the NDMAR1 channel 90 degrees demonstrates that the association of NR1 and Cx36 did not occur by chance. **B)** For comparison, sampling boxes were placed around NR1 clusters on AIIs while the Cx36 signal was hidden. With this sampling constraint, again all three signals have a correlated central peak, indicating that Cx36 and NR1 indeed that NMDA receptors on AII amacrine cells are very regularly associated with Cx36.

sampling box centered on Cx36 gap junctions on AIIs (Supplemental Figure 3A). The

central peak seen in all three channel averages indicates the association of all three

signals. NMDA receptors are expressed by a number of retinal neurons with dendrites

near to those of AII amacrine cells, such as ON retinal ganglion cells (Zhang and

Diamond, 2006; Kalbaugh et al., 2009), and much of the NR1 labeling seen is not on AII

amacrine cells. The association of Cx36 gap junctions with NR1 puncta was not due to

chance colocalization of the more numerous NR1 puncta, however, as 90° rotation of the

NR1 channel relative to the other two channels abolished the associated central peak in

the spatial average. As an independent measure we also examined the spatial average

centered around the NR1 puncta. The resulting central peak in the Cx36 channel

indicates a strong tendency for NR1 puncta at this level of the retina to colocalize with

Cx36 gap junctions (Supplemental Figure 3B). Thus, NMDA receptors are appropriately

localized to influence the coupling state of the AII amacrine network by modulating

Cx36 gap junctions.

**Blockade of NMDA receptors and inhibition of CamKII reduce phosphorylation of
Cx36 on AII amacrine cells**

In order to test the functional significance of NMDA receptor colocalization

with Cx36 gap junctions, we used an experimental paradigm we previously established to

assess the coupling state of Cx36 gap junctions by examining the relative

phosphorylation state of Cx36 at Ser293 (Cx36-P) (Kothmann et al., 2009). Using this

paradigm, we found that increased phosphorylation of Cx36 at Ser293, a site that

regulates coupling through these gap junctions (Ouyang et al., 2005), is strongly

111
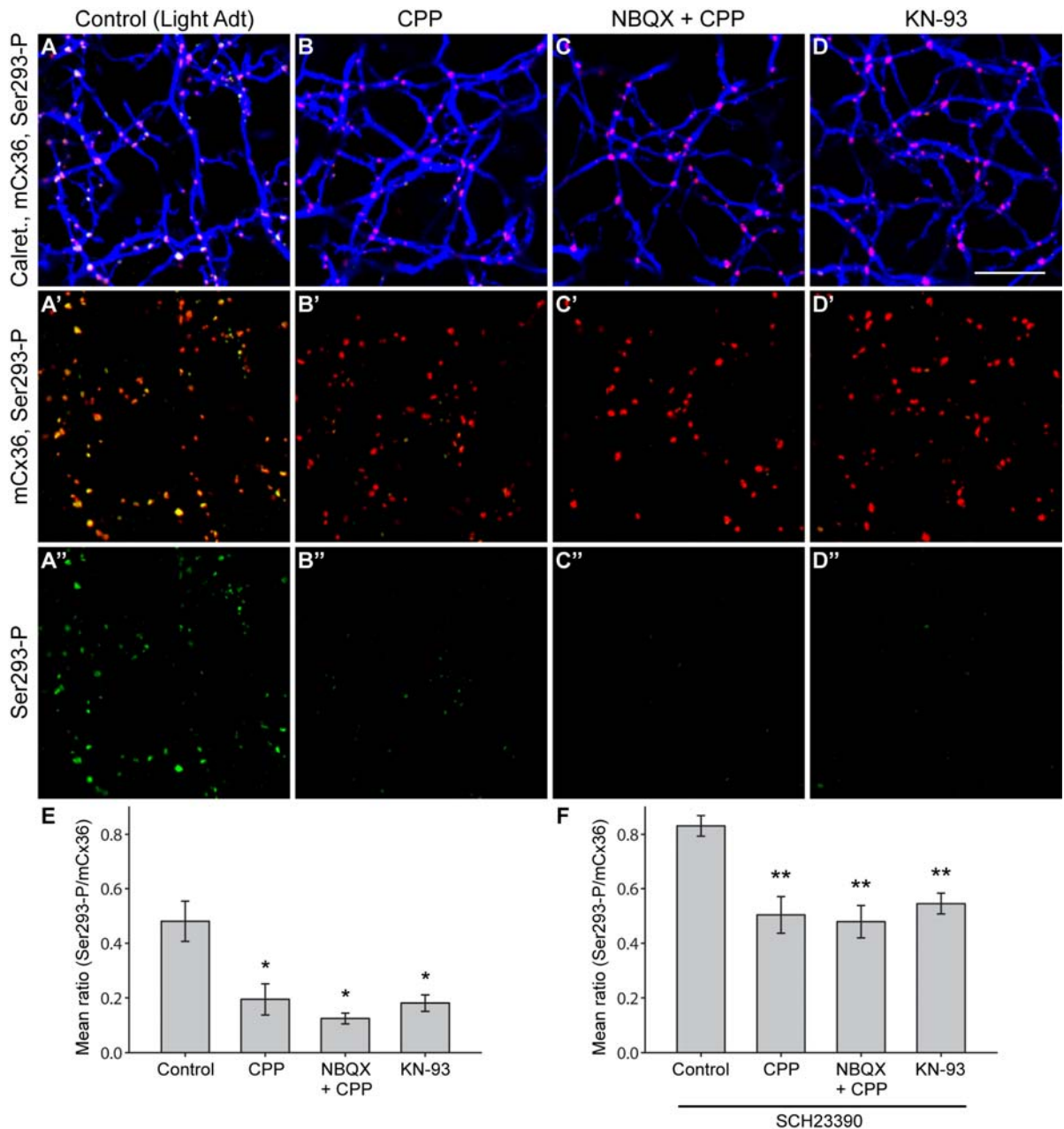
Figure 4 | Blockade of NMDA receptors and inhibition of CamKII reduce phosphorylation of Cx36 gap junctions on AII amacrine cells.
A) – A") Phosphorylation of Cx36 at Ser293 is heterogeneous in light-adapted retina. **B) – B")** Blockade of NMDA receptors (CPP, 10 μM) reduces phosphorylation of Cx36 at Ser293. **C) – C")** Blockade of AMPA/kainate (NBQX, 10 μM) and NMDA receptors has little additional effect over blockade of NMDA receptors alone. **D) – D")** Inhibition of CamKII (KN-93, 10 μM) reduced phosphorylation of Cx36 at Ser293. **E)** Summary of experiments (n = 4) shows that blockade of NMDA receptors significantly reduces mean phosphorylation of Cx36 on AII amacrine cells. Additional blockade of AMPA receptors does not significantly increase the magnitude of this effect. Inhibition of CamKII reduces phosphorylation of Cx36 to a similar extent as NMDA receptor blockade. **F)** The

112

experiments summarized in **E** were repeated with antagonist of dopamine D1 receptors (SCH23390, 50 µM) in the bath (n = 6). As shown previously, antagonism of D1 receptors increased mean phosphorylation of Cx36 on AIIs. It did not prevent the effects of NMDA receptor blockade or CamKII inhibition, indicating that both of the effects are independent of dopaminergic input to AII amacrine cells. Analysis was performed on single optical sections; images presented are 1 µm-deep z-stacks. Error bars are SEM, * $p < 0.05$, ** $p < 0.01$. Scale bar in **D** is 10 µm.

associated with increased coupling in the AII amacrine cell network. For the current experiments the superior portion of a light-adapted rabbit eyecup was cut into four retina-sclera pieces with a razor blade. These were incubated for 20 minutes in control Ames or Ames with glutamate receptor antagonist(s) added, and changes in phosphorylation were measured using an antibody specific for phospho-Ser293-Cx36 (Kothmann et al., 2007). Cx36-P was quantified as the average ratio of phospho-Ser293-Cx36 antibody fluorescence to monoclonal Cx36 antibody fluorescence at each individual gap junction plaque (for full details on Cx36-P quantification, see Methods). Phosphorylation of Cx36 plaques on AII amacrine cells is heterogeneous in light adapted retina (Figure 4A). Application of the NMDA receptor antagonist CPP (10 μM) reduced mean Cx36-P by 2.5-fold (Figure 4B, E), indicating that activation of NMDA receptors in light-adapted retina acts to increase phosphorylation of Cx36. Co-application of the AMPA receptor antagonist NBQX (10 μM) with CPP caused a slightly more robust reduction in Cx36-P, though not significantly different from CPP alone (Figure 4C, E).

Dopamine is a well-known regulator of coupling in the AII amacrine cell network (Hampson et al., 1992), with increased dopamine signaling causing reduced Cx36-P and reduced coupling (Kothmann et al., 2009). We tested whether the effect of NMDA receptor blockade on Cx36-P was due to modulation of neurons influencing dopamine release in the retina by repeating the experiment with the dopamine D1 receptor antagonist SCH23390 (50 μM) in the bath. D1 receptor blockade alone increased Cx36-P, as we reported previously (Kothmann et al., 2009), but it did not prevent the reduction in Cx36-P caused by CPP (Figure 4F). As before, inclusion of NBQX in the bath had no additional effect. Thus, blockade of NMDA receptors is
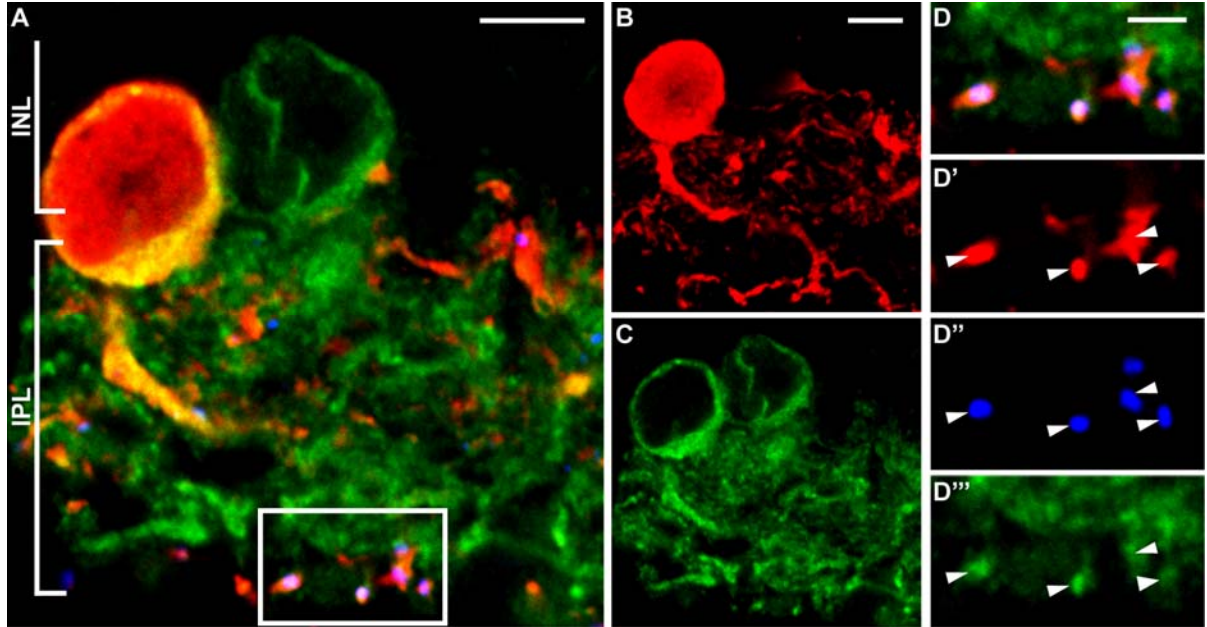
Figure 5 | Activated CamKII "hotspots" colocalize with Cx36 gap junctions on AII amacrine cell dendrites.

A) A single optical confocal section showing that activated CamKII, identified by antibodies against phospho-Thr286-CamKII (green) is widely distributed throughout the inner plexiform layer (IPL) of light-adapted retina. Strong labeling is seen in a ring around the soma of a calretinin-labeled AII amacrine cell (red) in the inner nuclear layer (INL), as well as in its stout primary dendrite (yellow). **B)** A 6 μm-deep z-stack of the calretinin label showing more fully the primary dendrite of the AII descending through the IPL and branching into fine dendrites. **C)** A single optical confocal section showing only the activated CamKII label. **D) – D''')** High magnification views of the area enclosed in the white rectangle in **A**. These single optical confocal sections show cross-sections through several of the fine dendrites of the AII amacrine cell (**D'**), and the Cx36 gap junctions (blue) on them (**D''**). Several of the Cx36 gap junctions are indicated by arrowheads, and when the activated CamKII label is viewed in isolation (**D'''**), it is evident that several of these Cx36 gap junctions are colocalized with "hotspots" of activated CamKII. Scale bars in **A** and **B** are 5 μm, scale bar in **D** is 2 μm.

sufficient to reduce phosphorylation of Cx36 in AII amacrine cells in light adapted retina, and is not due to modulation of the dopaminergic pathway which also regulates Cx36-P in AIIs.

In addition to requiring NMDA receptor activation and Ca^{2+} influx, the activity-dependent potentiation of Cx35-mediated electrical coupling in Mauthner cells also requires CamKII activation (Pereda et al., 1998). We therefore also tested if inhibition of CamKII influenced the phosphorylation state of Cx36 gap junctions on AII amacrine cells. Application of the CamKII inhibitor KN-93 (10 μM) reduced mean Cx36-P to a similar extent as blockade of NMDA receptors (Figure 4D, E). As was the case with NMDA receptor blockade, the reduction in Cx36-P caused by KN-93 persisted with dopamine D1 receptor antagonist in the bath (Figure 4F), indicating that CamKII inhibition reduces Cx36-P independent of dopamine signaling. These experiments indicate that in light-adapted retina, activation of NMDA receptors and CamKII activity are both required to maintain phosphorylation of Cx36 at Ser293.

Activated CamKII colocalizes with Cx36 gap junctions in AII amacrine cells

CamKII is a common mediator of activity-dependent plasticity in neurons (Colbran and Brown, 2004). In order to maintain specificity of targeting, CamKII is localized in postsynaptic density found at glutamatergic synapses. CamKII binds to multiple subunits of the NMDA receptor as well as to Cx36 gap junctions, and this binding is often facilitated by or requires autophosphorylation of the kinase at Thr286 (Colbran, 2004; Alev et al., 2008). We utilized antibodies against phospho-Thr286-CamKII, calretinin, and Cx36 to determine if the activated kinase is localized near Cx36
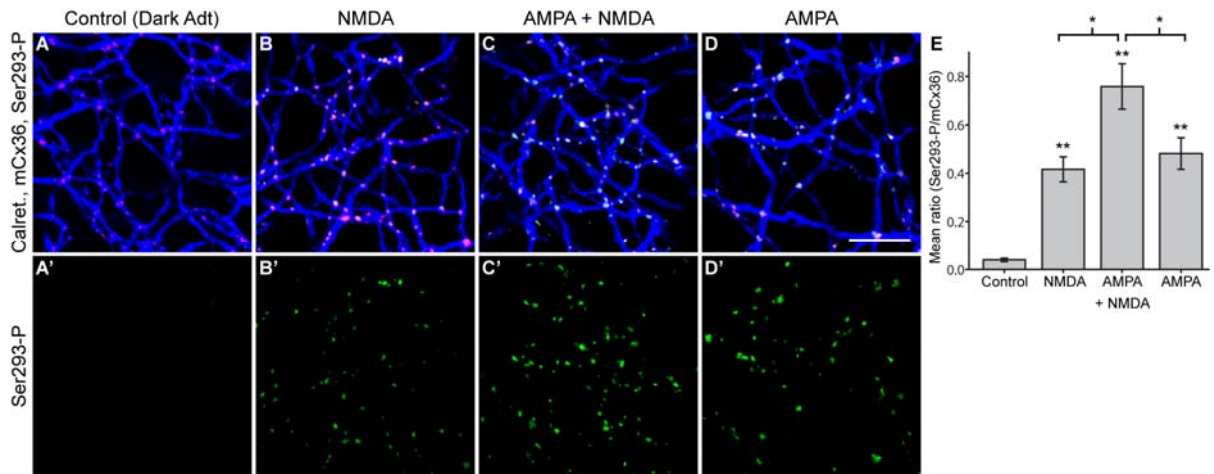
Figure 6 | Activation of NMDA receptors drives phosphorylation of Cx36 gap junctions on AII amacrine cells.
A) and A') Dark adaptation of the retina for 2 hours greatly reduced phosphorylation of Cx36 gap junctions at Ser293. **B) and B')** Application of NMDA (50 μM) drove increased phosphorylation of Cx36 at Ser293. **C) and C')** Addition of AMPA (5 μM) and NMDA drove increased phosphorylation of Cx36 at Ser293 more strongly than NMDA did alone. **D) and D')** Interestingly, application of AMPA alone also drove increased phosphorylation of Cx36 at Ser293. **E)** Summary of experiments (n = 6) shows that addition of NMDA to the bath drove phosphorylation of Cx36 back to control, light adapted levels (compare with Figure 4E). Application of AMPA drove increased phosphorylation as much as NMDA did. Addition of AMPA and NMDA drove phosphorylation significantly higher than NMDA or AMPA alone. Analysis was performed on single optical sections; images presented are 1 μm-deep z-stacks. Error bars are SEM, ** p < 0.01. Scale bar in **D** is 10 μm.

gap junctions in AII amacrine cells. In vertical sections from light-adapted retina there was strong phospho-Thr286-CamKII labeling throughout the IPL (Figure 5). The somas of a number of cells were ringed with phospho-Thr286-CamKII labeling, including many AII amacrine cells. Activated CamKII labeling was often strong in the primary dendrites of AIIs as well. Close inspection of the fine dendrites of AIIs in sublamina b of the IPL showed that hotspots of phospho-Thr286-CamKII labeling were often colocalized with Cx36 gap junctions on the AII network. These results indicate that activated CamKII is appropriately localized to influence the phosphorylation state of Cx36 gap junctions on AII amacrine cells, either by direct phosphorylation of the protein of by modulation of other proteins regulating phosphorylation of Cx36.

NMDA and AMPA drive phosphorylation of Cx36 on AII amacrine cells

We next asked whether activation of NMDA receptors could drive increased phosphorylation of Cx36 gap junctions. For these experiments we began by dark-adapting the superior portion of a rabbit eyecup for 100 minutes. The purpose for this was twofold. First, AII amacrine cells in well dark-adapted retinas have been shown to be relatively uncoupled (Bloomfield et al., 1997; Bloomfield and Volgyi, 2004). Thus we wished to investigate the phosphorylation state of Cx36 in AIIs after our retina-sclera preparations were dark-adapted. Second, as rod bipolar cells are ON-type bipolar cells and release glutamate in response to light, using dark-adapted retinas allowed us to examine the effects of NMDA application on relatively quiescent AII amacrine cells. After the initial dark-adaptation period, the eyecup was removed from the light-tight chamber under infrared illumination and cut into four retina-sclera pieces with a razor

118
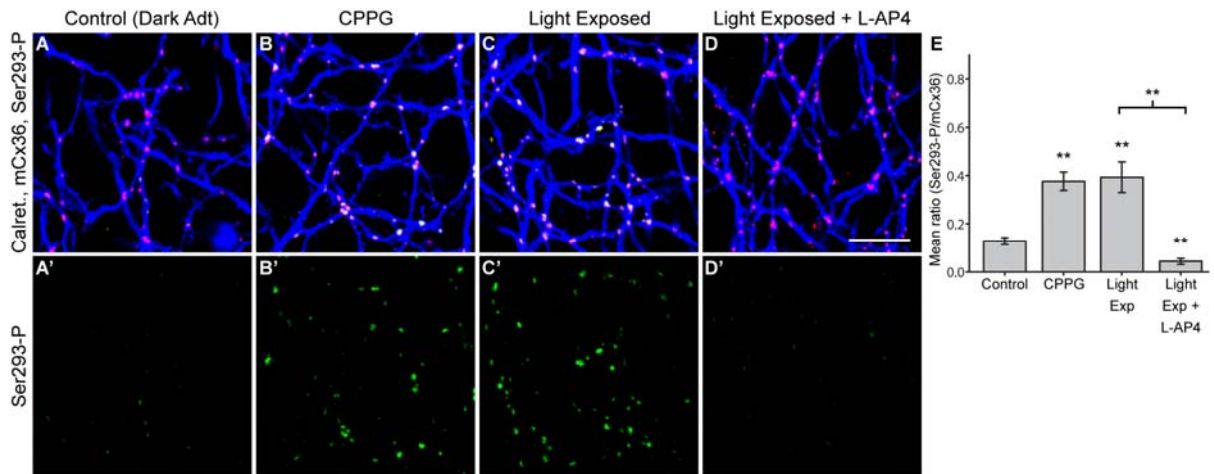
Figure 7 | Activation of ON-bipolar cells by CPPG or background light increment drive increased phosphorylation of Cx36 gap junctions on AII amacrine cells.
A) and A') Dark adaptation of the retina for 2 hours greatly reduced phosphorylation of Cx36 gap junctions at Ser293. **B) and B')** Depolarization of ON-type bipolar cells in darkness via antagonism of mGluR6 receptors (CPPG, 200 μM) drove increased phosphorylation of Cx36 at Ser293. **C) and C')** Exposure of dark-adapted retinas to photopic full-field background illumination also drove increased phosphorylation of Cx36 at Ser293. **D) and D')** The effect of increased background illumination was abolished when activation of ON-type bipolar cells was inhibited (L-AP4, 50 μM). **E)** Summary of experiments (n = 5) shows that activation of ON-type bipolar cells drove phosphorylation of Cx36 back to control, light adapted levels (compare with Figure 4E). Exposure of dark-adapted retinas to photopic background illumination drove phosphorylation to a similar extent as ON-type bipolar cell activation did. Activation of mGluR6 receptors on ON-type bipolar cells completely prevented the effects of increased background illumination, and actually reduced phosphorylation below control, dark-adapted levels (but compare with dark-adapted levels in Figure 5E). Analysis was performed on single optical sections; images presented are 1 μm-deep z-stacks. Error bars are SEM, ** $p < 0.01$. Scale bar in **D** is 10 μm.

119

blade. Pieces were separated into control Ames or Ames with glutamate agonist(s) added and placed back into the light-tight chamber for 20 additional minutes, after which phosphorylation of Cx36 was measured as before. Dark-adapting the retina for 120 minutes led to a dramatic reduction in Cx36-P (Figure 6A), in good agreement with the previous reports that AIIs are uncoupled in well dark-adapted retinas (Bloomfield et al., 1997; Bloomfield and Volgyi, 2004). Mean Cx36-P in dark-adapted retina was approximately 10-fold less than typical values obtained from in light-adapted retinas (Figure 4E). Addition of NMDA (50 μM) to the bath increased Cx36-P back to typical light-adapted levels (Figure 6B), indicating that NMDA receptor activation drives phosphorylation of Cx36. Addition of both AMPA (5 μM) and NMDA (50 μM) to the bath increased Cx36-P significantly above the levels cause by application of NMDA alone (Figure 6C). Interestingly, application of AMPA (5 μM) alone also increased Cx36-P (Figure 6D). These experiments support a role for NMDA-receptor mediated modulation of AII amacrine cell coupling via increased phosphorylation of Cx36 in AII amacrine cells. It is unclear from these experiments how AMPA receptors drive increased Cx36 phosphorylation. One simple explanation is that AMPA receptor-driven depolarization of AII amacrine cells may facilitate opening of NMDA receptors near Cx36 gap junctions, although these experiments cannot rule out other alternatives.

ON-Bipolar cell activation and background light increments drive phosphorylation of Cx36 on AII amacrine cells

Finally, we tested whether activation of ON-type bipolar cells could drive increased phosphorylation of Cx36 gap junctions on AII amacrine cells. Rod bipolar

cells provide the major glutamatergic input to AIIs on their fine dendrites, where the Cx36 gap junctions are located (Strettoi et al., 1992). The experimental setup was the same as described for the above experiments using dark-adapted retina. The mean level of Cx36-P was slightly higher in dark-adapted control pieces than in the above experiments (Figure 7A), but was still well reduced below levels seen in light-adapted retinas. Addition of CPPG (200 μM), an mGluR6 antagonist which causes depolarization in ON-type bipolar cells (citations), significantly increased mean Cx36-P (Figure 7B, E) to levels similar to those in light-adapted retina. At the same time as one retina-sclera piece was placed in Ames with CPPG added, another was place in Ames with L-AP4, an agonist of the mGluR6 receptor which hyperpolarizes ON-type bipolar cells. Then, after the control (dark-adapted) and CPPG retina-sclera pieces were re-secured within the light-tight chamber, the remaining two pieces (in either control Ames or Ames with L-AP4) were removed from the dark room and placed under the light-source (fluorescent lab lighting) used for light-adapted experiments for 15 minutes. This period of increased background illumination also significantly increased Cx36-P (Figure 7C, E) back to typical light-adapted levels. Inclusion of L-AP4 in the bath completely prevented this increase, and actually significantly reduced phosphorylation below control (dark-adapted) levels (Figure 7D, E). That pharmacological inactivation of ON-type bipolar cells reduced phosphorylation further than dark-adaptation alone suggests that in this set of experiments dark-adaptation was incomplete, perhaps due to exposure to dim point-sources of light in the dark room when the eyecup was removed from the light-tight chamber. This is further supported by the observation that dark-adaptation in previous experiments was sufficient to reduce Cx36-P to the same levels as seen in L-AP4 in these

experiments. These experiments provide evidence that increments in background lighting, mediated by ON-type bipolar cells, drive increased phosphorylation of Cx36 on AII amacrine cells. This agrees nicely with previous experiments that demonstrated increased coupling between AII amacrine cells under increasing background illumination (Bloomfield et al., 1997; Bloomfield and Volgyi, 2004).

Discussion

Although NMDA currents have been described in AII amacrine cells before (Hartveit and Veruki, 1997; Zhou and Dacheux, 2004), the physiological significance of these currents remain unknown. The results of the present study now describe a role for these NMDA receptors in driving increased phosphorylation of Cx36 gap junctions on AIIs, thereby increasing cell-cell coupling in the AII amacrine cell network. Indeed, driving increased phosphorylation of Cx36 under scotopic background illumination may be the primary purpose of NMDA receptors on AIIs, as our evidence indicates that they do not contribute to the light response of the cells under these conditions.

Our evidence indicates that the AII's NMDA receptors are extrasynaptic, as EPSCs in AIIs triggered by voltage steps in rod bipolar cells were nearly abolished by AMPA receptor blockade. This was confirmed by immunolabeling showing no relationship between NMDA receptors on AIIs and rod bipolar terminals or synaptic ribbons. It is also in agreement with electrophysiological data reported by others showing that spontaneous EPSCs in AIIs were solely mediated by AMPA receptors (Veruki et al., 2003). However, averaging of all rod bipolar-AII pairs did show a low-amplitude, NBQX-resistant current with slow kinetics, as would be predicted for

122

extrasynaptic NMDA receptors (citations). Since spillover of glutamate does occur at the

rod bipolar-AII synapse (Veruki et al., 2006), it is possible that this residual current

represents binding of spillover glutamate to the AIIs NMDA receptors. Future

experiments must be done to confirm this.

We found that the Cx36 and NMDA receptors are regularly colocalized or

closely associated in AII dendrites, and a functional relationship between them was

revealed by blockade of NMDA receptors in light-adapted retina, which reduced

phosphorylation of Cx36 at Ser293. This reduction in Cx36 phosphorylation indicates

reduced coupling between AII amacrine cells (Kothmann et al., 2009). The relationship

between NMDA receptors and Cx36 was confirmed by the finding that activation of the

receptors drives increased phosphorylation of Cx36 in dark-adapted retina. This is very

interesting, as AIIs should be hyperpolarized in the dark-adapted preparation. In the

absence of any depolarizing input, how do the NMDA receptors open? It is known that

NMDA receptors containing the NR2C or NR2D subunits are 5- to10-fold less sensitive

to the Mg^{2+} block than are the other NMDA receptors (Monyer et al., 1994). For

instance, NR1-NR2A current responses to NMDA are reduced by ~80% by 0.5 mM Mg^{2+}

at a holding potential of -60 mV, whereas NR1-NR2C responses are only reduced by

~50% (Monyer et al., 1992). Considering the physiological Mg^{2+} concentration in our

Ames solution (1.2 mM Mg^{2+}), we would predict that NMDA receptors on AIIs are NR1-

NR2C or NR1-NR2D heteromers. It is also known that ambient extracellular glutamate

in hippocampal slices is of sufficiently high concentration to activate NMDA receptors

and contributes to the excitability of pyramidal neurons (Sah et al., 1989). Similarly, in

retina NMDA receptors contribute to the basal noise in retinal ganglion cells (Gottesman

and Miller, 2003). In both of these examples the effect is observed at membrane potentials of -70 mV or more, well below the resting membrane potential of an AII (-46 mV, (Dunn et al., 2006). Our data indicate that despite the lack of direct glutamatergic input on the AIIs fine dendrites in dark-adapted retina, NMDA receptors are still responsive to exogenous agonist, potentially because of receptor subtype and/or the relatively depolarized resting membrane potential of AII amacrine cells.

It is more straightforward to imagine the circumstances that would activate NMDA receptors on AII amacrine cells *in vivo* under scotopic conditions, when they are depolarized directly by glutamate released by rod bipolar cells. Based on our results, we postulate that extracellular NMDA receptors, with their exceptional high affinity for glutamate (Olverman et al., 1984), sense the local excitation history in the vicinity of Cx36 gap junctions on AII dendrites. Such a situation fits with the observed increase in AII-AII coupling when background illumination exceeds the rod photoreceptor threshold, as this is when rod bipolar cells presynaptic to AIIs begin to release glutamate and AIIs are transiently depolarized by AMPA receptor activation. Further increases in background illumination within the scotopic range would cause larger numbers of rod bipolar cells to be active at a given time, further increasing extracellular glutamate and AII depolarization and thus further driving increased AII-AII coupling, as has been observed (Bloomfield et al., 1997; Bloomfield and Volgyi, 2004). Our data support such a scenario, as pharmacological activation of ON-type bipolar cells and activation by a background light increment both drive increased phosphorylation of Cx36 gap junctions on the AII network, indicating increased AII-AII coupling.

In light-adapted retina, AIIs receive significant input from coupled ON cone bipolar cells, sufficient to drive AII-mediated inhibition of OFF bipolar and ganglion cells (Manookin et al., 2008; Murphy and Rieke, 2008; Munch et al., 2009; van Wyk et al., 2009). Depolarization from this input should facilitate NMDA receptor activation by ambient and/or spillover glutamate, leading to increased Cx36 phosphorylation. This will be opposed by dopamine-driven dephosphorylation of Cx36 in daytime, light-adapted retina (Kothmann et al., 2009). The conflicting actions of these two pathways likely account for the heterogeneous phosphorylation of Cx36 gap junctions that we observe in light-adapted retina-sclera preparations. It is unknown if this same heterogeneity exists *in vivo*, as the bath volume (4 mL) used in our pharmacology experiments may dilute effective dopamine concentrations. In addition or perhaps alternatively, the observed heterogeneity may be due to differential regulation of AII-AII gap junctions and AII-cone bipolar gap junctions, as has been demonstrated (Mills and Massey, 1995). Our techniques do not currently distinguish between these gap junctions, but it seems likely that AII-AII gap junctional coupling may be preferentially decreased while AII-cone bipolar gap junctional coupling remains somewhat intact, given the existence of ON cone bipolar driven inhibition of ganglion cells via AII amacrine cell activation (Manookin et al., 2008; Murphy and Rieke, 2008; Munch et al., 2009; van Wyk et al., 2009) and the lesser effect of dopamine on AII-cone bipolar gap junctions (Xia and Mills, 2004). This could be due to expression of Cx45 on the ON bipolar cell side of these junctions (Han and Massey, 2005; Dedek et al., 2006), or the selective impact of cGMP-dependent signaling on the ON bipolar cell side of the gap junction only (Mills and Massey, 1995; Xia and Mills, 2004), or both.

Our data show that the effects of glutamate receptor blockade on Cx36 phosphorylation are not due to indirect modulation of extracellular dopamine in the retina, as they persist when the dopaminergic input to AII amacrine cells is blocked. Further evidence for this comes from the same set of experiments, since blockade of AMPA and NMDA receptors should reduce activation of the dopaminergic amacrine cell (Zhang et al., 2007; Hoshi et al., 2009), which would reduce extracellular dopamine and should increase Cx36 phosphorylation on AIIs (Kothmann et al., 2009). However, we observe the opposite; Cx36 phosphorylation was reduced in these experiments, whether or not D1 dopamine receptors were blocked. Thus we conclude from the experiments presented here and those conducted previously (Kothmann et al., 2009) that two pathways, one driving increased phosphorylation and mediated by NMDA receptor activation and the other driving decreased phosphorylation and mediated by dopamine signaling, are responsible for the inverted U-shaped pattern of coupling in the AII amacrine cell relative to background illumination. Furthermore, we infer from our data that there must be constitutive phosphatase activity which drives dephosphorylation of Cx36 in dark-adapted retina. The identity of the phosphatase and whether its activity is modulated remains unknown at present.

Chapter 5

Discussion

The experiments detailed in the previous chapters have significantly advanced our understanding of how signaling methods in the retina contribute to the regulation of gap junctional coupling in a particular retinal neuron, the AII amacrine cell. In order to reach this new level of understanding, we first developed and characterized phospho-specific antibodies against key residues of the gap junction protein Cx36. We then showed that light adaptation state and acute light exposure modulate the phosphorylation state of these residues in fish retina. These initial experiments highlighted the need for a method to study a retinal neuron expressing Cx36 that we could repeatedly identify. We chose the AII amacrine cell of mammalian retina for further study because it is easily and diffusely immunolabeled by antibodies against calretinin and because its coupling state is strongly modulated by dopamine signaling. Using rabbit retina to study regulation of the AII amacrine cell coupling we described the relationship between phosphorylation of Cx36 and coupling through these gap junctions. We discovered that dopamine-stimulated uncoupling of the AII is, as predicted, mediated by PKA activation, but that this pathway triggers dephosphorylation of Cx36 the requires activation of PP2A. Our experiments in this system also indicated that phosphorylation appears to modulate coupling by altering the channel properties of Cx36, rather than by alteration of trafficking of the protein. They also indicated that coupling is regulated locally at the level of individual gap junction plaques, rather than on a cell-by-cell basis. Finally, we demonstrated that increased coupling between AII amacrine cells is driven by activation of NMDA receptors and activation of CamKII. This increase in coupling was caused by activation of ON type bipolar cells by light increments.

Our findings show that two pathways, dopamine D1 receptor signaling and NMDA receptor activation, drive phosphorylation of Cx36 in opposite directions in AII amacrine cells. Together these two pathways can account for the characteristic inverted 'U'-shaped pattern of AII amacrine cell coupling in relation to background illumination. Additionally, we found that dark-adaptation strongly reduced Cx36 phosphorylation. These observations, along with the presence of two diametrically opposed pathways, provide the first independent confirmation of the inverted 'U'-shaped coupling-light relationship.

Horizontal cells in the rabbit retina also display an inverted 'U'-shaped coupling pattern in relation to background illumination (Xin and Bloomfield, 1999), and are also uncoupled by dopamine through D1 receptor-like signaling (Piccolino et al., 1984; Lasater, 1987). Based on these similarities to the AII amacrine cell network, we would predict that they also show increased coupling driven by presynaptic activity in photoreceptors. Regulation of horizontal cell coupling through phosphorylation of gap junction proteins they express, such as connexin 50 (O'Brien et al., 2006), remains a viable hypothesis at present. However, since neither horizontal cell uses Cx36 gap junctions, the exact intracellular cascades leading to increased coupling would not necessarily be the same. Indeed, other work in our lab has shown that regulation of coupling between zebrafish cone photoreceptors is also dependent on dopamine signaling, but that PKA activation increases coupling, exactly opposite of what we observe in AII amacrine cells (O'Brien et al., 2004). Coupled with our results presented here, it becomes clear that regulation of Cx36 is cell-type specific, and must be studied further on a cell-by-cell basis.

Many questions still remain about the role of phosphorylation in regulating Cx36-mediated coupling. Does phosphorylation itself alter the conformation of the protein, thereby changing the conductance or open probability of the channel? Alternatively, does it alter the affinity of Cx36 for protein binding partners, which then modulate coupling? Indeed, the two possibilities are not mutually exclusive, but solving them presents numerous technical challenges requiring careful biochemistry, electrophysiology, and structural studies.

Further questions exist about coupling in the AII amacrine cell network as well. Of great interest is whether regulatory pathways within the AII amacrine cell selectively modulate AII-AII gap junctions differently than they regulate AII-cone bipolar gap junctions. Anecdotally, I have observed that antagonism of NMDA receptors often leaves a population of small gap junctions on AIIs well phosphorylated. Many of these gap junctions do not appear to be at AII dendritic crossings, indicating that they are likely to be AII-cone bipolar gap junctions. Future studies are needed to determine if this is a reliable effect, and will require careful analysis and more concrete identification of AII-cone bipolar gap junctions. Additionally, before concluded differential regulation within AII amacrine cells, it must be shown that any selective effect of NMDA receptor antagonism is not selectively modulating Cx36 hemichannels on the bipolar cell side of the gap junction. Such channels have been reported in ON-cone bipolar cells that appear to be coupled to AIIs (Han and Massey, 2005). Most studies agree that Cx45 is expressed by the majority of bipolar cell types that couple to AIIs and forms heterotypic gap junctions with Cx36 on the AII side (Han and Massey, 2005; Maxeiner et al., 2005; Dedek et al., 2006), but the question of whether the AII-cone bipolar gap junctions are

homotypic, heterotypic, or Cx36/Cx45 bi-homotypic is still somewhat debated (Li et al., 2008).

The experiments presented in this work now provide a logical, integrated framework for studying regulation of Cx36-mediated coupling in other neuronal systems, where it is widely expressed, as well as in pancreatic β cells where it is involved in regulation of insulin secretion (Serre-Beinier et al., 2008; Wellershaus et al., 2008). In these systems, coupling can now be easily assessed through use of the phospho-specific antibodies developed and used in this work. Additionally, our results explain the mechanisms that underlie long-standing yet enigmatic observations of regulation of AII amacrine cell coupling by background illumination levels.

References

Ahn JH, McAvoy T, Rakhilin SV, Nishi A, Greengard P, Nairn AC (2007) Protein

    kinase A activates protein phosphatase 2A by phosphorylation of the B56delta

    subunit. Proc Natl Acad Sci U S A 104:2979-2984.

Alev C, Urschel S, Sonntag S, Zoidl G, Fort AG, Hoher T, Matsubara M, Willecke K,

    Spray DC, Dermietzel R (2008) The neuronal connexin36 interacts with and is

    phosphorylated by CaMKII in a way similar to CaMKII interaction with

    glutamate receptors. Proc Natl Acad Sci U S A 105:20964-20969.

Attwell D, Borges S, Wu SM, Wilson M (1987) Signal clipping by the rod output

    synapse. Nature 328:522-524.

Baldridge WH, Ball AK (1991) Background illumination reduces horizontal cell

    receptive-field size in both normal and 6-hydroxydopamine-lesioned goldfish

    retinas. Vis Neurosci 7:441-450.

Bedner P, Niessen H, Odermatt B, Willecke K, Harz H (2003) A method to determine

    the relative cAMP permeability of connexin channels. Exp Cell Res 291:25-

    35.

Bedner P, Niessen H, Odermatt B, Kretz M, Willecke K, Harz H (2006) Selective

    permeability of different connexin channels to the second messenger cyclic

    AMP. J Biol Chem 281:6673-6681.

Beierlein M, Gibson JR, Connors BW (2000) A network of electrically coupled

    interneurons drives synchronized inhibition in neocortex. Nat Neurosci 3:904-

    910.

Bekkers JM, Stevens CF (1989) NMDA and non-NMDA receptors are co-localized at individual excitatory synapses in cultured rat hippocampus. Nature 341:230-233.

Beyer EC, Berthoud VM (2009) The family of connexin genes. In: Connexins: A Guide (Harris AL, Locke D, eds), pp 3-26: Humana Press.

Bloomfield SA, Xin D (1997) A comparison of receptive-field and tracer-coupling size of amacrine and ganglion cells in the rabbit retina. Vis Neurosci 14:1153-1165.

Bloomfield SA, Volgyi B (2004) Function and plasticity of homologous coupling between AII amacrine cells. Vision Res 44:3297-3306.

Bloomfield SA, Volgyi B (2009) The diverse functional roles and regulation of neuronal gap junctions in the retina. Nat Rev Neurosci 10:495-506.

Bloomfield SA, Xin D, Persky SE (1995) A comparison of receptive field and tracer coupling size of horizontal cells in the rabbit retina. Vis Neurosci 12:985-999.

Bloomfield SA, Xin D, Osborne T (1997) Light-induced modulation of coupling between AII amacrine cells in the rabbit retina. Vis Neurosci 14:565-576.

Bostanci MO, Bagirici F (2007) Anticonvulsive effects of quinine on penicillin-induced epileptiform activity: an in vivo study. Seizure 16:166-172.

Buhl DL, Harris KD, Hormuzdi SG, Monyer H, Buzsaki G (2003) Selective impairment of hippocampal gamma oscillations in connexin-36 knock-out mouse in vivo. J Neurosci 23:1013-1018.

Burr GS, Mitchell CK, Keflemariam YJ, Heidelberger R, O'Brien J (2005) Calcium-dependent binding of calmodulin to neuronal gap junction proteins. Biochem Biophys Res Commun 335:1191-1198.

Carlen PL, Skinner F, Zhang L, Naus C, Kushnir M, Perez Velazquez JL (2000) The role of gap junctions in seizures. Brain Res Brain Res Rev 32:235-241.

Charpantier E, Cancela J, Meda P (2007) Beta cells preferentially exchange cationic molecules via connexin 36 gap junction channels. Diabetologia 50:2332-2341.

Cohen AI, Todd RD, Harmon S, O'Malley KL (1992) Photoreceptors of mouse retinas possess D4 receptors coupled to adenylate cyclase. Proc Natl Acad Sci U S A 89:12093-12097.

Colbran RJ (2004) Targeting of calcium/calmodulin-dependent protein kinase II. Biochem J 378:1-16.

Colbran RJ, Brown AM (2004) Calcium/calmodulin-dependent protein kinase II and synaptic plasticity. Curr Opin Neurobiol 14:318-327.

Condorelli DF, Parenti R, Spinella F, Trovato Salinaro A, Belluardo N, Cardile V, Cicirata F (1998) Cloning of a new gap junction gene (Cx36) highly expressed in mammalian brain neurons. Eur J Neurosci 10:1202-1208.

Connors BW (2009) Electrical signaling with neuronal gap junctions. In: Connexins: A Guide (Harris AL, Locke D, eds), pp 143-164: Humana Press.

Cook JE, Becker DL (1995) Gap junctions in the vertebrate retina. Microsc Res Tech 31:408-419.

Copenhagen DR, Green DG (1987) Spatial spread of adaptation within the cone network of turtle retina. J Physiol 393:763-776.

Dacey DM, Peterson BB, Robinson FR, Gamlin PD (2003) Fireworks in the primate
retina: in vitro photodynamics reveals diverse LGN-projecting ganglion cell
types. Neuron 37:15-27.

Deans MR, Gibson JR, Sellitto C, Connors BW, Paul DL (2001) Synchronous
activity of inhibitory networks in neocortex requires electrical synapses
containing connexin36. Neuron 31:477-485.

Deans MR, Volgyi B, Goodenough DA, Bloomfield SA, Paul DL (2002) Connexin36
is essential for transmission of rod-mediated visual signals in the mammalian
retina. Neuron 36:703-712.

Dearry A, Burnside B (1986) Dopaminergic regulation of cone retinomotor
movement in isolated teleost retinas: I. Induction of cone contraction is
mediated by D2 receptors. J Neurochem 46:1006-1021.

Dedek K, Schultz K, Pieper M, Dirks P, Maxeiner S, Willecke K, Weiler R, Janssen-
Bienhold U (2006) Localization of heterotypic gap junctions composed of
connexin45 and connexin36 in the rod pathway of the mouse retina. Eur J
Neurosci 24:1675-1686.

DeVries SH, Schwartz EA (1989) Modulation of an electrical synapse between
solitary pairs of catfish horizontal cells by dopamine and second messengers. J
Physiol 414:351-375.

DeVries SH, Qi X, Smith R, Makous W, Sterling P (2002) Electrical coupling
between mammalian cones. Curr Biol 12:1900-1907.

Dingledine R, Borges K, Bowie D, Traynelis SF (1999) The glutamate receptor ion
channels. Pharmacol Rev 51:7-61.

Djamgoz MB, Downing JE, Wagner HJ (1989) Amacrine cells in the retina of a
cyprinid fish: functional characterization and intracellular labelling with
horseradish peroxidase. Cell Tissue Res 256:607-622.

Djamgoz MB, Spadavecchia L, Usai C, Vallerga S (1990) Variability of light-evoked
response pattern and morphological characterization of amacrine cells in
goldfish retina. J Comp Neurol 301:171-190.

Dunn FA, Doan T, Sampath AP, Rieke F (2006) Controlling the gain of rod-mediated
signals in the Mammalian retina. J Neurosci 26:3959-3970.

Ekelund J, Slifstein M, Narendran R, Guillin O, Belani H, Guo NN, Hwang Y,
Hwang DR, Abi-Dargham A, Laruelle M (2007) In vivo DA D(1) receptor
selectivity of NNC 112 and SCH 23390. Mol Imaging Biol 9:117-125.

Fadool JM, Dowling JE (2007) Zebrafish: A model system for the study of eye
genetics. Prog Retin Eye Res.

Famiglietti EV, Jr., Kolb H (1975) A bistratified amacrine cell and synaptic cirucitry
in the inner plexiform layer of the retina. Brain Res 84:293-300.

Feigenspan A, Teubner B, Willecke K, Weiler R (2001a) Expression of neuronal
connexin36 in AII amacrine cells of the mammalian retina. J Neurosci 21:230-
239.

Feigenspan A, Teubner B, Willecke K, Weiler R (2001b) Expression of neuronal
connexin36 in AII amacrine cells of the mammalian retina. J Neurosci 21:230-
239.

Feigenspan A, Janssen-Bienhold U, Hormuzdi S, Monyer H, Degen J, Sohl G,
Willecke K, Ammermuller J, Weiler R (2004a) Expression of connexin36 in

cone pedicles and OFF-cone bipolar cells of the mouse retina. J Neurosci 24:3325-3334.

Feigenspan A, Janssen-Bienhold U, Hormuzdi S, Monyer H, Degen J, Sohl G, Willecke K, Ammermuller J, Weiler R (2004b) Expression of connexin36 in cone pedicles and OFF-cone bipolar cells of the mouse retina. J Neurosci 24:3325-3334.

Feng W, Zhang M (2009) Organization and dynamics of PDZ-domain-related supramodules in the postsynaptic density. Nat Rev Neurosci 10:87-99.

Field GD, Chichilnisky EJ (2007) Information processing in the primate retina: circuitry and coding. Annu Rev Neurosci 30:1-30.

Flores CE, Li X, Bennett MV, Nagy JI, Pereda AE (2008) Interaction between connexin35 and zonula occludens-1 and its potential role in the regulation of electrical synapses. Proc Natl Acad Sci U S A 105:12545-12550.

Gajda Z, Szupera Z, Blazso G, Szente M (2005) Quinine, a blocker of neuronal cx36 channels, suppresses seizure activity in rat neocortex in vivo. Epilepsia 46:1581-1591.

Gajda Z, Gyengesi E, Hermesz E, Ali KS, Szente M (2003) Involvement of gap junctions in the manifestation and control of the duration of seizures in rats in vivo. Epilepsia 44:1596-1600.

Gibson JR, Beierlein M, Connors BW (1999) Two networks of electrically coupled inhibitory neurons in neocortex. Nature 402:75-79.

Gonzalez-Nieto D, Gomez-Hernandez JM, Larrosa B, Gutierrez C, Munoz MD, Fasciani I, O'Brien J, Zappala A, Cicirata F, Barrio LC (2008) Regulation of

neuronal connexin-36 channels by pH. Proc Natl Acad Sci U S A 105:17169-17174.

Gottesman J, Miller RF (2003) N-methyl-D-aspartate receptors contribute to the baseline noise of retinal ganglion cells. Vis Neurosci 20:329-333.

Grunder T, Kohler K, Kaletta A, Guenther E (2000) The distribution and developmental regulation of NMDA receptor subunit proteins in the outer and inner retina of the rat. J Neurobiol 44:333-342.

Guldenagel M, Ammermuller J, Feigenspan A, Teubner B, Degen J, Sohl G, Willecke K, Weiler R (2001) Visual transmission deficits in mice with targeted disruption of the gap junction gene connexin36. J Neurosci 21:6036-6044.

Hampson EC, Vaney DI, Weiler R (1992) Dopaminergic modulation of gap junction permeability between amacrine cells in mammalian retina. J Neurosci 12:4911-4922.

Han Y, Massey SC (2005) Electrical synapses in retinal ON cone bipolar cells: subtype-specific expression of connexins. Proc Natl Acad Sci U S A 102:13313-13318.

Harsanyi K, Mangel SC (1992) Activation of a D2 receptor increases electrical coupling between retinal horizontal cells by inhibiting dopamine release. Proc Natl Acad Sci U S A 89:9220-9224.

Hartveit E, Veruki ML (1997) AII amacrine cells express functional NMDA receptors. Neuroreport 8:1219-1223.

Hempelmann A, Heils A, Sander T (2006) Confirmatory evidence for an association of the connexin-36 gene with juvenile myoclonic epilepsy. Epilepsy Res 71:223-228.

Hidaka S, Kato T, Miyachi E (2002) Expression of gap junction connexin36 in adult rat retinal ganglion cells. J Integr Neurosci 1:3-22.

Hidaka S, Kato T, Hashimoto Y (2005) Structural and functional properties of homologous electrical synapses between retinal amacrine cells. J Integr Neurosci 4:313-340.

Hidaka S, Maehara M, Umino O, Lu Y, Hashimoto Y (1993) Lateral gap junction connections between retinal amacrine cells summating sustained responses. Neuroreport 5:29-32.

Honkanen RE, Zwiller J, Moore RE, Daily SL, Khatra BS, Dukelow M, Boynton AL (1990) Characterization of microcystin-LR, a potent inhibitor of type 1 and type 2A protein phosphatases. J Biol Chem 265:19401-19404.

Hormuzdi SG, Pais I, LeBeau FE, Towers SK, Rozov A, Buhl EH, Whittington MA, Monyer H (2001) Impaired electrical signaling disrupts gamma frequency oscillations in connexin 36-deficient mice. Neuron 31:487-495.

Hoshi H, Liu WL, Massey SC, Mills SL (2009) ON inputs to the OFF layer: bipolar cells that break the stratification rules of the retina. J Neurosci 29:8875-8883.

Hu EH, Bloomfield SA (2003) Gap junctional coupling underlies the short-latency spike synchrony of retinal alpha ganglion cells. J Neurosci 23:6768-6777.

Iuvone PM, Galli CL, Garrison-Gund CK, Neff NH (1978) Light stimulates tyrosine hydroxylase activity and dopamine synthesis in retinal amacrine neurons. Science 202:901-902.

Jahromi SS, Wentlandt K, Piran S, Carlen PL (2002) Anticonvulsant actions of gap junctional blockers in an in vitro seizure model. J Neurophysiol 88:1893-1902.

Kalbaugh TL, Zhang J, Diamond JS (2009) Coagonist release modulates NMDA receptor subtype contributions at synaptic inputs to retinal ganglion cells. J Neurosci 29:1469-1479.

Kolb H, Famiglietti EV (1974) Rod and cone pathways in the inner plexiform layer of cat retina. Science 186:47-49.

Kothmann WW, Massey SC, O'Brien J (2009) Dopamine-stimulated dephosphorylation of connexin 36 mediates AII amacrine cell uncoupling. J Neurosci 29:14903-14911.

Kothmann WW, Li X, Burr GS, O'Brien J (2007) Connexin 35/36 is phosphorylated at regulatory sites in the retina. Vis Neurosci 24:363-375.

Kramer SG (1971) Dopamine: A retinal neurotransmitter. I. Retinal uptake, storage, and light-stimulated release of H3-dopamine in vivo. Invest Ophthalmol 10:438-452.

Kreuzberg MM, Deuchars J, Weiss E, Schober A, Sonntag S, Wellershaus K, Draguhn A, Willecke K (2008) Expression of connexin30.2 in interneurons of the central nervous system in the mouse. Mol Cell Neurosci 37:119-134.

Krizaj D, Gabriel R, Owen WG, Witkovsky P (1998) Dopamine D2 receptor-
mediated modulation of rod-cone coupling in the Xenopus retina. J Comp
Neurol 398:529-538.

Kwak BR, Hermans MM, De Jonge HR, Lohmann SM, Jongsma HJ, Chanson M
(1995) Differential regulation of distinct types of gap junction channels by
similar phosphorylating conditions. Mol Biol Cell 6:1707-1719.

Lamb TD, Simon EJ (1976) The relation between intercellular coupling and electrical
noise in turtle photoreceptors. J Physiol 263:257-286.

Lampe PD (1994) Analyzing phorbol ester effects on gap junctional communication:
a dramatic inhibition of assembly. J Cell Biol 127:1895-1905.

Lampe PD, Lau AF (2004) The effects of connexin phosphorylation on gap junctional
communication. Int J Biochem Cell Biol 36:1171-1186.

Lampe PD, TenBroek EM, Burt JM, Kurata WE, Johnson RG, Lau AF (2000)
Phosphorylation of connexin43 on serine368 by protein kinase C regulates
gap junctional communication. J Cell Biol 149:1503-1512.

Landisman CE, Connors BW (2005) Long-term modulation of electrical synapses in
the mammalian thalamus. Science 310:1809-1813.

Landisman CE, Long MA, Beierlein M, Deans MR, Paul DL, Connors BW (2002)
Electrical synapses in the thalamic reticular nucleus. J Neurosci 22:1002-
1009.

Lankheet MJ, Przybyszewski AW, van de Grind WA (1993) The lateral spread of
light adaptation in cat horizontal cell responses. Vision Res 33:1173-1184.

Lasater EM (1987) Retinal horizontal cell gap junctional conductance is modulated
by dopamine through a cyclic AMP-dependent protein kinase. Proc Natl Acad
Sci U S A 84:7319-7323.

Lee EJ, Han JW, Kim HJ, Kim IB, Lee MY, Oh SJ, Chung JW, Chun MH (2003) The
immunocytochemical localization of connexin 36 at rod and cone gap
junctions in the guinea pig retina. Eur J Neurosci 18:2925-2934.

Leonard SK, Ferry-Leeper P, Mailman RB (2006) Low affinity binding of the
classical D1 antagonist SCH23390 in rodent brain: potential interaction with
A2A and D2-like receptors. Brain Res 1117:25-37.

Li H, Chuang AZ, O'Brien J (2009) Photoreceptor coupling is controlled by connexin
35 phosphorylation in zebrafish retina. J Neurosci 29:15178-15186.

Li W, Trexler EB, Massey SC (2002) Glutamate receptors at rod bipolar ribbon
synapses in the rabbit retina. J Comp Neurol 448:230-248.

Li X, Olson C, Lu S, Kamasawa N, Yasumura T, Rash JE, Nagy JI (2004) Neuronal
connexin36 association with zonula occludens-1 protein (ZO-1) in mouse
brain and interaction with the first PDZ domain of ZO-1. Eur J Neurosci
19:2132-2146.

Li X, Kamasawa N, Ciolofan C, Olson CO, Lu S, Davidson KG, Yasumura T,
Shigemoto R, Rash JE, Nagy JI (2008) Connexin45-containing neuronal gap
junctions in rodent retina also contain connexin36 in both apposing
hemiplaques, forming bihomotypic gap junctions, with scaffolding
contributed by zonula occludens-1. J Neurosci 28:9769-9789.

Lieschke GJ, Currie PD (2007) Animal models of human disease: zebrafish swim into view. Nat Rev Genet 8:353-367.

Long MA, Landisman CE, Connors BW (2004) Small clusters of electrically coupled neurons generate synchronous rhythms in the thalamic reticular nucleus. J Neurosci 24:341-349.

Long MA, Deans MR, Paul DL, Connors BW (2002) Rhythmicity without synchrony in the electrically uncoupled inferior olive. J Neurosci 22:10898-10905.

Maier N, Guldenagel M, Sohl G, Siegmund H, Willecke K, Draguhn A (2002) Reduction of high-frequency network oscillations (ripples) and pathological network discharges in hippocampal slices from connexin 36-deficient mice. J Physiol 541:521-528.

Manookin MB, Beaudoin DL, Ernst ZR, Flagel LJ, Demb JB (2008) Disinhibition combines with excitation to extend the operating range of the OFF visual pathway in daylight. J Neurosci 28:4136-4150.

Marc RE, Liu WL, Muller JF (1988) Gap junctions in the inner plexiform layer of the goldfish retina. Vision Res 28:9-24.

Mas C, Taske N, Deutsch S, Guipponi M, Thomas P, Covanis A, Friis M, Kjeldsen MJ, Pizzolato GP, Villemure JG, Buresi C, Rees M, Malafosse A, Gardiner M, Antonarakis SE, Meda P (2004) Association of the connexin36 gene with juvenile myoclonic epilepsy. J Med Genet 41:e93.

Massey SC, Mills SL (1999) Antibody to calretinin stains AII amacrine cells in the rabbit retina: double-label and confocal analyses. J Comp Neurol 411:3-18.

Massey SC, O'Brien JJ, Trexler EB, Li W, Keung JW, Mills SL, O'Brien J (2003) Multiple neuronal connexins in the mammalian retina. Cell Commun Adhes 10:425-430.

Maxeiner S, Dedek K, Janssen-Bienhold U, Ammermuller J, Brune H, Kirsch T, Pieper M, Degen J, Kruger O, Willecke K, Weiler R (2005) Deletion of connexin45 in mouse retinal neurons disrupts the rod/cone signaling pathway between AII amacrine and ON cone bipolar cells and leads to impaired visual transmission. J Neurosci 25:566-576.

McCracken CB, Roberts DC (2006) A single evoked afterdischarge produces rapid time-dependent changes in connexin36 protein expression in adult rat dorsal hippocampus. Neurosci Lett 405:84-88.

Mills SL, Massey SC (1991) Labeling and distribution of AII amacrine cells in the rabbit retina. J Comp Neurol 304:491-501.

Mills SL, Massey SC (1995) Differential properties of two gap junctional pathways made by AII amacrine cells. Nature 377:734-737.

Mills SL, Massey SC (2000) A series of biotinylated tracers distinguishes three types of gap junction in retina. J Neurosci 20:8629-8636.

Mills SL, O'Brien JJ, Li W, O'Brien J, Massey SC (2001a) Rod pathways in the mammalian retina use connexin36. J Comp Neurol 436:336-350.

Mills SL, O'Brien JJ, Li W, O'Brien J, Massey SC (2001b) Rod pathways in the mammalian retina use connexin 36. J Comp Neurol 436:336-350.

Mills SL, Xia XB, Hoshi H, Firth SI, Rice ME, Frishman LJ, Marshak DW (2007)
Dopaminergic modulation of tracer coupling in a ganglion-amacrine cell
network. Vis Neurosci 24:593-608.

Mitropoulou G, Bruzzone R (2003) Modulation of perch connexin35 hemi-channels
by cyclic AMP requires a protein kinase A phosphorylation site. J Neurosci
Res 72:147-157.

Mitsuhashi S, Matsuura N, Ubukata M, Oikawa H, Shima H, Kikuchi K (2001)
Tautomycetin is a novel and specific inhibitor of serine/threonine protein
phosphatase type 1, PP1. Biochem Biophys Res Commun 287:328-331.

Monyer H, Burnashev N, Laurie DJ, Sakmann B, Seeburg PH (1994) Developmental
and regional expression in the rat brain and functional properties of four
NMDA receptors. Neuron 12:529-540.

Monyer H, Sprengel R, Schoepfer R, Herb A, Higuchi M, Lomeli H, Burnashev N,
Sakmann B, Seeburg PH (1992) Heteromeric NMDA receptors: molecular
and functional distinction of subtypes. Science 256:1217-1221.

Moreno AP, Saez JC, Fishman GI, Spray DC (1994) Human connexin43 gap junction
channels. Regulation of unitary conductances by phosphorylation. Circ Res
74:1050-1057.

Morkve SH, Veruki ML, Hartveit E (2002) Functional characteristics of non-NMDA-
type ionotropic glutamate receptor channels in AII amacrine cells in rat retina.
J Physiol 542:147-165.

Munch TA, da Silveira RA, Siegert S, Viney TJ, Awatramani GB, Roska B (2009) Approach sensitivity in the retina processed by a multifunctional neural circuit. Nat Neurosci.

Murphy GJ, Rieke F (2008) Signals and noise in an inhibitory interneuron diverge to control activity in nearby retinal ganglion cells. Nat Neurosci 11:318-326.

Negishi K, Teranishi T (1990) Close tip-to-tip contacts between dendrites of transient amacrine cells in carp retina. Neurosci Lett 115:1-6.

Neve KA, Seamans JK, Trantham-Davidson H (2004) Dopamine receptor signaling. J Recept Signal Transduct Res 24:165-205.

Nir I, Harrison JM, Haque R, Low MJ, Grandy DK, Rubinstein M, Iuvone PM (2002) Dysfunctional light-evoked regulation of cAMP in photoreceptors and abnormal retinal adaptation in mice lacking dopamine D4 receptors. J Neurosci 22:2063-2073.

O'Brien J, al-Ubaidi MR, Ripps H (1996) Connexin 35: a gap-junctional protein expressed preferentially in the skate retina. Mol Biol Cell 7:233-243.

O'Brien J, Nguyen HB, Mills SL (2004) Cone photoreceptors in bass retina use two connexins to mediate electrical coupling. J Neurosci 24:5632-5642.

O'Brien J, Bruzzone R, White TW, Al-Ubaidi MR, Ripps H (1998) Cloning and expression of two related connexins from the perch retina define a distinct subgroup of the connexin family. J Neurosci 18:7625-7637.

O'Brien JJ, Li W, Pan F, Keung J, O'Brien J, Massey SC (2006) Coupling between A-type horizontal cells is mediated by connexin 50 gap junctions in the rabbit retina. J Neurosci 26:11624-11636.

Olverman HJ, Jones AW, Watkins JC (1984) L-glutamate has higher affinity than other amino acids for [3H]-D-AP5 binding sites in rat brain membranes. Nature 307:460-462.

Ouyang X, Winbow VM, Patel LS, Burr GS, Mitchell CK, O'Brien J (2005) Protein kinase A mediates regulation of gap junctions containing connexin35 through a complex pathway. Brain Res Mol Brain Res 135:1-11.

Pais I, Hormuzdi SG, Monyer H, Traub RD, Wood IC, Buhl EH, Whittington MA, LeBeau FE (2002) Sharp wave-like activity in the hippocampus in vitro in mice lacking the gap junction protein connexin 36. J Neurophysiol 89:2046-2054.

Pan F, Paul DL, Bloomfield SA, Volgyi B Connexin36 is required for gap junctional coupling of most ganglion cell subtypes in the mouse retina. J Comp Neurol 518:911-927.

Partida GJ, Lee SC, Haft-Candell L, Nichols GS, Ishida AT (2004) DARPP-32-like immunoreactivity in AII amacrine cells of rat retina. J Comp Neurol 480:251-263.

Patel LS, Mitchell CK, Dubinsky WP, O'Brien J (2006) Regulation of gap junction coupling through the neuronal connexin Cx35 by nitric oxide and cGMP. Cell Commun Adhes 13:41-54.

Pereda A, O'Brien J, Nagy JI, Bukauskas F, Davidson KG, Kamasawa N, Yasumura T, Rash JE (2003) Connexin35 mediates electrical transmission at mixed synapses on Mauthner cells. J Neurosci 23:7489-7503.

Pereda AE, Faber DS (1996) Activity-dependent short-term enhancement of
intercellular coupling. J Neurosci 16:983-992.

Pereda AE, Bell TD, Chang BH, Czernik AJ, Nairn AC, Soderling TR, Faber DS
(1998) Ca2+/calmodulin-dependent kinase II mediates simultaneous
enhancement of gap-junctional conductance and glutamatergic transmission.
Proc Natl Acad Sci U S A 95:13272-13277.

Perez Velazquez JL, Carlen PL (2000) Gap junctions, synchrony and seizures. Trends
Neurosci 23:68-74.

Piccolino M, Neyton J, Gerschenfeld HM (1984) Decrease of gap junction
permeability induced by dopamine and cyclic adenosine 3':5'-monophosphate
in horizontal cells of turtle retina. J Neurosci 4:2477-2488.

Ribelayga C, Cao Y, Mangel SC (2008) The circadian clock in the retina controls
rod-cone coupling. Neuron 59:790-801.

Rieke F, Rudd ME (2009) The challenges natural images pose for visual adaptation.
Neuron 64:605-616.

Rodieck RW (1998) The first steps in seeing. Sunderland, MA: Sinauer Associates.

Roska B, Werblin F (2001) Vertical interactions across ten parallel, stacked
representations in the mammalian retina. Nature 410:583-587.

Roska B, Molnar A, Werblin FS (2006) Parallel processing in retinal ganglion cells:
how integration of space-time patterns of excitation and inhibition form the
spiking output. J Neurophysiol 95:3810-3822.

Sah P, Hestrin S, Nicoll RA (1989) Tonic activation of NMDA receptors by ambient
glutamate enhances excitability of neurons. Science 246:815-818.

Schubert T, Degen J, Willecke K, Hormuzdi SG, Monyer H, Weiler R (2005) Connexin36 mediates gap junctional coupling of alpha-ganglion cells in mouse retina. J Comp Neurol 485:191-201.

Schwartz EA (1975a) Rod-rod interaction in the retina of the turtle. J Physiol 246:617-638.

Schwartz EA (1975b) Cones excite rods in the retina of the turtle. J Physiol 246:639-651.

Schwartz EA (1975c) Rod-rod interaction in the retina of the turtle. J Physiol 246:617-638.

Schwartz EA (1975d) Cones excite rods in the retina of the turtle. J Physiol 246:639-651.

Serre-Beinier V, Bosco D, Zulianello L, Charollais A, Caille D, Charpantier E, Gauthier BR, Diaferia GR, Giepmans BN, Lupi R, Marchetti P, Deng S, Buhler L, Berney T, Cirulli V, Meda P (2008) Cx36 makes channels coupling human pancreatic {beta} - cells, and correlates with insulin expression. Hum Mol Genet.

Siegert S, Scherf BG, Del Punta K, Didkovsky N, Heintz N, Roska B (2009) Genetic address book for retinal cell types. Nat Neurosci 12:1197-1204.

Sitaramayya A, Crabb JW, Matesic DF, Margulis A, Singh V, Pulukuri S, Dang L (2003) Connexin 36 in bovine retina: lack of phosphorylation but evidence for association with phosphorylated proteins. Vis Neurosci 20:385-395.

Smith RG, Vardi N (1995) Simulation of the AII amacrine cell of mammalian retina: functional consequences of electrical coupling and regenerative membrane properties. Vis Neurosci 12:851-860.

Smith RG, Freed MA, Sterling P (1986) Microcircuitry of the dark-adapted cat retina: functional architecture of the rod-cone network. J Neurosci 6:3505-3517.

Soderling TR, Derkach VA (2000) Postsynaptic protein phosphorylation and LTP. Trends Neurosci 23:75-80.

Sohl G, Degen J, Teubner B, Willecke K (1998) The murine gap junction gene connexin36 is highly expressed in mouse retina and regulated during brain development. FEBS Lett 428:27-31.

Sohl G, Guldenagel M, Beck H, Teubner B, Traub O, Gutierrez R, Heinemann U, Willecke K (2000) Expression of connexin genes in hippocampus of kainate-treated and kindled rats under conditions of experimental epilepsy. Brain Res Mol Brain Res 83:44-51.

Srinivas M, Rozental R, Kojima T, Dermietzel R, Mehler M, Condorelli DF, Kessler JA, Spray DC (1999) Functional properties of channels formed by the neuronal gap junction protein connexin36. J Neurosci 19:9848-9855.

Strettoi E, Dacheux RF, Raviola E (1990) Synaptic connections of rod bipolar cells in the inner plexiform layer of the rabbit retina. J Comp Neurol 295:449-466.

Strettoi E, Raviola E, Dacheux RF (1992) Synaptic connections of the narrow-field, bistratified rod amacrine cell (AII) in the rabbit retina. J Comp Neurol 325:152-168.

Svenningsson P, Nishi A, Fisone G, Girault JA, Nairn AC, Greengard P (2004) DARPP-32: an integrator of neurotransmission. Annu Rev Pharmacol Toxicol 44:269-296.

Teranishi T, Negishi K (1994) Double-staining of horizontal and amacrine cells by intracellular injection with lucifer yellow and biocytin in carp retina. Neuroscience 59:217-226.

Teranishi T, Negishi K, Kato S (1984) Dye coupling between amacrine cells in carp retina. Neurosci Lett 51:73-78.

Teubner B, Degen J, Sohl G, Guldenagel M, Bukauskas FF, Trexler EB, Verselis VK, De Zeeuw CI, Lee CG, Kozak CA, Petrasch-Parwez E, Dermietzel R, Willecke K (2000) Functional expression of the murine connexin 36 gene coding for a neuron-specific gap junctional protein. J Membr Biol 176:249-262.

Thompson JD, Higgins DG, Gibson TJ (1994) CLUSTAL W: improving the sensitivity of progressive multiple sequence alignment through sequence weighting, position-specific gap penalties and weight matrix choice. Nucleic Acids Res 22:4673-4680.

Tsang VC, Wilkins PP (1991) Optimum dissociating condition for immunoaffinity and preferential isolation of antibodies with high specific activity. J Immunol Methods 138:291-299.

Urschel S, Hoher T, Schubert T, Alev C, Sohl G, Worsdorfer P, Asahara T, Dermietzel R, Weiler R, Willecke K (2006) Protein kinase A-mediated phosphorylation of connexin36 in mouse retina results in decreased gap

junctional communication between AII amacrine cells. J Biol Chem 281:33163-33171.

Uusisaari M, Smirnov S, Voipio J, Kaila K (2002) Spontaneous epileptiform activity mediated by GABA(A) receptors and gap junctions in the rat hippocampal slice following long-term exposure to GABA(B) antagonists. Neuropharmacology 43:563-572.

Van Der Giessen RS, Koekkoek SK, van Dorp S, De Gruijl JR, Cupido A, Khosrovani S, Dortland B, Wellershaus K, Degen J, Deuchars J, Fuchs EC, Monyer H, Willecke K, De Jeu MT, De Zeeuw CI (2008) Role of olivary electrical coupling in cerebellar motor learning. Neuron 58:599-612.

van Veen TA, van Rijen HV, Jongsma HJ (2000) Electrical conductance of mouse connexin45 gap junction channels is modulated by phosphorylation. Cardiovasc Res 46:496-510.

van Wyk M, Wassle H, Taylor WR (2009) Receptive field properties of ON- and OFF-ganglion cells in the mouse retina. Vis Neurosci 26:297-308.

Vaney DI (1985) The morphology and topographic distribution of AII amacrine cells in the cat retina. Proc R Soc Lond B Biol Sci 224:475-488.

Vaney DI (1991) Many diverse types of retinal neurons show tracer coupling when injected with biocytin or Neurobiotin. Neurosci Lett 125:187-190.

Vardi N, Smith RG (1996) The AII amacrine network: coupling can increase correlated activity. Vision Res 36:3743-3757.

Veruki ML, Hartveit E (2002a) AII (Rod) amacrine cells form a network of
electrically coupled interneurons in the mammalian retina. Neuron 33:935-
946.

Veruki ML, Hartveit E (2002b) Electrical synapses mediate signal transmission in the
rod pathway of the mammalian retina. J Neurosci 22:10558-10566.

Veruki ML, Morkve SH, Hartveit E (2003) Functional properties of spontaneous
EPSCs and non-NMDA receptors in rod amacrine (AII) cells in the rat retina.
J Physiol 549:759-774.

Veruki ML, Morkve SH, Hartveit E (2006) Activation of a presynaptic glutamate
transporter regulates synaptic transmission through electrical signaling. Nat
Neurosci 9:1388-1396.

Veruki ML, Oltedal L, Hartveit E (2008) Electrical Synapses Between AII Amacrine
Cells: Dynamic Range and Functional Consequences of Variation in
Junctional Conductance. J Neurophysiol 100:3305-3322.

Virshup DM, Shenolikar S (2009) From promiscuity to precision: protein
phosphatases get a makeover. Mol Cell 33:537-545.

Volgyi B, Deans MR, Paul DL, Bloomfield SA (2004) Convergence and segregation
of the multiple rod pathways in mammalian retina. J Neurosci 24:11182-
11192.

Wagner HJ, Wagner E (1988) Amacrine cells in the retina of a teleost fish, the roach
(Rutilus rutilus): a Golgi study on differentiation and layering. Philos Trans R
Soc Lond B Biol Sci 321:263-324.

Wark B, Fairhall A, Rieke F (2009) Timescales of inference in visual adaptation. Neuron 61:750-761.

Wellershaus K, Degen J, Deuchars J, Theis M, Charollais A, Caille D, Gauthier B, Janssen-Bienhold U, Sonntag S, Herrera P, Meda P, Willecke K (2008) A new conditional mouse mutant reveals specific expression and functions of connexin36 in neurons and pancreatic beta-cells. Exp Cell Res 314:997-1012.

Witkovsky P (2004) Dopamine and retinal function. Doc Ophthalmol 108:17-40.

Witkovsky P, Nicholson C, Rice ME, Bohmaker K, Meller E (1993) Extracellular dopamine concentration in the retina of the clawed frog, Xenopus laevis. Proc Natl Acad Sci U S A 90:5667-5671.

Witkovsky P, Svenningsson P, Yan L, Bateup H, Silver R (2007) Cellular localization and function of DARPP-32 in the rodent retina. Eur J Neurosci 25:3233-3242.

Wu SM, Yang XL (1988) Electrical coupling between rods and cones in the tiger salamander retina. Proc Natl Acad Sci U S A 85:275-278.

Xia XB, Mills SL (2004) Gap junctional regulatory mechanisms in the AII amacrine cell of the rabbit retina. Vis Neurosci 21:791-805.

Xin D, Bloomfield SA (1997) Tracer coupling pattern of amacrine and ganglion cells in the rabbit retina. J Comp Neurol 383:512-528.

Xin D, Bloomfield SA (1999) Dark- and light-induced changes in coupling between horizontal cells in mammalian retina. J Comp Neurol 405:75-87.

Yang XD, Korn H, Faber DS (1990) Long-term potentiation of electrotonic coupling at mixed synapses. Nature 348:542-545.

Yang XL, Wu SM (1989) Modulation of rod-cone coupling by light. Science 244:352-354.

Yeager M (2009) Gap junction channel structure. In: Connexins: A Guide (Harris AL, Locke D, eds), pp 27-75: Humana Press.

Zampighi GA, Planells AM, Lin D, Takemoto D (2005) Regulation of lens cell-to-cell communication by activation of PKCgamma and disassembly of Cx50 channels. Invest Ophthalmol Vis Sci 46:3247-3255.

Zhang DQ, Zhou TR, McMahon DG (2007) Functional heterogeneity of retinal dopaminergic neurons underlying their multiple roles in vision. J Neurosci 27:692-699.

Zhang J, Wu SM (2004) Connexin35/36 gap junction proteins are expressed in photoreceptors of the tiger salamander retina. J Comp Neurol 470:1-12.

Zhang J, Diamond JS (2006) Distinct perisynaptic and synaptic localization of NMDA and AMPA receptors on ganglion cells in rat retina. J Comp Neurol 498:810-820.

Zhou C, Dacheux RF (2004) All amacrine cells in the rabbit retina possess AMPA-, NMDA-, GABA-, and glycine-activated currents. Vis Neurosci 21:181-188.

Zoidl G, Meier C, Petrasch-Parwez E, Zoidl C, Habbes HW, Kremer M, Srinivas M, Spray DC, Dermietzel R (2002) Evidence for a role of the N-terminal domain in subcellular localization of the neuronal connexin36 (Cx36). J Neurosci Res 69:448-465.

Vita

William Wade Kothmann was born in Austin, Texas on August 15th, 1981 to Don William Kothmann and Sheila Gregg Kothmann. After graduating from Round Rock High School, Round Rock, Texas in 1999, he entered Southwestern University in Georgetown, Texas. He earned a Bachelor of Arts with a major in psychology from Southwestern in May, 2003. In August of 2004 he entered The University of Texas Health Science Center at Houston Graduate School of Biomedical Sciences.